

**DETECTION OF AUTOMATIC DEPENDENT
SURVEILLANCE – BROADCAST SIGNALS USING
STRATOSPHERIC AND ORBITAL PLATFORMS**

**DÉTECTION DES SIGNAUX DE LA SURVEILLANCE
DÉPENDANTE AUTOMATIQUE EN MODE DIFFUSION
EN UTILISANT DES PLATES-FORMES
STRATOSPHERIQUES ET ORBITALES**

A Thesis Submitted

to the Division of Graduate Studies of the Royal Military College of Canada

by

Raymond Francis, B.A.Sc.
Second Lieutenant

In Partial Fulfillment of the Requirement for the Degree of

Master of Science in Physics

April 2010

© This Thesis may be used within the Department of National
Defence but copyright for open publication remains the property of the author.



Library and Archives
Canada

Published Heritage
Branch

395 Wellington Street
Ottawa ON K1A 0N4
Canada

Bibliothèque et
Archives Canada

Direction du
Patrimoine de l'édition

395, rue Wellington
Ottawa ON K1A 0N4
Canada

Your file *Votre référence*
ISBN: 978-0-494-64543-7
Our file *Notre référence*
ISBN: 978-0-494-64543-7

NOTICE:

The author has granted a non-exclusive license allowing Library and Archives Canada to reproduce, publish, archive, preserve, conserve, communicate to the public by telecommunication or on the Internet, loan, distribute and sell theses worldwide, for commercial or non-commercial purposes, in microform, paper, electronic and/or any other formats.

The author retains copyright ownership and moral rights in this thesis. Neither the thesis nor substantial extracts from it may be printed or otherwise reproduced without the author's permission.

In compliance with the Canadian Privacy Act some supporting forms may have been removed from this thesis.

While these forms may be included in the document page count, their removal does not represent any loss of content from the thesis.

AVIS:

L'auteur a accordé une licence non exclusive permettant à la Bibliothèque et Archives Canada de reproduire, publier, archiver, sauvegarder, conserver, transmettre au public par télécommunication ou par l'Internet, prêter, distribuer et vendre des thèses partout dans le monde, à des fins commerciales ou autres, sur support microforme, papier, électronique et/ou autres formats.

L'auteur conserve la propriété du droit d'auteur et des droits moraux qui protègent cette thèse. Ni la thèse ni des extraits substantiels de celle-ci ne doivent être imprimés ou autrement reproduits sans son autorisation.

Conformément à la loi canadienne sur la protection de la vie privée, quelques formulaires secondaires ont été enlevés de cette thèse.

Bien que ces formulaires aient inclus dans la pagination, il n'y aura aucun contenu manquant.


Canada

ABSTRACT

Author: Francis, Raymond; Degree: MSc Physics; Granting institution: Royal Military College of Canada; Date of qualification: April 2010; Title: Detection of Automatic Dependent Surveillance – Broadcast Signals using Stratospheric and Orbital Platforms

The possibility of using the Automatic Dependent Surveillance – Broadcast (ADS-B) system for monitoring air traffic from orbit is examined. Experimental work is described which successfully demonstrated reception using a stratospheric balloon of ADS-B signals sent over the 1090 MHz Extended Squitter system. A model is developed of the signal propagation from aircraft to satellites in various orbits, including atmospheric effects. The resulting power level at the orbital altitude is used to determine the net receiver gain needed to reliably detect the signals from orbit. A model of the effect on detectability of signal collisions is developed and resulting design parameters determined. ADS-B signals are concluded to be detectable with a gain of 0-5 dB from LEO and 30 dB from GEO orbits, for aircraft populations of up to 4000 in the sensor's field of view.

List of keywords:

ADS-B, air traffic surveillance, Automatic Dependent Surveillance – Broadcast, aviation, Extended Squitter, high-altitude balloon, Mode S, satellite, signal propagation, space missions

RÉSUMÉ

Auteur: Francis, Raymond; Diplôme: MSc Physique; Établissement accordant: Collège militaire royal du Canada; Date d'admission: avril 2010; Titre: Détection des signaux de la Surveillance dépendante automatique en mode diffusion en utilisant des plates-formes stratosphériques et orbitales

La possibilité d'utiliser le système de Surveillance dépendante automatique en mode diffusion (« ADS-B ») pour la surveillance de la circulation aérienne par un système orbitale est examiné. Des travaux expérimentaux sont décrits dans lesquels on démontre que les signaux transmis par l'ADS-B sur le système de « squitter long de 1090 MHz » peuvent être reçus par une sonde qui est transportée sur un ballon stratosphérique. Un modèle de la propagation des signaux des aéronefs aux satellites en plusieurs différents types d'orbites est développé. Le modèle inclut les effets atmosphériques et ionosphériques. La puissance du signal résultante est employée pour déterminer le gain net nécessaire pour la réception fiable des signaux ADS-B par des plates-formes orbitales. Un modèle de l'effet de collision causé par la réception de plusieurs signaux ADS-B en même temps est développé, et les paramètres de dessin résultants sont déterminés. Les signaux ADS-B sont détectables avec un gain de 0-5 dB en orbite basse tandis que pour un satellite en orbite géostationnaire, une antenne de 30 dB est nécessaire pour l'observation des aéronefs. Le capteur sur le satellite peut observer jusqu'à 4000 aéronefs dans son champ de visée.

Mots clés: ADS-B, aviation, ballon-sonde en haute altitude, missions spatiales, Mode S, propagation de signaux, satellite, squitter long, Surveillance dépendante automatique en mode diffusion, surveillance de circulation aérienne

Contents

List of Tables	vi
List of Figures	vii
List of Acronyms	ix
1 Introduction	1
1.1 Air Traffic Management	1
1.2 The use of ADS-B	2
1.3 Canadian implementation	4
1.4 Orbital sensors	6
1.5 Automatic Identification System (AIS)	6
1.6 Satellite augmentation of ADS-B	7
1.7 Objective and outline	8
2 Stratospheric Detection Experiments	10
2.1 Introduction	10
2.2 The FLOAT experiment	10
2.3 Mission Concept	12
2.4 Mission Profile	12
2.5 Payload system	15
2.6 Tracking	16
2.7 Operational and regulatory aspects	16
2.8 The first flight of FLOAT	17
2.9 Test and revision program	18
2.10 FLOAT-2 mission	19
3 Stratospheric Detection Results	20
3.1 Introduction	20
3.2 The FLOAT-2 dataset	20
3.3 Detection region	22
3.4 Detection rate	28
3.5 Detection cases of particular interest	31
3.5.1 Long-range detections	31
3.5.2 Estimates of the line-of-sight reception range	34
3.5.3 Estimate of the vertical detection range	37
3.6 Technical performance of the payload	38
3.6.1 ADS-B Detection without the payload antenna	38

3.6.2	Interruption to ADS-B recording	40
3.6.3	Interruptions to temperature recording	42
4	Orbital Detection: Methodology	43
4.1	Introduction	43
4.2	Background	44
4.2.1	1090 MHz Extended Squitter	44
4.2.2	Signal modulation and message format	44
4.2.3	Transmission characteristics	46
4.2.3.1	Transmitted power	46
4.2.3.2	Transmission frequency	46
4.2.3.3	Timing of messages	46
4.2.3.4	Transmitter antenna characteristics	48
4.2.3.5	Polarization	48
4.2.3.6	Transmitting diversity	48
4.2.3.7	Reception range	48
4.2.3.8	Transmission criteria	49
4.2.3.9	Other information	49
4.3	Orbital geometry	50
4.4	Link Budget	51
4.4.1	Gain of the ADS-B antenna	52
4.4.2	Free-space path loss	53
4.4.3	Atmospheric propagation effects	53
4.4.3.1	Neutral atmosphere absorption	54
4.4.3.2	Attenuation by precipitation and clouds	55
4.4.3.3	Atmospheric refraction	55
4.4.3.4	Atmospheric loss factor	56
4.4.3.5	Ionospheric refraction	57
4.4.3.6	Ionospheric attenuation	57
4.4.3.7	Scintillation fading	58
4.4.4	Received power	59
4.4.5	Signal-to-noise ratio	59
4.4.6	Parabolic receiver antenna	60
4.5	Doppler effect	62
4.6	Signal collisions	63
4.6.1	Probability of signal collision	64
4.6.2	Allowed detection time and probability	66
5	Orbital Detection: Theoretical Results	68
5.1	Introduction	68
5.2	Orbital geometry	69
5.3	Link Budget	74
5.3.1	Free-space path loss	74
5.3.2	Neutral atmosphere absorption	76
5.3.3	Atmospheric refraction	77

5.3.4	Ionospheric refraction	79
5.3.5	Ionospheric attenuation	80
5.3.6	Overall implication of atmospheric effects	81
5.3.7	Received power	81
5.3.8	Signal-to-noise ratio	85
5.4	The LEO case	89
5.5	The GEO case	93
5.6	Constellations and hybrid systems	100
5.7	The stratospheric balloon case revisited	104
5.8	Doppler effect	107
5.9	Signal collisions	108
5.9.1	System design parameters and strategy	116
5.9.2	Addressing the aircraft population limit	117
6	Considerations for implementation	119
6.1	Introduction	119
6.2	Motivation	119
6.3	International co-ordination	120
6.4	Stakeholders	122
6.5	System characteristics	122
6.6	Implementation	123
6.7	Further evolution	124
7	Summary, Conclusion, and Future work	125
7.1	Summary	125
7.2	Key findings	126
7.3	Future work	128
	Bibliography	131
	CURRICULUM VITAE	138

List of Tables

3.1	Data statistics for FLOAT-2 mission	22
3.3	Aircraft types detected by FLOAT-2	22
3.5	Parameters of long-range detections	33
4.1	ADS-B message broadcast rates by message type	47
5.1	Parameters for LEO orbits, 10 dB link margin criterion	89
5.3	Parameters for LEO orbits, 7 dB link margin criterion	89
5.5	Parameters for GEO constellation, with elimination of low-latitude coverage gaps	101
5.7	Number of aircraft allowed in the field of view for detection failure probability and integration time	115

List of Figures

1.1	Comparison of ADS-B and radar antenna installations	3
1.2	Nav Canada proposed area of ADS-B surveillance.	5
2.1	FLOAT mission profile	13
2.2	The FLOAT balloon system in flight	14
3.1	Plot of all aircraft position reports recorded by FLOAT-2	24
3.2	Plot of aircraft position reports recorded by FLOAT-2 (detail)	25
3.3	Plot of aircraft position reports recorded by FLOAT-2 during the high-altitude segment.	26
3.4	Path of the FLOAT-2 balloon and payload	27
3.5	Detection results for aircraft with known ADS-B equipment	30
3.6	Position reports from N627JB	35
3.7	Position reports from N706TW	36
3.8	Aircraft tracked on the surface at Toronto-Pearson	37
3.9	Position reports from C-GJWS	39
3.10	Evolution of external and internal temperatures during the ADS-B signal reception gap	40
4.1	1090 MHz ES message format	45
4.2	1090 MHz ES data block allocations	45
4.3	Orbital geometry	50
4.4	Quarter-wave monopole antenna radiation pattern	52
4.5	Effect of atmospheric refraction	55
4.6	Radiation pattern of a typical parabolic reflector antenna	61
5.1	Aircraft horizontal range (L) vs. nadir angle (θ)	70
5.2	Elevation angle (α) vs. nadir angle (θ)	72
5.3	Propagation distance (d_{prop}) vs. nadir angle (θ)	73
5.4	Free-space path loss (L_s) vs. nadir angle (θ)	75
5.5	Neutral atmosphere attenuation (A_a) vs. elevation angle at the aircraft (α)	76
5.6	Attenuation due to neutral atmosphere absorption (A_a) vs. nadir angle (θ)	77
5.7	Attenuation factor due to atmospheric refraction (L_r) vs. elevation angle (α)	78

5.8	Attenuation factor due to atmospheric refraction (L_r) vs. elevation angle (α), detail	78
5.9	Critical frequency for ionospheric transmission vs. elevation angle	79
5.10	Critical frequency for ionospheric transmission vs. elevation angle, detail	80
5.11	Received isotropic power vs. nadir angle θ	82
5.12	Received isotropic power (P_r) vs. aircraft horizontal range (L)	84
5.13	E_b/N_o vs. nadir angle	86
5.14	E_b/N_o vs. aircraft horizontal range	87
5.15	Range and signal strength comparison for LEO orbits	90
5.16	Comparison of antenna cases at low Earth orbit (LEO)	91
5.17	Detection region and central null for a satellite at 400 km	92
5.18	Central lobe of parabolic antenna radiation pattern	94
5.19	Performance of 1.96 m parabolic antenna at geostationary altitude	94
5.20	Detection area for GEO case: 100°W longitude	95
5.21	Canadian Air Defence Identification Zone	97
5.22	Gander Oceanic Control Area	98
5.23	Position of the Gander Oceanic CTA within the area of coverage	98
5.24	ADS-B coverage over South America for a geostationary satellite at 100°W	99
5.25	ADS-B coverage over the Pacific Ocean for a geostationary satellite at 100°W	99
5.26	Variation in received signal strength with angular separation	101
5.27	GEO constellation arrangement strategy	102
5.28	Polar detection gap in the GEO constellation with 10 dB link margin	102
5.29	Link margin vs. range for a balloon-borne sensor at 30 km	104
5.30	Comparison of reception ranges for various balloon altitudes	106
5.31	Comparison of link margin and range for stratospheric and orbital platforms	106
5.32	Probability of no collisions vs. Number of aircraft in view	110
5.33	Expected number of aircraft successfully detected vs. Number of aircraft in view	110
5.34	Detection Probability by number of aircraft and integration time	111
5.35	Detection failure probability by number of aircraft and integration time	112
5.36	Relationship between key signal collision parameters	114

List of Acronyms

ACC	Area Control Centre
ADIZ	Air Defence Identification Zone
ADS-B	Automatic Dependent Surveillance – Broadcast
AIC	Aeronautical Information Circular
AIM	Aeronautical Information Manual
AIP	Aeronautical Information Publication
AIS	Automatic Identification System
ANS&A	Air Navigation Services and Airspace
APRS	Automatic Packet Reporting System
ASL	above sea level
ASM	Application of Separation Minima
ATCRBS	Air Traffic Control Radar Beacon System
ATS	Air Traffic Services
BLAST	Balloon-borne Large Aperture Submillimeter Telescope
BSO	Balloon Safety Officer
CAR	Canadian Aviation Regulations
CSA	Canadian Space Agency
CTA	Control Area
CVFR	Controlled VFR
DAH	Designated Airspace Handbook
DFAIT	Department of Foreign Affairs and International Trade

DME	Distance Measuring Equipment
DND	Department of National Defence
DRDC	Defence Research and Development Canada
EDT	Eastern Daylight Saving Time
ES	Extended Squitter
ESA	European Space Agency
EUMETSAT	European Organisation for the Exploitation of Meteorological Satellites
EUROCAE	European Organization for Civil Aviation Equipment
EUROCONTROL	European Organisation for the Safety of Air Navigation
FAA	Federal Aviation Administration
FIC	Flight Information Centre
FIR	Flight Information Region
FLOAT	Flying Laboratory for Observation of ADS-B Transmissions
GBT	Green Bank Telescope
GEO	geostationary orbit
GNSS	Global Navigation Satellite Systems
GPS	Global Positioning System
GTAA	Greater Toronto Airports Authority
IATA	International Air Transport Association
ICAO	International Civil Aviation Organization
IFR	Instrument Flight Rules
ISS	International Space Station
IMO	International Maritime Organization
LEO	low Earth orbit
MAIT	manufacturing, assembly, integration, and testing
MANTRA	Middle Atmosphere Nitrogen Trend Assessment

Mbps	megabit per second
MEO	medium Earth orbit
MOPS	Minimum Operational Performance Standards
MSG	Meteosat Second Generation
NAT	North Atlantic
NM	nautical mile
NOAA	National Oceanic and Atmospheric Administration
NORAD	North American Aerospace Defense Command
NOTAM	Notice to Airmen
NTS	Nanosatellite Tracking Ships
PCW	Polar Communications and Weather
PPM	Pulse Position Modulation
RMC	Royal Military College of Canada
RTCA	Radio Technical Commission for Aeronautics
SOLAS	International Convention for the Safety of Life at Sea
SPG	Systems Planning Group
SSO	sun-synchronous orbit
TACAN	Tactical Air Navigation
TC	Transport Canada
TDMA	time-division multiple access
TIS-B	Traffic Information Services – Broadcast
UAT	Universal Access Transceiver
UTC	Co-ordinated Universal Time
UHF	Ultra High Frequency
VDL Mode 4	VHF Data Link Mode 4
VFR	Visual Flight Rules
VHF	Very High Frequency
WAAS	Wide Area Augmentation System

Chapter 1

Introduction

1.1 Air Traffic Management

The modern air traffic management system has traditionally relied on radar systems to inform Air Traffic Services (ATS) of the positions of aircraft in their area of responsibility. While this technology has proven very reliable, radar installations are expensive, and in many areas are impractical to install. For this reason, the airspace covering large areas of the Earth's surface, such as over the open ocean, lacks radar positioning services, and as a result ATS has no direct source of aircraft position information in these areas.

In areas where no surveillance information is available, separation between aircraft is often assured by procedural means. Aircraft can, for example, be assigned to different flight altitudes, with sufficient spacing to ensure that aircraft in adjacent altitude bands do not simultaneously enter the same position in space, given the potential errors in altimetry and procedure. Lateral spacing is similarly effected. Such position and altitude assignments are directed by ATS based on projected motion of the aircraft and reported position. To account for uncertainties in instrumentation, the infrequent availability of accurate position information, and the potential for unannounced deviations from planned flight paths, the margins between assigned aircraft positions must be large. In the North Atlantic (NAT) region, the International Civil Aviation Organization (ICAO) mandates separation minima which are in some cases as wide as 120 nautical miles (NM) (222 km) laterally, 60 minutes of flight distance longitudinally (along the direction of flight), and up to 4000 feet (1219 m) vertically (NAT ASM, 2009).

In recent years, a new technology called Automatic Dependent Surveillance – Broadcast (ADS-B) has come into use in some regions. In this system, aircraft regu-

larly broadcast messages containing position, itinerary, and identification information, which can be received by nearby aircraft or ATS ground receivers. The navigational information contained in these messages is derived from on-board navigation systems, generally with reference to Global Navigation Satellite Systems (GNSS), and are transmitted automatically, without intervention from the aircraft crew. The ADS-B system is termed ‘dependent’ surveillance because it relies upon the reported position information from the aircraft, while ‘independent’ surveillance systems such as radar require no active participation from the aircraft.

1.2 The use of ADS-B

In operation, ADS-B-equipped aircraft exchange navigation data by a variety of datalink technologies using both Very High Frequency (VHF) and Ultra High Frequency (UHF) bands.

Two modes are possible, and are distinguished by terminology adopted by ICAO (ICAO ADS-B, 2003) and the International Air Transport Association (IATA) (Martis, 2007). In “ADS-B Out”, aircraft transmit ADS-B navigation messages in a defined format, at regular intervals, without regard to the presence of receivers. In “ADS-B In”, aircraft receive the ADS-B messages sent by other aircraft, and on-board equipment processes them to produce a cockpit display of nearby air traffic. ADS-B Out is a precondition for ADS-B In services (ICAO ADS-B, 2003), since the signals must be transmitted by air traffic to be available for processing on-board. ADS-B In capability is required for aircraft to be able to independently provide separation from each other, but even without ADS-B In, it is possible for ATS to obtain surveillance information from aircraft equipped for ADS-B Out, using dedicated ground receivers (Wright, 2009).

The use of such ground stations offers a significant cost advantage, compared to conventional surveillance radar (ICAO, 2003b). While radar ground stations require active antennas which radiate power, the ADS-B ground stations are equipped with passive, receiving elements, since the transmitted messages originate with the aircraft. Some remotely-located ADS-B ground stations installed in Australia are powered by co-located solar arrays, since the stations require only 100W of power to operate (Dunstone, 2005). These antennas can also be designed to be of fixed, omnidirectional character, rather than the rotating elements needed for surveillance radar. The lack of mechanical systems and greatly reduced operating power make ADS-B ground stations significantly cheaper to install and operate (FAA, 2007). Figure 1.1 shows

a combined radar and ADS-B installation in Australia, with a large, rotating, active radar antenna and a small, fixed, passive ADS-B antenna labeled below it.



Figure 1.1: Comparison of ADS-B and radar antenna installations. Image from Dunstone (2005).

For this reason, organizations which provide air traffic services, as well as other stakeholders, have advocated the replacement or extension of radar surveillance systems with surveillance based on ADS-B. The European Organisation for the Safety of Air Navigation (EUROCONTROL) plans to use it in areas where existing radars have reached the end of their service lives, and the cost of replacement is prohibitive (PSC ADS-B-NRA, 2008). The Federal Aviation Administration (FAA), in the United States, also plans to implement ADS-B surveillance, partly motivated by reasons of cost (FAA, 2003). In Canada, Nav Canada plans to use ADS-B to extend surveillance to remote areas unserved by radar (Nav Canada, 2008). IATA has also advocated the general adoption of ADS-B as a replacement for radar surveillance, anticipating cost savings to be passed on to its member airlines (IATA, 2007).

1.3 Canadian implementation

In Canada, conventional radar systems have been limited to the southern part of the country (Nav Canada, 2008), leaving large parts of the sparsely settled northern regions unserved by ATS surveillance. In particular, Hudson Bay has long been a gap in radar coverage, due to the impracticality of installing radar stations inside this large inlet of the Arctic Ocean. Recently, Nav Canada has installed ADS-B ground stations around the perimeter of Hudson Bay, to allow provision of ADS-B surveillance in place of radar (Nav Canada, 2008). Service commenced on 15 January 2009, with ADS-B equipped aircraft given priority in certain sectors of the Hudson Bay airspace (AIC 21/09, 2009). It is planned to expand service in the Hudson Bay region, including restrictions on non-ADS-B-equipped aircraft, over the coming years as more aircraft become equipped.

Following the Hudson Bay implementation, expansion of ADS-B coverage to other areas is already underway (Wright, 2009). The second area for ADS-B service includes the northeast coast of Canada, as well as Greenland. This will allow Nav Canada to provide ADS-B surveillance both inside Canadian Domestic Airspace, and oceanic airspace for which it is the ICAO-delegated ATS provider. A map showing this coverage is given in Figure 1.2.

A further expansion is planned to cover most of the Northern Domestic Airspace which does not have radar coverage (Nav Canada, 2008), (Wright, 2009).

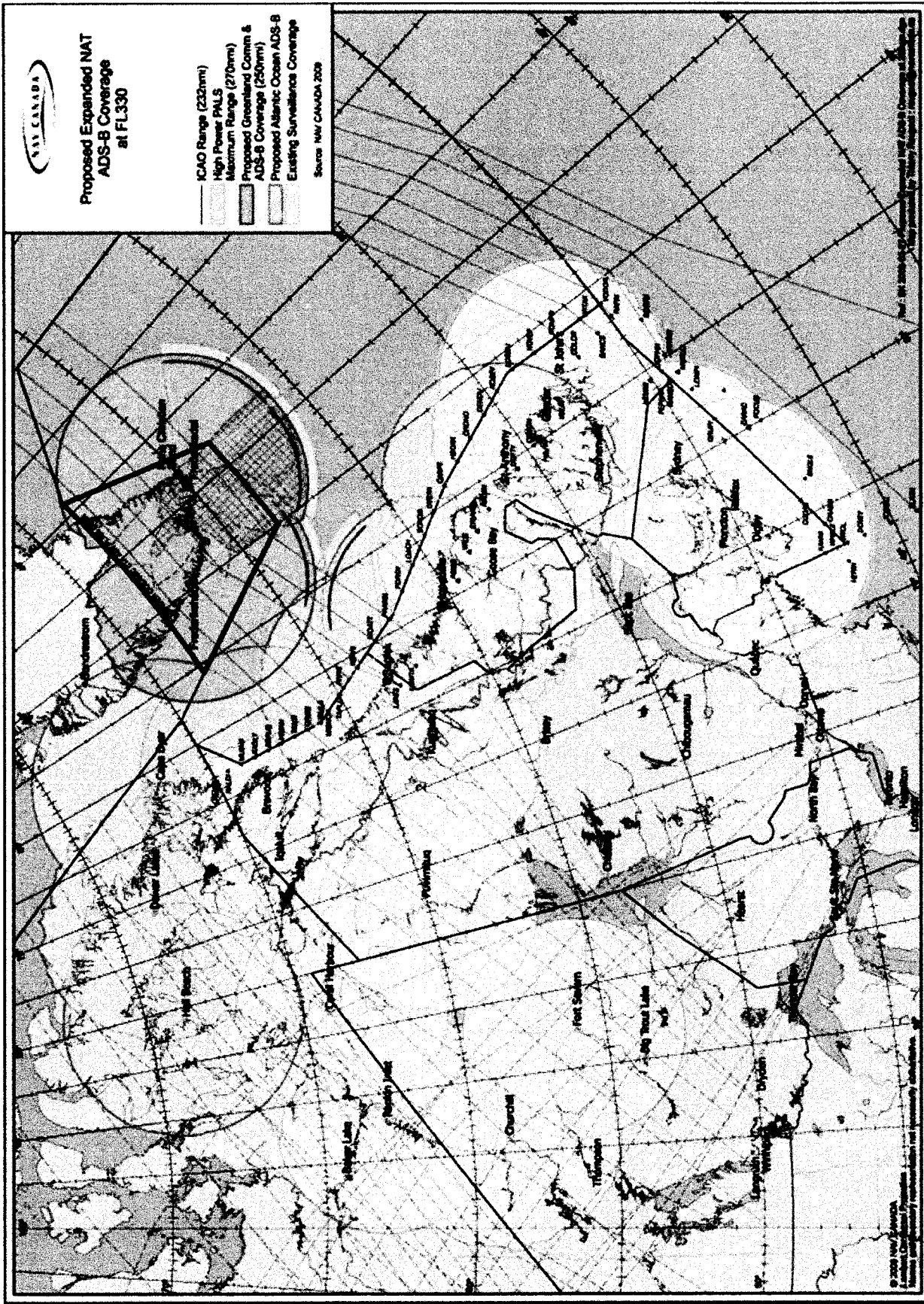


Figure 1.2: Nav Canada proposed area of ADS-B surveillance. Existing radar and ADS-B coverage is in green, the next phase of domestic expansion is in orange. The pink area indicates planned Nav Canada coverage based in Greenland, to serve North Atlantic traffic. Image from Cochrane (2008)

1.4 Orbital sensors

Despite plans for expansion and worldwide adoption, there is a limit to the coverage of ground stations which applies as much to ADS-B as to radar. Since it is impractical to install ADS-B receivers at sea, ground station coverage will never extend beyond line-of-sight from shore. Over the open ocean, gaps in coverage will remain. This situation is partially rectified by the adoption of ADS-B In technology, which allows aircraft to see and avoid each other. Such a scenario nonetheless requires all aircraft to be equipped for both ADS-B Out and ADS-B In, so that all aircraft are both transmitting and interpreting messages. This entails an additional cost for installation and maintenance to be born by operators, and it also leaves oceanic controllers on shore without surveillance information.

A possible solution is the deployment of ADS-B receivers on orbital platforms. Satellite-based receivers could function in the same way as the existing ADS-B ground stations, receiving ADS-B messages from aircraft and relaying them to ATS agencies. A suitable network of such sensors could provide continuous coverage over defined areas of the ocean, and could allow continuous provision of surveillance information from takeoff to landing for a transoceanic flight. Such information could replace or supplement the current dependence on periodic position reports over the ocean, increasing the timeliness and accuracy of the information available to ATS. This would allow reduced spacing requirements to be applied to transoceanic flights, allowing aircraft to follow more direct and efficient routings. This in turn would result in reductions in fuel consumption and engine emissions. Additionally, this more accurate and timely surveillance information would improve the the reliability of separation procedures in increasingly crowded airspace, making greater safety of transoceanic traffic a further expected benefit of such a service. These benefits could also be felt over remote land areas, or any region where radar service is unavailable or aging and prohibitively expensive to replace.

1.5 Automatic Identification System (AIS)

AIS is a transponder system used by seagoing vessels which provides a function similar to that of ADS-B. The International Maritime Organization (IMO) mandates the installation of AIS on vessels of greater than 300 gross tonnage traveling internationally, as well as cargo ships of 500 gross tonnage and all passenger ships (SOLAS, 2002, Ch.V, Reg.19, Sec.2.4). Equipped ships transmit messages containing identifica-

tion and navigational information, which can be detected both by other vessels and by coastal fixed stations used by maritime traffic authorities. These signals are broadcast on VHF frequencies of 161.975 MHz and 162.025 MHz (MSC.140(76), 2002).

Satellite-based sensors to detect AIS signals and relay them to Earth have already been flown, and more are planned. A commercially-developed satellite from Canada named NTS, for *Nanosatellite Tracking Ships*, was launched in April 2008 (Pranajaya et al., 2009), and has successfully tracked AIS signals from low Earth orbit (LEO). The European Space Agency (ESA) has deployed two AIS receivers aboard the International Space Station (ISS), called NORAIS and LUXAIS, launched in September 2009 (ESA, 2009a). Future missions are in development, including AISSat-1 for the Norwegian government (Bonin et al., 2009), and M3MSat (*Maritime Monitoring and Messaging Microsatellite*) for the Canadian (Bédard & Spaans, 2007).

The current and planned space missions aimed at monitoring AIS signals from orbit provide a precedent for orbital traffic monitoring which might be adapted to the case of ADS-B.

1.6 Satellite augmentation of ADS-B

Investigations have already been made into augmenting an ADS-B surveillance system with information delivered by satellite. The University of Alaska has conducted experiments in mountainous regions of Alaska where ADS-B transmitters often do not have line-of-sight to ground stations (FAA, 2002). In this trial, an aircraft's position information was relayed over a satellite telephony link to ATS, using the Iridium constellation. This system, however, required a separate satellite telephony transceiver to be installed aboard the aircraft, and for navigational information to be separately encoded into the satellite telephony link. Widespread adoption of this system would require all aircraft to be equipped both for ADS-B Out, and for satellite telephony. This would also impose a significant new traffic volume on the chosen telephony system, possibly requiring a guaranteed bandwidth service.

Erçetin et al. (2000) also investigated the use of satellite communication for exchanging air traffic information between aircraft and ATS. However, this work also focused on the use of dedicated satellite communication systems such as Iridium, Globalstar, and services in higher orbits including geostationary (GEO). The authors envisaged a transition from terrestrial radio systems for both control instructions and surveillance information, to the use of satellite communication systems as the primary carrier of this information. Such a system would, like that trialled in Alaska, require

aircraft to be equipped for satellite communication.

In addition to the new equipment required to be certified and installed on most or all aircraft, a further complication arises from a system which passes surveillance information over satellite telecom systems. Any such system would be dependent on the availability, serviceability, and durability of the chosen satellite communications network. In general, satellite communication systems are not interoperable; each uses different allocated frequencies and encoding protocols. As such, it would be necessary either to choose a single provider, or to develop a mechanism for merging incoming data from multiple systems, as well as guaranteeing service availability on all used systems. Significant program risk may exist in the event that a single commercial provider is chosen. For example, were the Iridium constellation chosen as the carrier for air navigation data, the possibility of interruption to aeronautical communication services exists should the Iridium constellation cease operations. Such a cessation could occur due to financial difficulties of the operating company, or due to failure to promptly renew the constellation at the end of the lifetime of the current batch of satellites, due to technical, financial, or other barriers.

A system using orbital sensors to detect ADS-B signals themselves, which are already transmitted by ADS-B Out-equipped aircraft, would not require new equipment aboard aircraft, and would not be subject to the difficulties resulting from the use of satellite communication networks. The orbital sensor spacecraft, or payload, could be a dedicated system used only by the ATS system, and be operated by, or on behalf of, the national or international ATS authority.

1.7 Objective and outline

This thesis will explore the concept of using orbital sensors to detect ADS-B signals from aircraft. Key work includes modeling the strength of the signals available on orbit to characterize net receiver gain and the type of antenna that would be needed on-orbit, and investigating natural phenomena which could affect signal reception. To this end, the outline of the remainder of the thesis is as follows:

- **Chapter 2:** Experimental work in detecting ADS-B signals using stratospheric platforms is presented, including the design and conduct of the experiments and considerations for those wishing to pursue similar research.
- **Chapter 3:** The results of the stratospheric detection experiments are presented, including a description of the dataset obtained and the aircraft detected,

the range of the ADS-B detector, and the technical performance of the payload system. Implications are drawn from the results of key aspects to be studied, which are addressed in following chapters.

- **Chapter 4:** A model is developed of ADS-B signal propagation from the transmitting aircraft to a sensor at altitudes ranging from the stratosphere to various orbits of interest. Atmospheric effects are included, as well as the effect of relative motion between the aircraft and the sensor. Additionally, a model is developed of the probability of signal collisions – overlapping signals from simultaneously-transmitting aircraft – which could prevent interpretation of the signals.
- **Chapter 5:** The results of the analysis described in the preceding chapter are presented. The central result is the value of the net gain required at the receiver to reliably detect ADS-B signals in various orbits. The probability of signal collisions is also determined, and the values of the resulting system performance parameters given.
- **Chapter 6:** Following from the scientific and technical results related in the preceding chapter, a brief overview of the the programmatic considerations for development and deployment of a space-based ADS-B surveillance system is given.
- **Chapter 7:** The work is summarized. Key findings are listed, and suggestions for future work to expand and refine the concept are given.

Chapter 2

Stratospheric Detection of ADS-B Signals: Experimental work

2.1 Introduction

This chapter describes experimental work in monitoring ADS-B signals from air traffic using balloon-borne platforms carried into the stratosphere. The experiment program is described in section 2.2, followed by an overview of the mission concept (2.3) and a description of key mission phases (2.4). The design of the experiment is given in more detail in the discussion of the payload design (2.5) and tracking system (2.6). The operational and regulatory constraints applicable to any effort to extend or replicate this work are discussed in section 2.7. Finally, the conduct of the experiments is presented in sections 2.8 through 2.10.

The data gathered in these experiments was subsequently analyzed to characterize the performance of the experiment and for input to the analysis of ADS-B signal detection from Earth orbit. These results are presented later in Chapter 3.

2.2 The FLOAT experiment

The *Flying Laboratory for Observation of ADS-B Transmissions* (FLOAT) was a stratospheric research balloon experiment developed and operated by the Royal Military College of Canada (RMC). Two high-altitude balloon flights took place in May and June 2009, each carrying as payload a device capable of detecting ADS-B transmissions using the 1090 MHz Extended Squitter (ES), one of several datalink technologies used to carry ADS-B information, which is used for ADS-B-based ATS

provision in Canada (Nav Canada, 2008).

The FLOAT mission was developed by a student team as part of the post-graduate and fourth-year undergraduate Space Mission Design courses at RMC, supervised by a professor. Primary funding for the project was provided by Defence Research and Development Canada (DRDC) – Ottawa, whose statement of work directed RMC to conduct the experiment with an aim both to detecting ADS-B signals and to laying the groundwork for a future microsatellite mission to do the same from orbit (DRDC, 2008).

The mission's goal was to demonstrate and characterize the detection of ADS-B signals from the stratosphere (FLOAT-RP-RMC-0001, 2009). The project had the additional objectives of laying the groundwork for future balloon and satellite missions by testing hardware and software for these where appropriate, and developing practices and procedures for use in these later missions. A further stated goal was the educational development of the students involved, echoing comments to the same in the directive from DRDC (DRDC, 2008). Thus both the direction from the funding agency and the objectives for mission planning saw FLOAT in the context of educational development and of future evolution to a satellite platform, in addition to the immediate goal of monitoring air traffic from the stratosphere.

The development program was rapid, but comprehensive. The student team, composed of two post-graduate and three undergraduate students, began work in January 2009 in the context of a winter-semester design project. By early April of the same year, the design was complete and virtually all hardware was delivered. The design was presented to both internal and external parties on April 8th, 2009, after which a fast-paced manufacturing, assembly, integration, and testing (MAIT) phase was carried out. After the payload achieved flight readiness, a first operational flight took place on 26 May 2009, launching from the airport at Wingham, Ontario. A second flight was carried out on 12 June 2009 to improve the dataset and resolve technical issues encountered during the first.

The data collected by the FLOAT payload represented the first-ever collection of ADS-B data from a stratospheric balloon platform. The successful completion of the program marked the establishment of a high-altitude research capability at RMC, and the beginning of an ongoing ADS-B research program at the College.

2.3 Mission Concept

The FLOAT system carried a receive-only ADS-B detector, capable of detecting and recording signals from aircraft using the 1090 MHz ES. The system was carried by a self-bursting stratospheric sounding balloon, capable of reaching altitudes higher than 90,000 feet (27,432 metres) above sea level (ASL). Airline traffic commonly cruises at altitudes from 29,000 to 43,000 feet ASL (TC AIM, 2009, section RAC 11.21.3). For redundancy, observed ADS-B data was to be both recorded on-board for later recovery, and transmitted by radio to a ground station at the launch site.

The system was designed as a lightweight payload, to allow its accommodation on a sounding balloon of the type used by meteorological agencies for daily upper air monitoring. The total payload mass was 3.0 kg, with no requirement for system attitude control or pointing. This architecture greatly reduced the cost and simplified the operation, compared to an alternate mission architecture using a long-duration equal-pressure balloon of the kind often used for scientific missions, such as the MANTRA (Quine et al., 2002) and BLAST (Pascale et al., 2008) experiments.

2.4 Mission Profile

The mission profile for the FLOAT experiment is shown in Figure 2.1. In accordance with aviation convention, altitudes are expressed as ‘Flight Levels’, where ‘FL600’ indicates an altitude of 60,000 feet ASL.

The FLOAT payload canister is suspended below its recovery parachute, which is in turn suspended below the helium balloon. In this configuration, shown in Figure 2.2, it is released manually from the launch site, rising to an uncontrolled burst at or slightly above FL900. With the balloon destroyed, the parachute is released from tension and opens to slow the descent of the payload. Following the landing, the payload is recovered by a retrieve crew sent from the launch site. Throughout this time, from launch to landing, ADS-B data is collected by the onboard receiver, and both stored and transmitted to the ground station. The primary launch site was at Petawawa, Ontario, inside restricted airspace; the ceiling of this area, designated CYR511, is also shown in Figure 2.1.

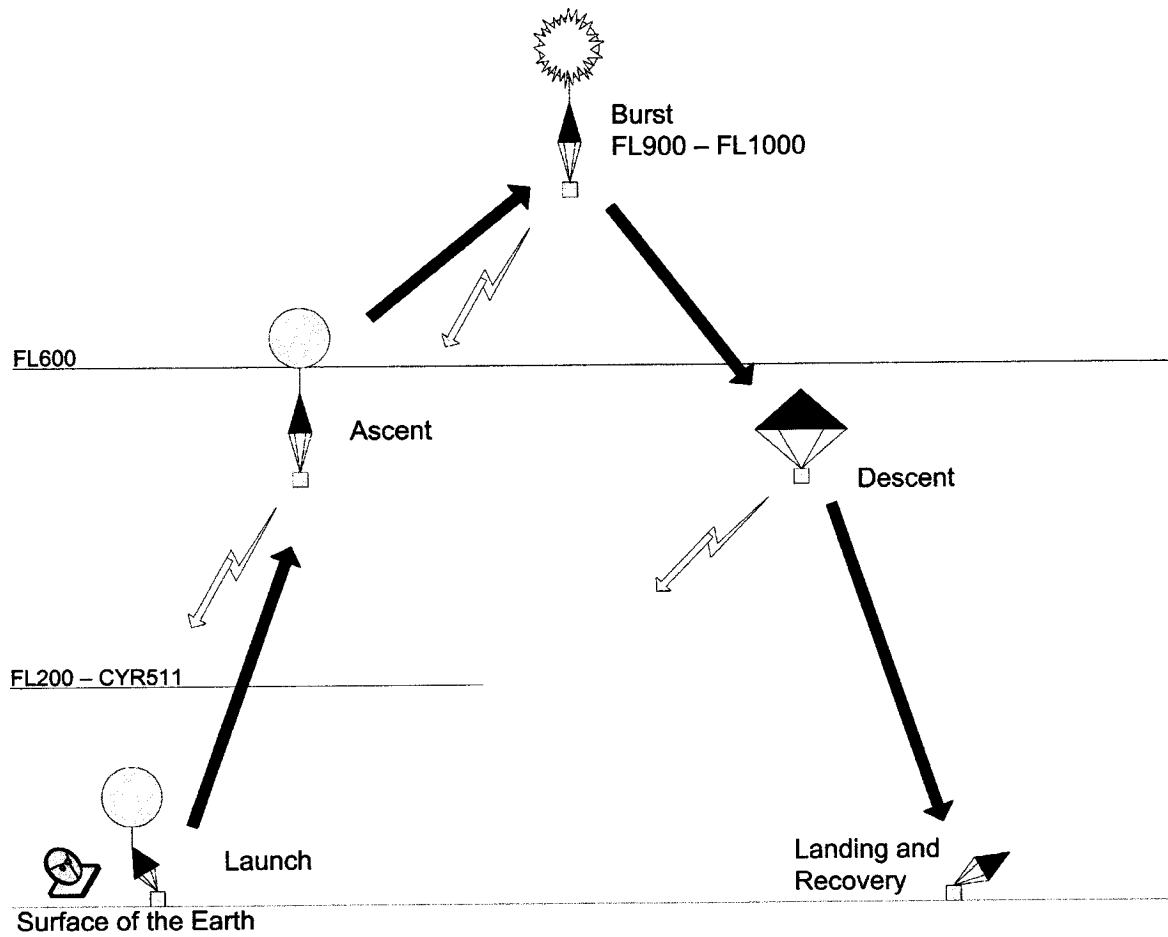


Figure 2.1: FLOAT mission profile. Image from FLOAT-RP-RMC-0001 (2009)



Figure 2.2: The FLOAT balloon system in flight

2.5 Payload system

The FLOAT payload system consisted of an insulated canister containing the sensor systems and supporting hardware. The total mass of the payload system, including the parachute and its rigging, was 3.0 kg. It was designed with a ten-hour operational lifetime, sufficient for preflight checks, launch process, flight operations, and estimated recovery time, with a two-hour margin.

The primary sensor was a commercial ADS-B detector and antenna. A key additional sensor was the onboard Global Positioning System (GPS) receiver, whose data was used both for tracking and as part of the science return. Also included was a secondary payload, a thermocouple acting as temperature sensor, whose role was to record the air temperature both inside and outside the canister during the flight. This temperature information was intended for later technical analysis and potential fault diagnosis, but it also served to provide a sounding of the atmospheric temperature profile.

The operations of these sensor subsystems were supported by an onboard computer, which controlled their operation and recorded the observed data. This data was stored both on the computer's own hard disk, and on a redundant solid-state storage device. Additionally, a UHF radio was used to send the data to the ground station as it was recorded. These support subsystems, and the sensor elements, were provided with electrical power by a system of batteries and a power regulation unit.

All of these components were housed together in a payload canister designed to protect the components during the mission. The canister was built of rigid insulating polymer foam faced with aluminum foil, and sealed with aluminum tape. This canister was designed to insulate the payload components from the cold environment of the stratosphere, where air temperatures as low as -56°C are experienced (Lydolph, 1985). It was also designed to protect the internal components from the force of impact during landing, and to be buoyant and leak-resistant, for the eventuality of a water landing. Aside from the radar-reflective external layer, the key external features of the canister were the housing for the secondary tracking system, the antennas for the ADS-B and GPS receivers and telemetry radio, and the external end of the thermocouple wire of the temperature sensor. The canister also carried markings identifying the payload and its launching authority, as required by the relevant regulations, and to aid in the recovery of the payload in the event the retrieve team was unable to locate it.

2.6 Tracking

To allow recovery of the payload and to meet the requirement to inform ATS of the balloon system's position, it was necessary to provide tracking capability for the system. Additionally, knowledge of the ADS-B receiver's position at the time of signal reception was relevant to the later analysis of the data, and to confirmation that the payload had reached the stratosphere. To these ends, several strategies were employed to monitor the position of the payload:

- **Onboard GPS receiver:** A high-precision GPS receiver of the type used on small satellites was carried in the payload canister. The position information was recorded as part of the science data, including the transmission to the launch site.
- **Commercial personal tracking device:** As a secondary tracking system, a personal tracking device was included, housed separately from the other payload systems and using its own self-contained power supply. This device, the size of a large mobile phone, is designed for personal tracking when traveling in remote areas. It regularly transmits short messages to a satellite communications constellation containing position information derived from its own GPS receiver. With an altitude limit of 21,400 feet ASL, the primary use of this system was for payload recovery, but it also served as a backup in the event that a loss of telemetry prevented access to data from the primary GPS receiver.
- **Radar reflectivity:** The payload canister was faced with a layer of aluminum foil and aluminum tape, for reflectivity to air traffic radar.
- **Automatic Packet Reporting System (APRS):** A transmitter connected to the onboard GPS receiver broadcast the payload's geographic position and altitude regularly on amateur radio frequencies. These signals were to be relayed by local receivers using the automated APRS network, to be visible on an internet interface. Due to unsatisfactory performance, the system was not used on the second balloon flight.

2.7 Operational and regulatory aspects

Operation of high-altitude research balloons carries implications for the safety of aviation, and as such is subject to regulation by the responsible airspace authorities.

In Canada, Transport Canada regulates aeronautical activities, while Nav Canada manages and operates the airspace system. The development and operation of the FLOAT mission was carried out in co-operation with both agencies.

Unoccupied free balloons – that is, those which carry no crew and are not tethered to the Earth’s surface – are governed by the Canadian Aviation Regulations (CAR, 2009). CAR 602.42 requires that balloons with gas envelopes larger than 3.256 m^3 not be launched without prior authorization. A helium balloon of sufficient buoyancy to lift the FLOAT payload had an estimated volume of 5.3 m^3 at launch (FLOAT-RP-RMC-0001, 2009), necessitating approval from Transport Canada. This approval was contingent on compliance with the Canadian Procedures for Large Unmanned Balloon Operations (Transport Canada, 2003) (*‘Balloon Procedures’*).

The Balloon Procedures set out operating rules and requirements for the balloon system and payload. Important among these requirements is the obligation to notify airspace users through the issuance of Notices to Airmen (NOTAMs), following the instructions laid out in the Canadian NOTAM Procedures Manual (Nav Canada, 2007). These NOTAMs serve as notice to airspace users of current or imminent activities; advance warning of the planned operation is also provided in the Aeronautical Information Publication (AIP Canada), in the form of an AIP Supplement, several weeks ahead of the balloon launch.

The Balloon Procedures also require the appointment of a Balloon Safety Officer (BSO), responsible for the safe conduct of the balloon operation (Transport Canada, 2003). The BSO directs the launch and airborne operation, and maintains contact with the relevant ATS authority throughout the pre-flight, flight, and termination phases of the mission. To comply with this requirement, the FLOAT experiment was both planned and operated in co-ordination with Transport Canada’s National Aviation Operations Centre, and Nav Canada’s NOTAM Office, Toronto Area Control Centre (ACC) and London Flight Information Centre (FIC).

2.8 The first flight of FLOAT

Following the test and integration phase, the first flight of the FLOAT payload took place on 26 May, 2009. Because of predicted wind drift during the flight and the anticipated landing area, the alternate launch site at the Wingham, Ontario airport (airport code CPR7) was used. The launch occurred at 12:21 local time, and the payload remained healthy and collected data after release.

Twenty minutes into the ascent, at an altitude of approximately 22,000 ft, teleme-

try from the payload was lost. Communication could not be re-established during the flight. The secondary tracking system, however, remained active, and using it, the payload was tracked to its landing site in a field 55 km east of the launch site. The total flight time was 2 hours, 4 minutes.

The post-flight analysis revealed that a failure of the onboard computer occurred 20 minutes after launch, attributed either to disruption of the spinning hard disk by turbulence encountered by the balloon, or to a momentary interruption of the power supply to the computer. As a result, no data was collected after that point. As well, during the landing, the computer's hard disk was rendered unserviceable due to the impact acceleration, and the ADS-B antenna was separated from the payload.

Despite this difficulty, the dataset for the first 20 minutes of flight was complete, and contained all expected elements, including ADS-B messages from aircraft. The flight also served to qualify the launch procedures, the operations plan, the payload recovery strategy, and the flight system consisting of balloon and parachute. The payload canister protected the hardware, and, with the exception of the hard disk, all internal components survived the flight, and performed as designed.

With some successful data collection and retirement of many of the technical risks associated with RMC's first balloon project, the flight was considered proof of the mission concept.

2.9 Test and revision program

With the positive appraisal of the mission concept, plans were made to launch a second flight to achieve the science goals. The second flight campaign made use of surviving equipment, flight spares, and extra material remaining from the preparation of the first mission. To address the problems that led to the failure of the first mission, a rapid-paced program was undertaken to analyze the technical faults, make modifications to the design to address those faults, and test and integrate the modified payload system.

Key changes included replacement of the flight computer's spinning hard disk with a solid-state model, and removal of the APRS transmitter system, which was a heavy draw on the power system and which performed below expectations in providing tracking data. Software modifications were also made to improve the ability of the computer to recover from power losses, and the power management system was carefully inspected and in some cases fitted with improved wiring and insulation. The system was again thoroughly tested, this time with knowledge gained from the

performance on the first flight.

Close collaboration with the regulating agencies and the smooth operation of the first flight allowed a rapid approval for a second launch, which occurred only 18 days after the first.

2.10 FLOAT-2 mission

The *FLOAT-2* mission took place on 12 June, 2009, using the same launch site at Wingham as the previous flight. The payload system, carrying the same sensor suite as the first mission but reflecting the revisions made in response to the outcome of that flight, was launched at 11:31 local time. Once again the payload remained healthy in the initial ascent.

This time, the payload successfully recorded data throughout its flight. Following an ascent to an altitude of 92,950 feet (28.3 km) ASL, the payload descended by parachute and came to rest in a tree 90 km east of the launch site after a flight of 2 hours, 25 minutes. Telemetry was unreliable during the late phases of the flight, but the secondary tracking system once again allowed recovery of the payload.

Shortly after recovery, it was ascertained that a complete data set had been recorded by the payload, with ADS-B, GPS, and temperature data as planned. All hardware survived the flight, with the exception of the ADS-B antenna, which was torn from its mount during the landing in the tree. The dataset was archived for later analysis at RMC, bringing the FLOAT program to a successful conclusion.

Chapter 3

Stratospheric Detection of ADS-B Signals: Experimental results

3.1 Introduction

This chapter presents the results of the FLOAT experiment, the design and conduct of which was described in chapter 2. The discussion begins with a description of the dataset obtained, in section 3.2. The geographical extent of the successful aircraft tracking is then described, in section 3.3. The performance of the ADS-B sensor is further investigated in section 3.4, by comparing the list of aircraft detected with a list of those known to be present and transmitting ADS-B signals at the time of the experiment. In section 3.5, several particular cases of aircraft detected by the FLOAT payload are investigated to refine the estimate of performance, and to introduce key parameters which limit the depth of analysis that can be made of the FLOAT dataset. These same parameters are explored in greater depth in chapters 4 and 5, where a general model of ADS-B signal propagation to orbital platforms is developed and applied.

The chapter concludes, in section 3.6, with a discussion of the technical performance of the FLOAT payload, of interest for interpreting the instrument's performance, and for any efforts to reproduce the experiment.

3.2 The FLOAT-2 dataset

The FLOAT-2 mission was successful in observing ADS-B transmissions from aircraft, meeting the mission's primary science goal. During the flight of 2 hours, 25 minutes,

2076 individual messages were received from aircraft. The ADS-B data was logged by the commercial software associated with the ADS-B receiver in separate files at intervals of one minute. In the event that no messages were detected in the corresponding one-minute period, no file was created. This occurred nine times during the flight. As well, there is a single longer period when data recording was greatly reduced, spanning 13.6 minutes during the payload's descent by parachute. During this period, only two ADS-B messages were detected, much less than the average of 15.8 per minute for the remainder of the flight. This interruption to the recording is discussed in section 3.6.2 below.

In addition to the ADS-B data, GPS data for the payload position was recorded every 7 seconds throughout the flight. Temperature data was also recorded continually, with a two interruptions of approximately three minutes in length (see section 3.6.3 below).

The portion of the flight in which the balloon was above an altitude of 60,000 feet (18288 metres) ASL is discussed separately as the high-altitude segment. This altitude is used operationally by the regulatory agencies as a reference for when the balloon was safely above air traffic (Nav Canada, 2007), because it represents the upper boundary of the class B airspace in which the cruise portion of long-distance airline flights are conducted. These flights typically cruise at 29,000 to 43,000 ft ASL (TC AIM, 2009); the highest aircraft detected by FLOAT-2 were in cruise at 40,000 ft. With FLOAT-2's height limit near 93,000 ft, this definition of the high-altitude segment places the cruise-phase aircraft between 20,000 and 61,000 ft below the detector. For comparison, a ground station at sea level would find itself 29,000 to 40,000 ft below the same aircraft.

FLOAT-2 operated above 60,000 ft for 48 minutes. During this time, the payload recorded 954 ADS-B messages. This is 46.0% of the mission total, in a period representing 33.1% of the overall flight time. During the high-altitude segment, the range of altitudes reported by detected aircraft were from 525 to 40,000 ft ASL. A summary of the aircraft population detected is given in Table 3.1.

The aircraft operators listed include passenger and cargo airlines, as well as private aircraft. Aircraft types included a variety of models from the three largest commercial aircraft manufacturers, suggesting that the results are not limited by hardware model or transmitter type. The aircraft types recorded are given in Table 3.3.

Table 3.1: Data statistics for FLOAT-2 mission

Altitude range	Airborne	Above FL600
Duration	145 minutes	48 minutes
Balloon drift distance	90.4 km	7.1 km
ADS-B messages	2076	954
Distinct Aircraft	41	18
Operators	20	13
Aircraft types	11	9
Nationality of Registration	8	6

Table 3.3: Aircraft types detected by FLOAT-2

Manufacturer	Aircraft models detected
Airbus	A300, A310, A319, A320, A330
Boeing	B737, B747, B757, B767, B777
Canadair (Bombardier)	CL600

3.3 Detection region

A series of figures is presented on the following pages, showing the geographical spread of the detected aircraft. In Figure 3.1, an overview is shown of the experiment region. The view is wide enough to include the positions of all detected aircraft. For each recorded ADS-B message, the position reported is plotted as a red point. At the centre of the image, a circular placemark indicates the balloon position at burst; its diameter is large enough to cover the entire region of the balloon's drift during the high-altitude segment.

Using the burst position as a reference, circles are plotted at three radii to divide the area into three regions. In the inner region, the density of ADS-B reports is very high. The tracks of aircraft detected within the region often end at or shortly before 200 km from the burst point. A circle of radius 194 km, centred on the burst point, contains these tracks well.

A larger region surrounding this has numerous tracks, particularly to the south. The density is noticeably lower, however, with fewer distinct aircraft detected, and in several cases gaps in the tracks of individual aircraft. These reports are contained

within a circle of 313 km radius, centred on the burst point.

A 545 km circle is also plotted. It contains all aircraft detected during the flight. Only a few aircraft lie outside the 313 km circle, and are in general at much larger distances, each detected five or fewer times in short succession. These long-range detections occurred very early in the flight, and are discussed in section 3.5.1. The farthest of these, over the eastern end of Lake Superior, was 528 km from the balloon at the time of detection.

Figure 3.2 provides a closer view of the central detection region. At this scale, parallel tracks of several aircraft are easier to differentiate. The track of the balloon from launch to landing is also shown, with the burst point still visible. The position of the Toronto-Pearson airport (airport code CYYZ) is visible from the tracks of several aircraft conducting the approach, landing, and taxi phases of their flights, forming loops of position marks to the southeast of the balloon track. Some of these aircraft were tracked from their entry into detection range (approximately 200 km) to their position at the terminal, or, for departing aircraft, from the apron through departure and cruise to a range of some 200 km from the balloon.

Figure 3.3 provides a similar close-range view, this time including all of the position reports detected while the balloon was above 60,000 ft ASL. The balloon track is not shown, since during this segment of the flight, total drift was limited to 7.1 km, over an area almost entirely covered by the placemark showing the balloon's burst point. Since this represents only a portion of the flight, the number of reports is reduced. However, even at this higher altitude, most aircraft which are tracked continuously still disappear from the record at ranges of approximately 200 km.

Finally, the ground track of the balloon is shown in Figure 3.4. The timings and positions of key events are shown, with the times given in local time at the launch site, Eastern Daylight Saving Time (EDT) (UTC-4h) on the date of the flight, 12 June 2009.

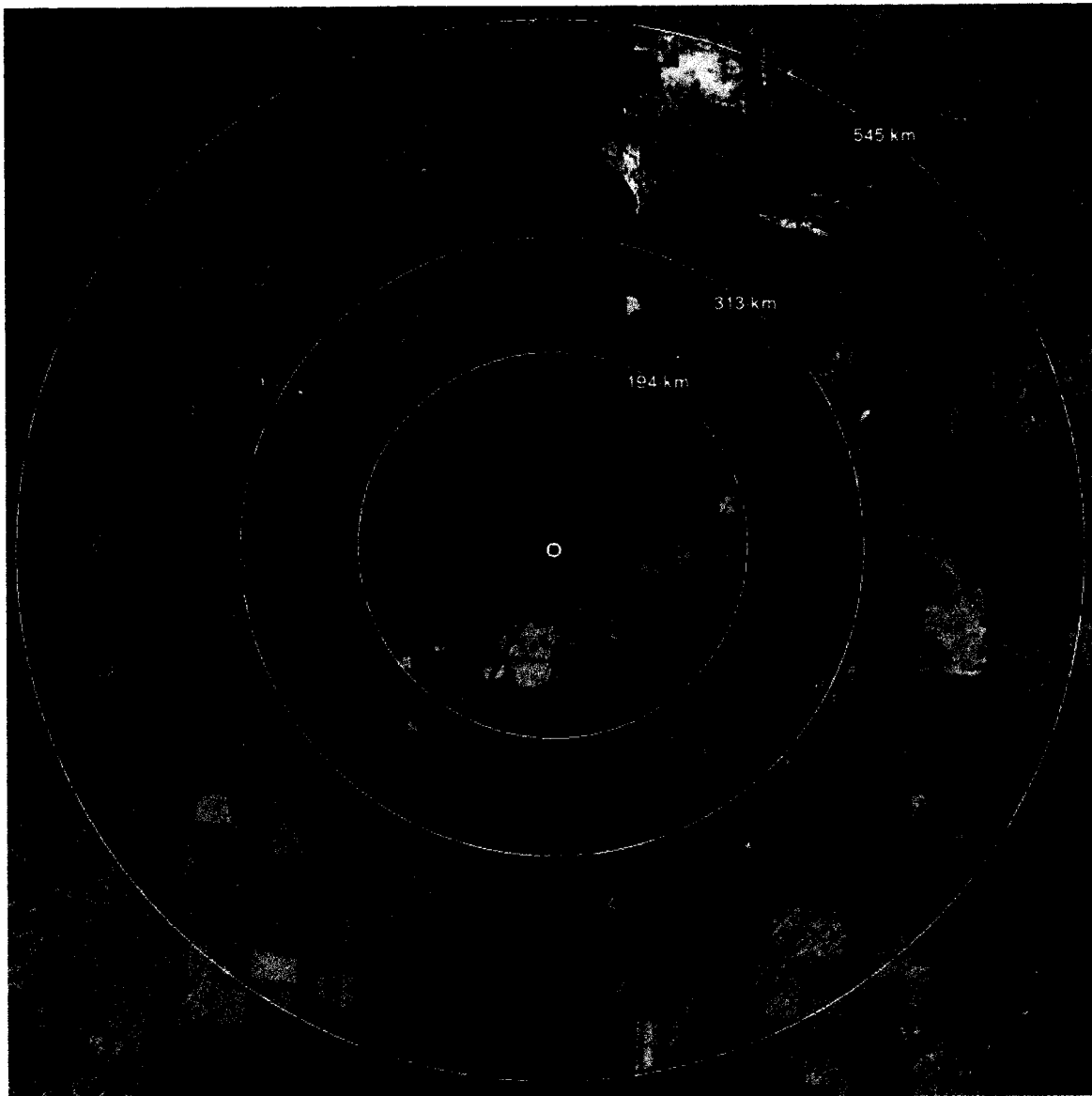


Figure 3.1: Plot of all aircraft position reports recorded by FLOAT-2. Each red mark corresponds to a recorded ADS-B position message. The central white and black marker indicates the position of the balloon at burst, with the white circles giving radius from this position. Image prepared using Google Earth.

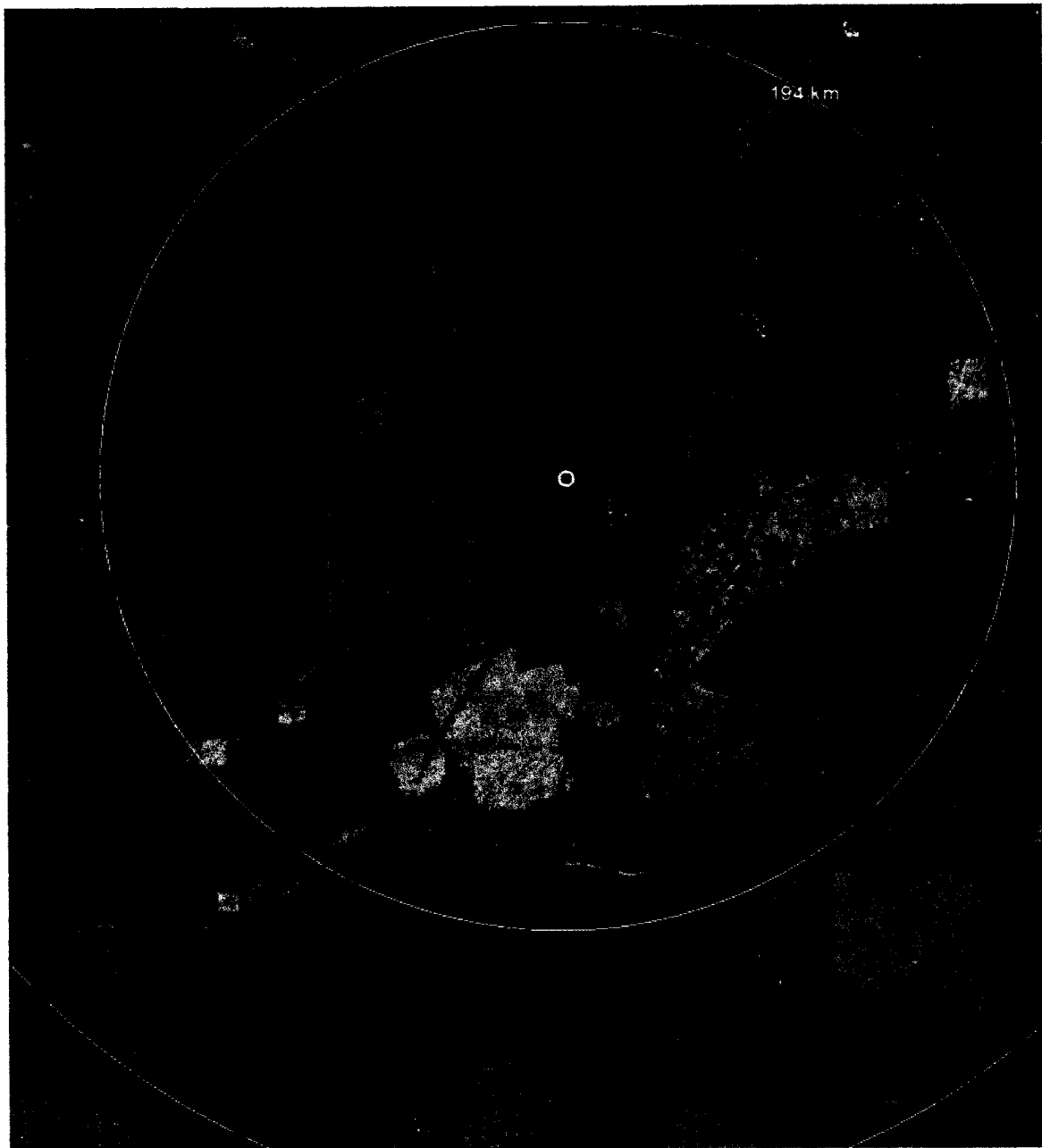


Figure 3.2: Plot of aircraft position reports recorded by FLOAT-2 (detail). Each red mark corresponds to a recorded ADS-B position message. The blue line indicates the path of the balloon-borne sensor. Looping aircraft tracks below and to the right of the balloon path indicate the position of the approach paths to parallel runways at Toronto Pearson airport. Image prepared using Google Earth.

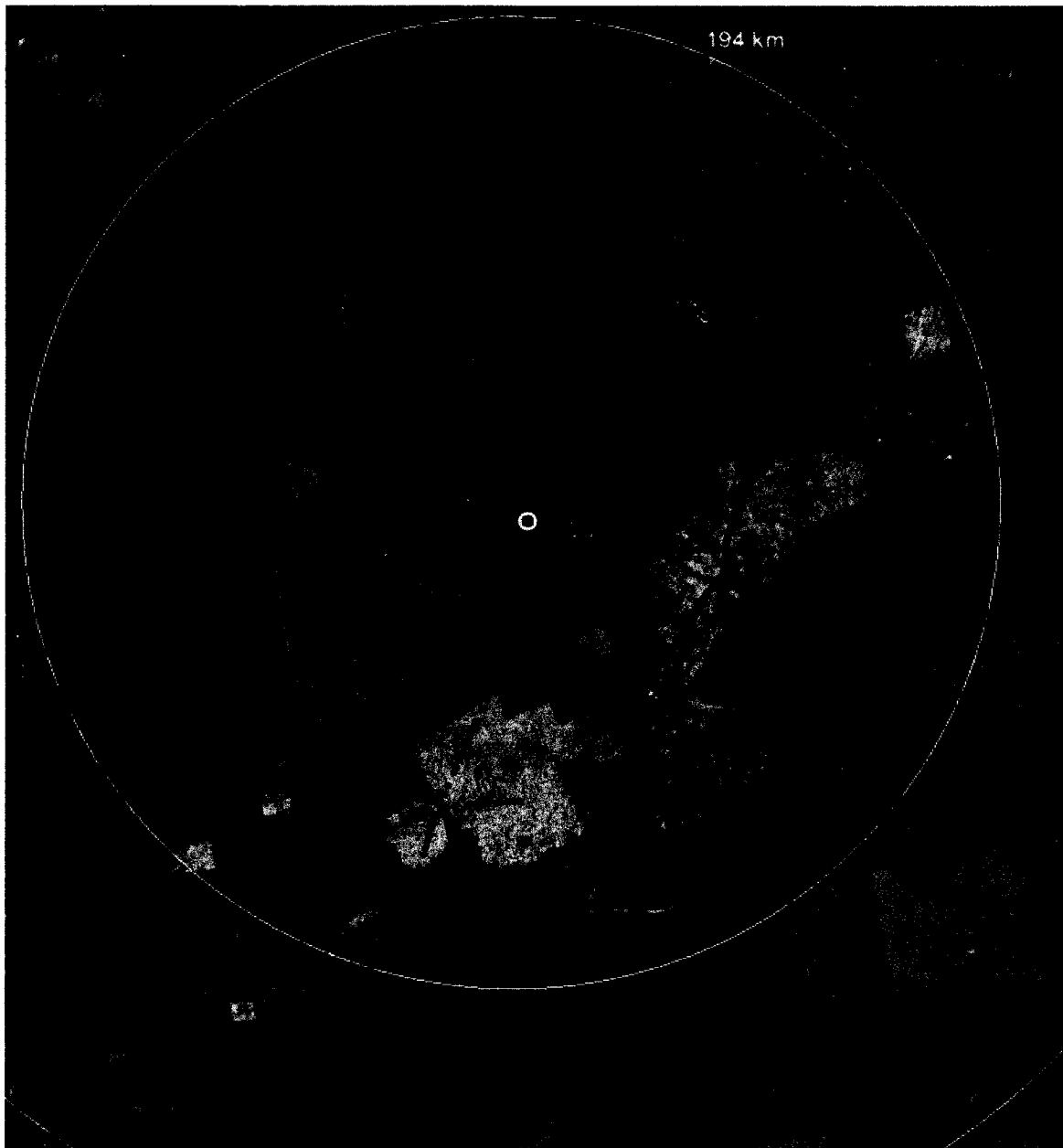


Figure 3.3: Plot of aircraft position reports recorded by FLOAT-2 during the high-altitude segment. Each red mark corresponds to a recorded ADS-B position message. Image prepared using Google Earth.

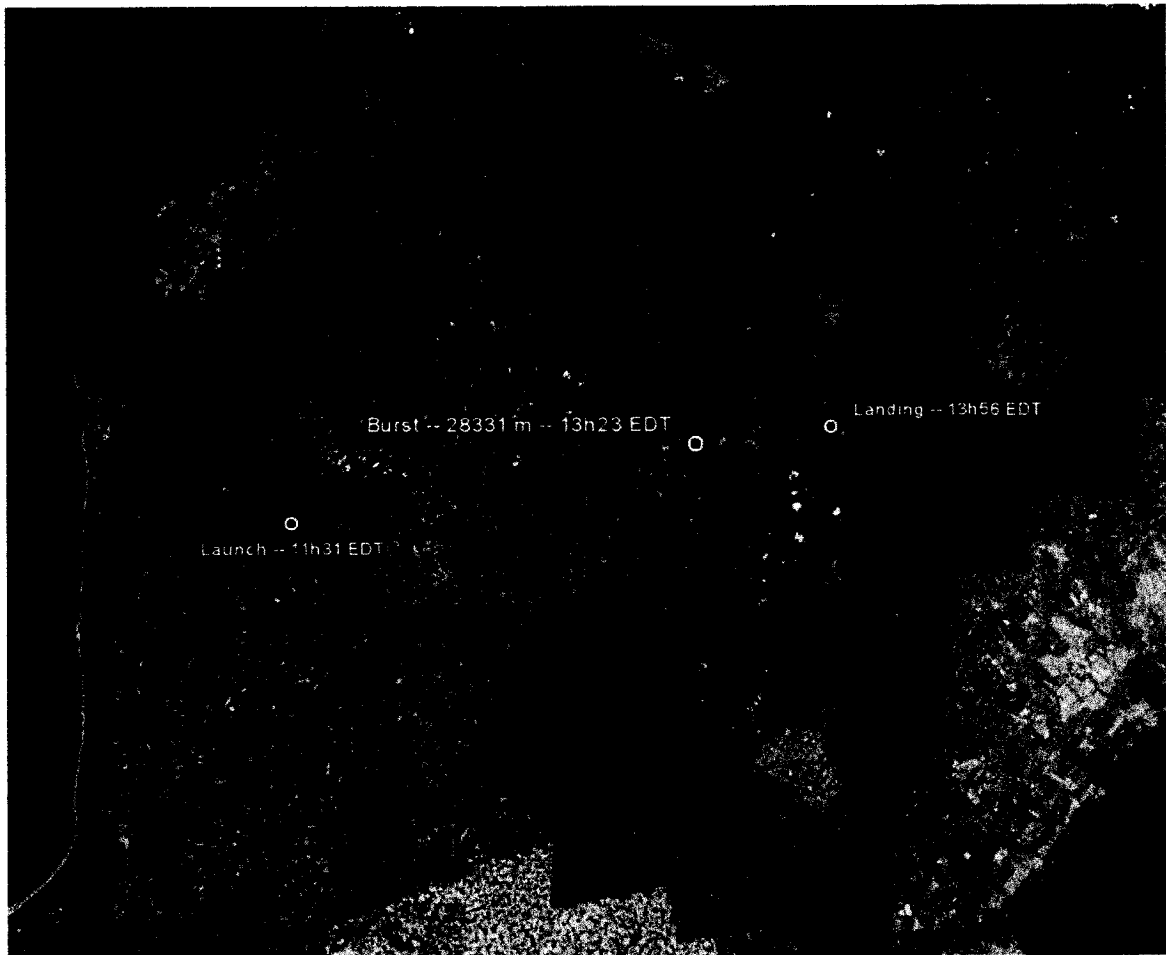


Figure 3.4: Path of the FLOAT-2 balloon payload, indicated by the blue line. The path from the burst point to landing indicates the descent by parachute. Image prepared using Google Earth.

3.4 Detection rate

While a count of the number of messages and aircraft detected by the system is of interest, a key question in rating the performance of an air traffic surveillance system is whether it succeeds in detecting all of the aircraft in its field of view. Complete knowledge of the aircraft population present in a parcel of airspace, and their positions, is essential for ATS to ensure safe separation of all aircraft. An ADS-B sensor such as that carried on FLOAT can only detect aircraft which are transmitting ADS-B messages, so the relevant question for this experiment is whether FLOAT-2 was able to detect all ADS-B-equipped aircraft which were present, and over what area.

Following the experiment, Nav Canada provided data listing all aircraft which operated in the vicinity of the balloon flight (Burrige, pers. comm., 2009). This record includes aircraft surrounding the launch point to a radius of approximately 450 km, called hereafter the test region. Further information provided by Nav Canada (Burrige, pers. comm., 2010) established a list of all aircraft which are registered with Nav Canada as having certified ADS-B equipment on board. Numerous aircraft operate with non-certified ADS-B equipment, which broadcast position messages but are not yet certified and thus can not be used for surveillance. Information was obtained from several airlines which allowed a compilation of aircraft in this group (Maloney, pers. comm., 2010 ; Zargarpur, pers. comm., 2010). This is not a list of all aircraft which transmit ADS-B signals; it includes only those airline fleets for which information is available, gathered from the certification list at Nav Canada, or directly from the airlines for aircraft which are not yet certified. Aircraft with non-certified equipment belonging to operators not surveyed may have been present, but cannot be accounted for. However, the list of equipped aircraft which is available represents the fleets of 18 operators, including airlines from 14 countries, plus Nav Canada's own fleet, for a total of 437 aircraft known to be ADS-B equipped.

Correlation of the list of known-equipped aircraft with the list of aircraft present in the test region during the experiment period allowed the identification of 10 aircraft which were known to be in the vicinity of the detector and transmitting ADS-B data, during the operation period of the experiment. These 10 aircraft are called hereafter the detection candidates, and detection results for them are shown in Figure 3.5. Of the 10 aircraft, three were detected by the ADS-B receiver aboard FLOAT-2. Their positions are marked in Figure 3.5 with yellow points, and the extension of their tracks to the edge of the test region given as a yellow line, constructed from the daily flight record provided by Nav Canada. The aircraft are identified in the figure by their

registration marks: C-FITL, C-FITU, and C-FIUL. The tracks of C-FITL and C-FITU are nearly coincident; based on the Nav Canada record, these aircraft are both on intercontinental flights to Toronto from Europe (Paris and Frankfurt, respectively), giving them similar flight paths. Both aircraft are first tracked by FLOAT-2 at a range close to 200 km, and are subsequently followed to their arrival at Toronto. C-FIUL, meanwhile, is a departure from Toronto to Tokyo on a polar route, which is tracked first on its climb-out from Pearson airport, and followed until 13:50 EDT, when the FLOAT-2 payload is in the final minutes of its descent.

One of the 10 detection candidates entered the test region two minutes before the end of the payload's descent, remaining more than 300 km distant as it approached from the east. The entry position of this aircraft, C-GZWS, is marked with a red point in Figure 3.5. It is consistent with the detection pattern observed thus far to conclude that this aircraft, though ADS-B-equipped, was beyond the detector's range.

The remaining six untracked aircraft in the set of detection candidates were all intercontinental flights from points in Europe to the United States. These tracks are shown as red lines in Figure 3.5. They pass through the northwest portion of the test region, with the closest approach to the balloon track never closer than 240 km, and the actual range to the balloon farther at all times.

Another aircraft on a similar route, from Amsterdam to Houston, is N78013. This aircraft does not have certified ADS-B equipment (Zargapur, pers. comm., 2010), but does carry uncertified equipment (Burridge, pers. comm, 2010). A single message from N78013 was detected; its position is marked in Figure 3.5 with a yellow point. Its position is 261 km from the location of the FLOAT-2 sensor at the time of reception. The flight path of the aircraft is not shown; it is so close to one of the tracks shown in red as to be indiscernible at the scale of the image. This aircraft is one of those detected during the brief operation of the first FLOAT mission as well. In that case, the aircraft flew on a different route, and was detected reliably over a period of ten minutes, with ranges to the balloon varying from approximately 80 to 120 km. This suggests that this aircraft, with its equipment, antenna, and power level, is reliably detectable by the FLOAT instrument, when it is within range.

Of all these flights passing through the northwest edge of the region on similar tracks, only one is detected, and that by only one ADS-B message. A reasonable explanation for their near-complete non-detection by FLOAT-2 is that these flights passed through the region at a short distance beyond the detection range.

Taking the 10 detection candidates together it is possible to conclude that, of all aircraft known to be ADS-B-equipped, every one which passed within approximately

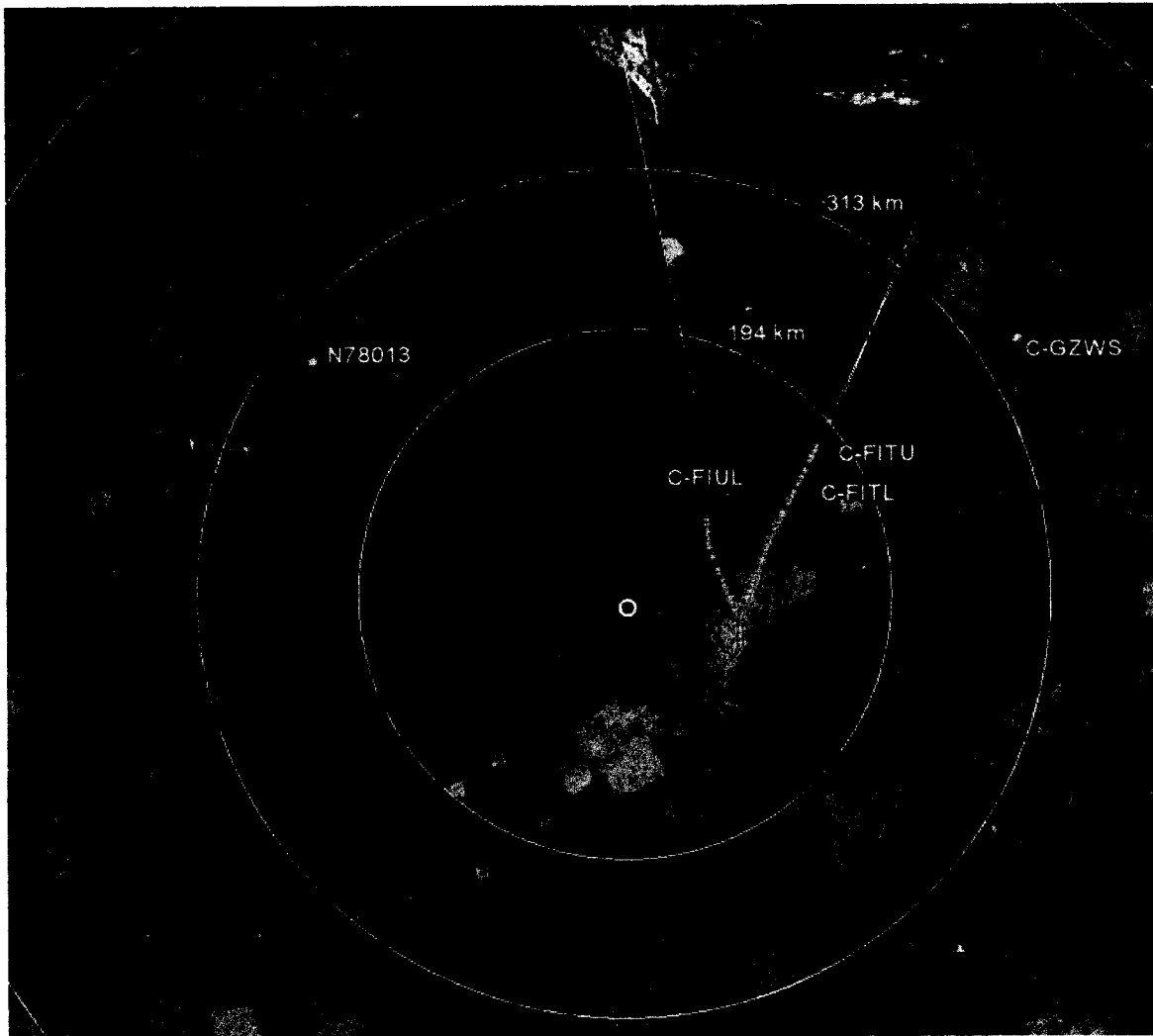


Figure 3.5: Detection results for aircraft with known ADS-B equipment. Aircraft detected are shown in yellow; those not detected are shown in red. Aircraft tracks shown as lines are based on reference data, as is the position of aircraft C-GZWS, shown with a dot because its reference path is too short to plot as a line. Yellow dots indicate the ADS-B-reported positions of aircraft detected by FLOAT-2. The blue line shows the path of the balloon, with the burst point marked with a black and white circle.

200 km of the FLOAT-2 payload was detected. However, this conclusion can not confidently be expanded to the claim that the FLOAT instrument is capable of detecting all ADS-B-equipped aircraft over that range. Firstly, though the success rate is 100%, the set remains small with only 3 aircraft. These three do represent the candidates from a much larger list of 437, but success for three out of three trials cannot be taken as a guarantee of success in general. A larger collection of data would be necessary to extend the appraisal of FLOAT's performance. Secondly, a key variable in the detection range has not been taken into account. The standards for ADS-B allow aircraft to transmit the signals at a range of power levels (DO-260B, 2009) between 75 and 500 Watts. Such a variation in transmitter power will greatly affect the detection range for a given receiver. Accounting for this variation, however, would require knowledge of the transmitter power and antenna characteristics for the particular aircraft observed during the experiment. This information is not currently available, though requests to several aircraft operators are pending. The topic of varying transmitter power will be further discussed in section 4.2.3.1.

Despite these limitations, the performance of FLOAT-2 is promising. In addition to the 3 aircraft which are part of fleets known to be ADS-B-equipped, 38 other aircraft were detected and tracked over horizontal ranges of up to 528 km, with performance decreasing beyond approximately 200 km. Vertical ranges of up to 85,000 ft (25.9 km) were achieved. Further refinement of the determination of FLOAT's performance would require more rich 'ground truth' data; that is, greater knowledge of the actual aircraft population present during the experiment, particularly with regard to ADS-B equipage and transmitter power. Some inferences can nonetheless be made from particular cases observed in the FLOAT-2 results, and these will be explored in the following sections.

3.5 Detection cases of particular interest

3.5.1 Long-range detections

As previously discussed in section 3.3, several detections occur at unusually large ranges of 300 km and more from the detector. Their positions are visible in Figure 3.1 as isolated red points to the southwest, west, and northwest of the central detection cluster.

The bulk of aircraft detected by FLOAT-2 were followed continually along their flight paths, generally disappearing from view at ranges of approximately 200 km,

with some disappearing sooner, and some tracked beyond that range to nearly 300 km. Four aircraft depart from this pattern, and are detected for only a few messages in short succession, at ranges from 299 to 528 km.

These detections all occurred in the first ten minutes of the balloon's ascent, when it was at low altitude. The aircraft are detected at very shallow elevation angles, with the balloon less than one degree above the horizon, as viewed from the transmitting aircraft. Details are presented in Table 3.5.

The elevation angle of the balloon, viewed from the transmitter, is the angle above the horizon at which a signal from the aircraft's ADS-B transmitter must pass to propagate to the balloon by line of sight. This angle is calculated using the altitudes of the aircraft and balloon, the horizontal distance between them, and the curvature of the Earth – the details of this geometry are developed in detail in section 4.3. For the four cases presented in Table 3.5, the line-of-sight path is very close to the horizon, with values mostly near 0.25° , and never exceeding 0.63° . Given the potential for signals passing this close to the horizon to be obstructed or refracted, it is possible that the signals received by FLOAT-2 did not propagate by line of sight.

Were the FLOAT instrument capable of detecting signals from ranges of 300 to 528 km, it would be expected to observe many aircraft within this range, over longer periods, as it did for aircraft at ranges up to approximately 200 km. Such long-distance reception would be expected to improve as the payload rose to higher altitudes, giving it a wider field of view. Instead, for the four long-range cases, messages from the aircraft were received for only a brief time, at low altitude, for a short period of the ascent, giving a small band of aircraft-to-balloon geometries in which signals were detected. It is possible that these short detection windows represent the periods when the propagation geometry was suitable for interception of signals refracted by the Earth's atmosphere.

Even UHF signals such as those of the 1090 MHz ES ADS-B system will be refracted by the atmosphere, for very shallow elevation angles. This effect can be seen at angles of less than one degree in the neutral atmosphere, a phenomenon which will be explored analytically in section 4.4.3.3. For the ionosphere, signals will be refracted back towards the Earth's surface if they are transmitted at angles less than the frequency-dependent critical angle, which for 1090 MHz is 0.47° . This behaviour in ionospheric refraction will be considered in subsequent chapters as the concept of ADS-B surveillance is extended to Earth-orbiting platforms. The relevant techniques, including calculation of the critical angle, are elaborated in section 4.4.3.5, with results given in section 5.3.4.

Table 3.5: Parameters of long-range detections

Aircraft registration	Number of messages received	Range of detection times, local EDT (Balloon launch 11:31)	Balloon altitude metres (feet)	Aircraft altitude metres (feet)	Aircraft horizontal range kilometres	Balloon elevation above horizon, viewed from transmitter
VT-ALL	4	11:32 - 11:34	549 - 1440 (1801 - 4724)	9754 (32000)	299 - 311	0.06 - 0.24°
N648JB	5	11:35 - 11:36	1704 - 2017 (5591 - 6618)	10957 - 10972 (35950 - 36000)	356 - 364	0.27 - 0.32°
N530NK	3	11:38 - 11:41	1394 - 3879 (4573 - 12726)	8725 - 9761 (28625 - 32025)	321 - 352	0.25 - 0.63°
PH-AOL	1	11:40	3747 (12293)	12192 (40000)	528	0.24°

3.5.2 Estimates of the line-of-sight reception range

An inspection of Figure 3.1 shows numerous aircraft tracked by FLOAT-2, with several consistently tracked for some distance before disappearing from view. Two cases in particular are inspected to estimate the range at which this occurs. One, registered N627JB, takes off from an airport inside the detection range, and leaves it on a path nearly radially away from the balloon. The second, registered N706TW, passes briefly through the edge of the detection range on a nearly tangential path.

Eight messages were received from N627JB. Their positions are plotted in Figure 3.6. The first message received reports an altitude of 1750 ft (533 m) ASL, and the aircraft climbs steadily as it moves southward on a heading of 172 degrees. It appears that this aircraft departed from the Buffalo Niagara International Airport (KBUF); the first message was received from a position less than 1 km from the end of the main runway at that airport. As it flies south, it moves farther from the FLOAT-2 balloon. The position of the balloon is shown at the time of the last reception from this aircraft, 12:10 EDT. At this time, the aircraft was 242 km from FLOAT-2, at an altitude of 17150 ft (5227 m) ASL. The balloon itself was somewhat higher, at 40364 ft (12303 m).

The second case of interest is that of N706TW. This aircraft, flying in a nearly straight line, is recorded in eleven messages spanning 8.4 minutes. Its path is shown in Figure 3.7, along with the position of the balloon near the middle of the detection period. The total drift of the balloon during this period was less than 2 km, making the drift indiscernible at this scale.

The aircraft is first detected at a range of 188 km. Its path, nearly tangential to the payload's detection area, approaches as close as 183 km, as the aircraft passes the balloon. The final message is received from a range of 209 km. During the detection period, the aircraft descends from 37950 ft (11567 m) ASL to 33075 ft (10081 m). The balloon rises from 73435 ft (22383 m) ASL to 80078 ft (24408 m) during the same time.

The range limit estimates given by these two aircraft agree, roughly, with the estimate obtained by visual inspection described in section 3.3, where it was concluded that the range lies near 200 km, with some aircraft detected somewhat beyond. The differences in estimated range may be due to several factors, including transmitted power, the variation of transmitter gain across the transmitter antenna pattern, and the variation in straight-line distance, and thus the path loss, that comes with varying altitudes. The effect of these variables on the detectability of ADS-B signals will be explored in detail in subsequent chapters.

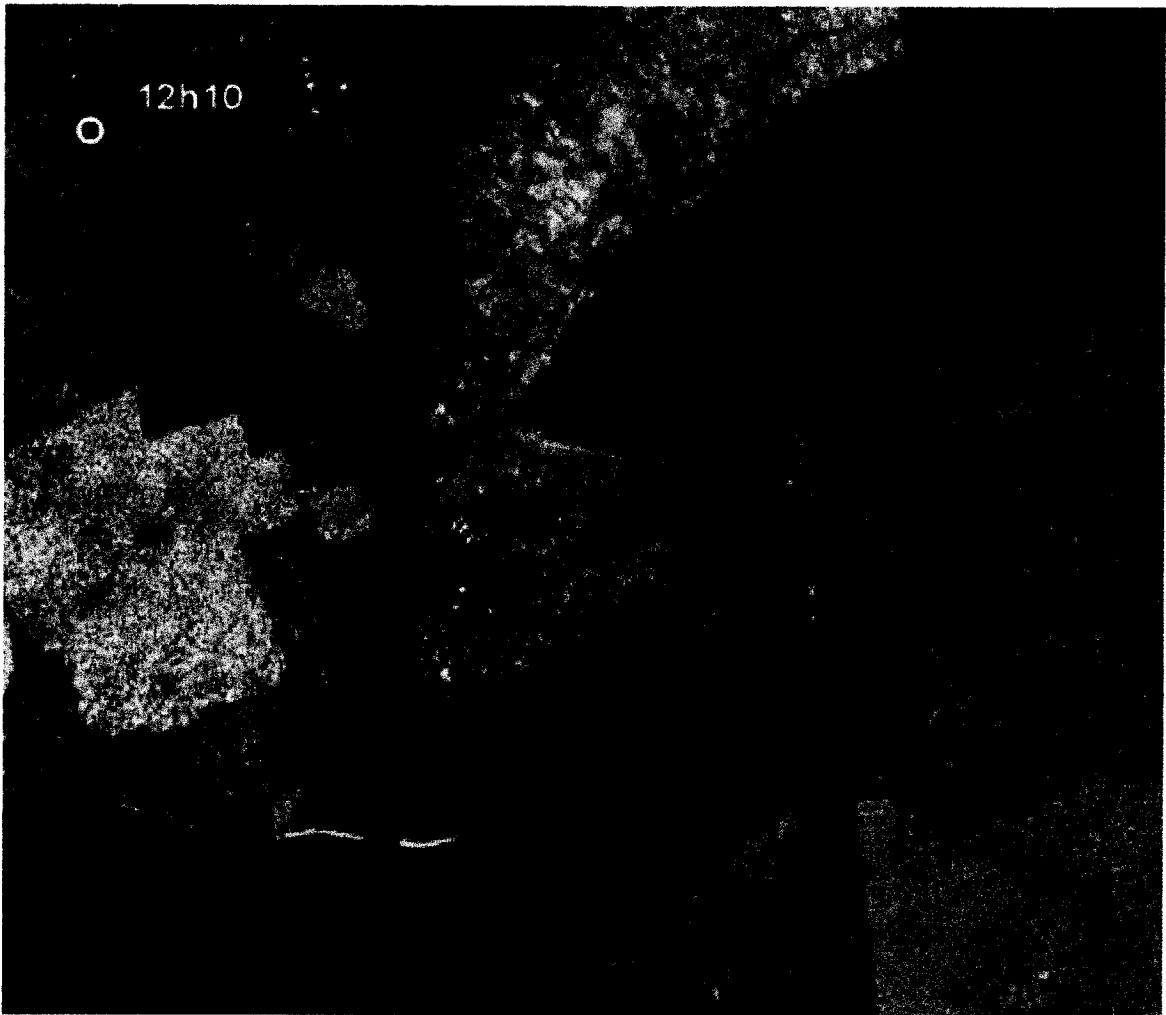


Figure 3.6: Position reports from N627JB. The aircraft position reported in each message is plotted as a red dot. The black and white dot indicates the balloon position at the time the last message was received.

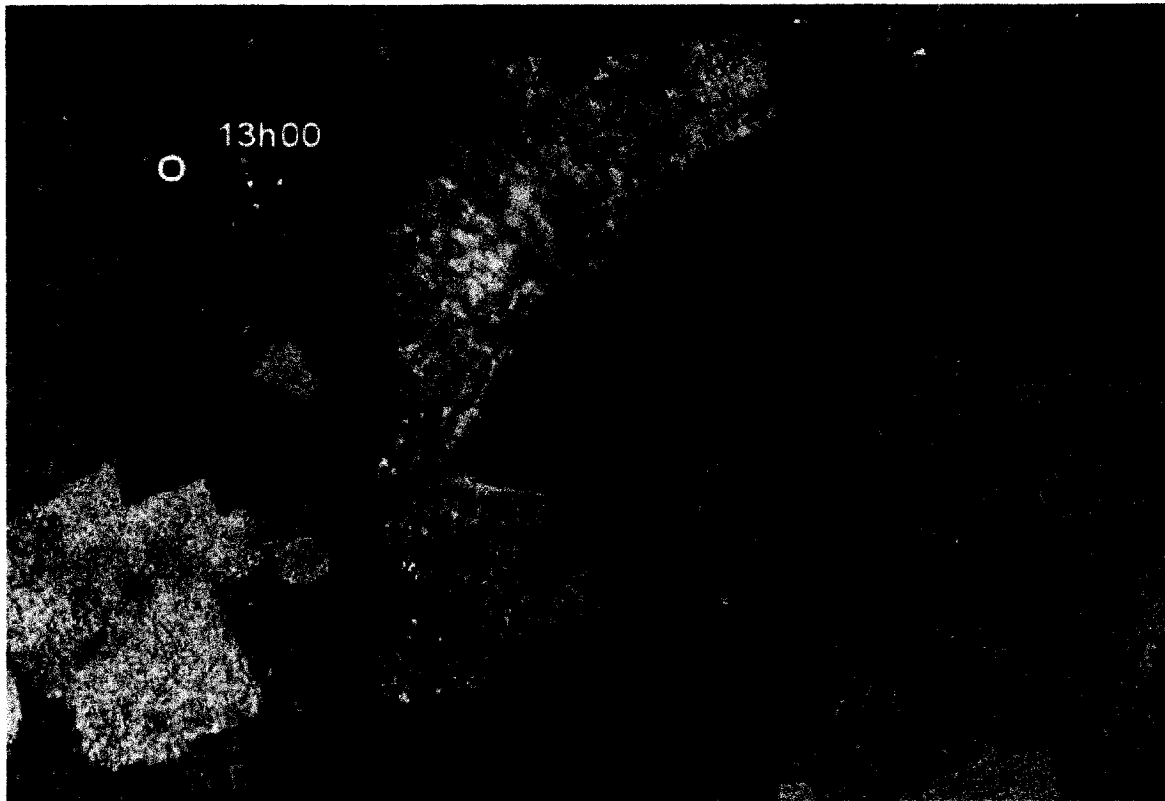


Figure 3.7: Position reports from N706TW. The aircraft position reported in each message is plotted as a red dot. The black and white dot indicates the balloon position at the middle of the detection period for this aircraft.

3.5.3 Estimate of the vertical detection range

Nine aircraft were tracked by FLOAT-2 while they were on the surface at Toronto's Pearson airport. Their positions, shown in Figure 3.8 as red dots, are precise enough to show the movement of aircraft on runways, taxiways, and aprons. The messages from these aircraft are, as might be expected, those which report the lowest altitude in the FLOAT-2 dataset; Pearson has an elevation of 569 ft ASL (GTAA, 2008). These messages were received over nearly the entire flight, from ten minutes after launch to four minutes before landing, with the exception of a 32 minute period surrounding the highest point of the balloon's flight. No signals were detected from the surface at Pearson when the balloon was at an altitude greater than 85,200 ft (25970 m) ASL; during this time the balloon was approximately 80 km northwest of Pearson airport.

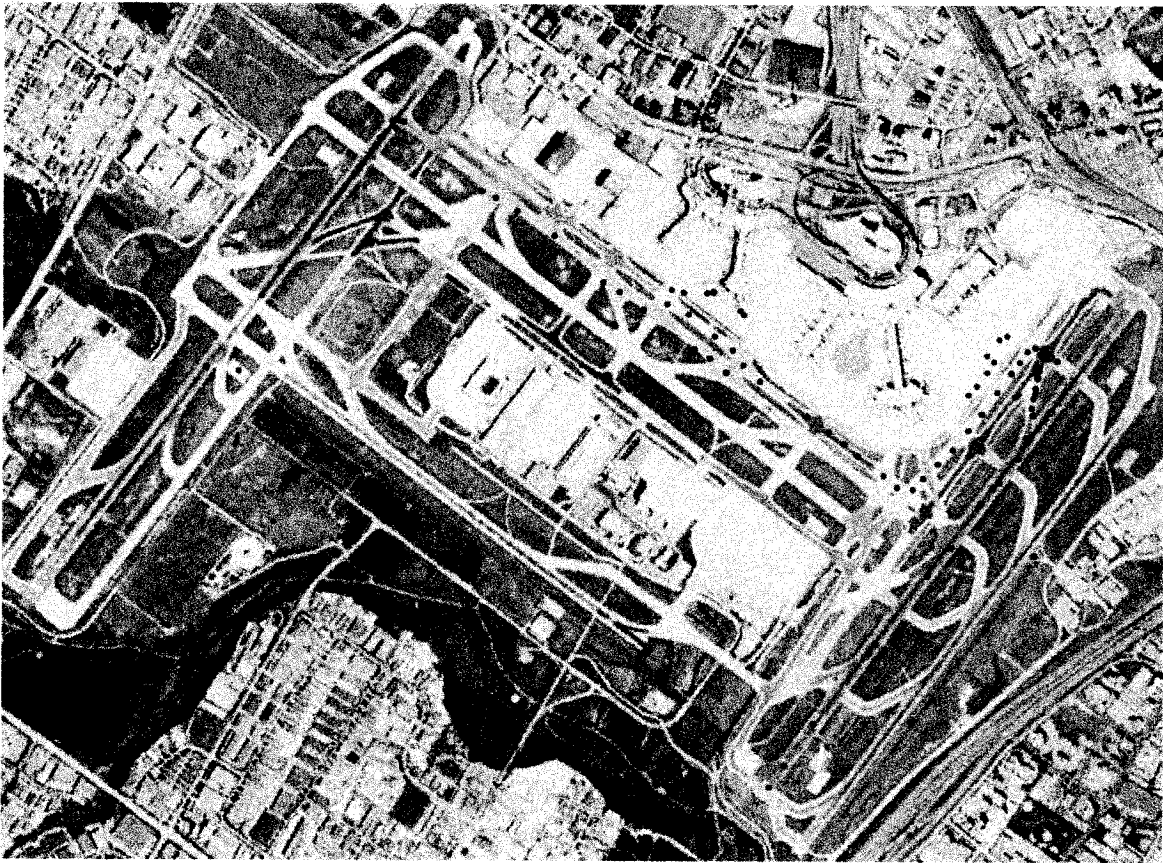


Figure 3.8: Aircraft tracked on the surface at Toronto-Pearson. Each red mark corresponds to an ADS-B position message. Image prepared using Google Earth.

In addition to the increasing distance from these transmitters on the surface, the antenna patterns of both the transmitter and receiver likely play a role in limiting the vertical range. While aircraft were readily detected at horizontal ranges of 100-200

km, they could not be detected when 80 km distant on the surface if the balloon was above 85,200 ft. It appears, then, the range is greatly reduced when the receiver is horizontally near, but at high altitude.

The FLOAT ADS-B payload used a full-wavelength monopole antenna with a vertical axis; such an antenna has a gain null along its axis (Orfanidis, 2008), greatly decreasing the reception from targets near the balloon's nadir. The antennas used for ADS-B transmitters aboard aircraft also have nulls along their vertical axes (DO-260B, 2009). As a result, when the receiver is at a relatively high angle of elevation as viewed from the transmitter, there will be reduced gain at both antennas. This effect, where aircraft are less detectable at nadir and the region of poor reception varies with altitude, has implications for the development of orbital ADS-B sensors, and will be examined in chapters 4 and 5.

3.6 Technical performance of the payload

Following the partial success of the first mission, a rapid test and revision program resulted in minor redesign and improvement of several payload systems. The significantly improved performance of the payload during the FLOAT-2 mission demonstrated the value of those adjustments. On FLOAT-2, the payload operated to a large extent nominally, and returned a very complete dataset. The hardware survived with most components in suitable condition for re-use, and no subsystem experienced a catastrophic failure, with the exception of the loss of the ADS-B antenna in the landing.

Nonetheless, certain behaviour of the on-board systems was unexpected. Three particular cases of the recorded data being more or less extensive than expected are discussed below.

3.6.1 ADS-B Detection without the payload antenna

Following its descent by parachute, the FLOAT-2 payload came to rest in a tree 90 km east of the launch site, where it remained suspended at an elevation of 1663 ft (507 m) ASL until the arrival of the recovery team. GPS and temperature data continued to be recorded, and the onboard computer continued to operate. However, during the landing, the ADS-B antenna was torn from its mount, ending the detection of aircraft, with one exception. Over a 90 second period beginning 3 hours, 2 minutes after the landing, 8 ADS-B messages were recorded from an airliner registered C-GJWS. This

aircraft was on descent towards Pearson airport, and was first detected at a horizontal range of 11.9 km and an altitude of 11425 ft (3482 m) ASL. It continued to descend, approaching as close as 10.4 km to the payload before the final message, at a range of 15.4 km and altitude of 9450 ft (2880 m).

Such reception by excitation of only the antenna stub is highly dependent on the orientation of the payload and the power, gain pattern, and other characteristics of the transmitter. It therefore provides little information about the range or sensitivity of the payload. Nonetheless, it indicates that all the payload's key hardware not only survived the landing, but continued to operate through it, and for hours afterward.

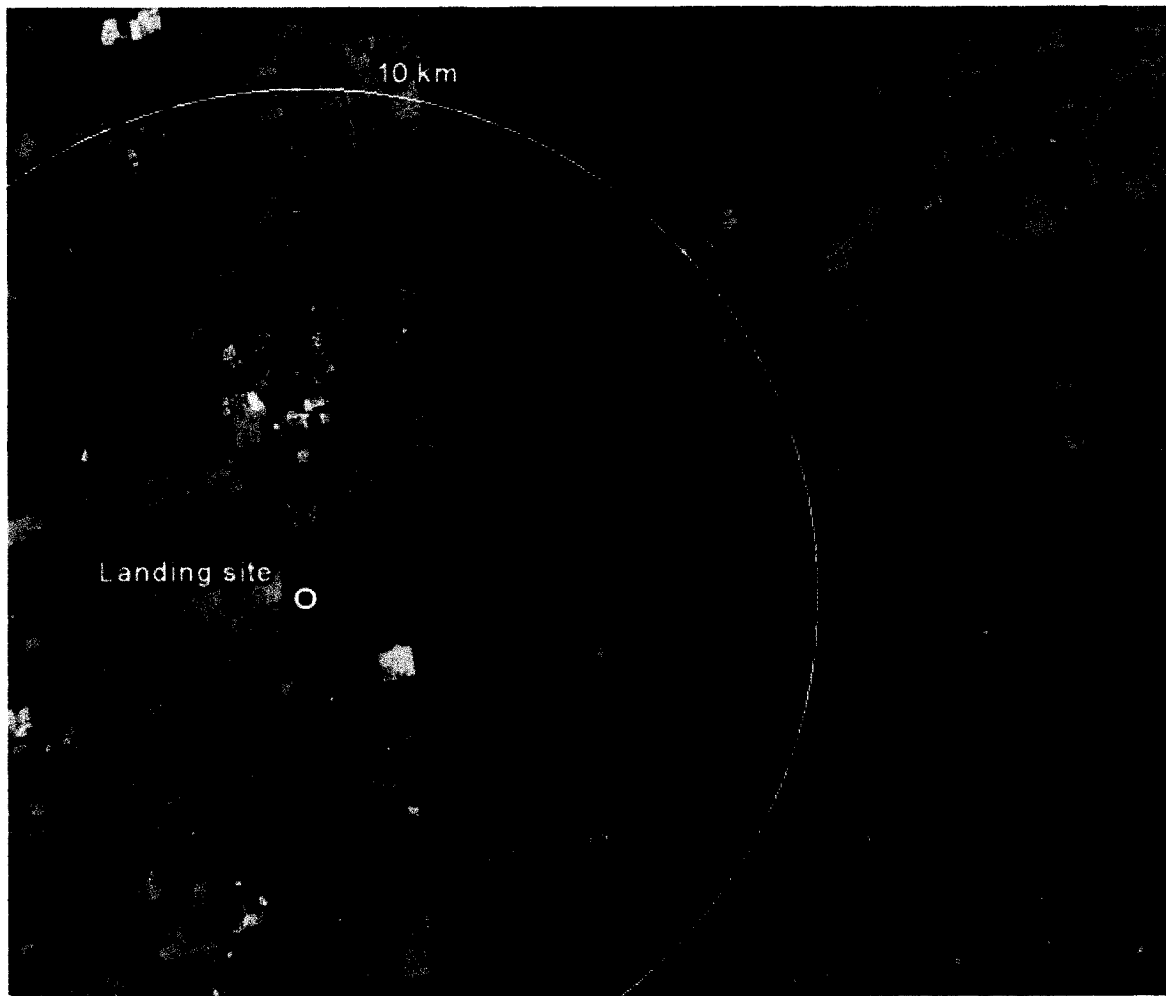


Figure 3.9: Position reports from C-GJWS. The aircraft position reported in each message is plotted as a red dot. Image prepared using Google Earth.

3.6.2 Interruption to ADS-B recording

ADS-B data was recorded continually throughout the flight of FLOAT-2, with the exception of a period of 13.6 minutes during the descent by parachute, during which only two ADS-B messages are recorded. This is a significant reduction compared to the the average of 15.8 ADS-B messages per minute recorded during the remainder of the flight. The gap is not explained by a lack of aircraft in the detection area, since some aircraft are tracked, on the same scheduled flight, both before and after the gap.

FLOAT carried a temperature sensor which continually measured the temperature of the air inside the payload canister and of the air outside. A record of these two temperatures is given for the period surrounding the ADS-B reception gap in Figure 3.10. On the horizontal axis, '0' marks the reception of the last message before the gap, shown as the grey band. The gap ends at 13.6 minutes.

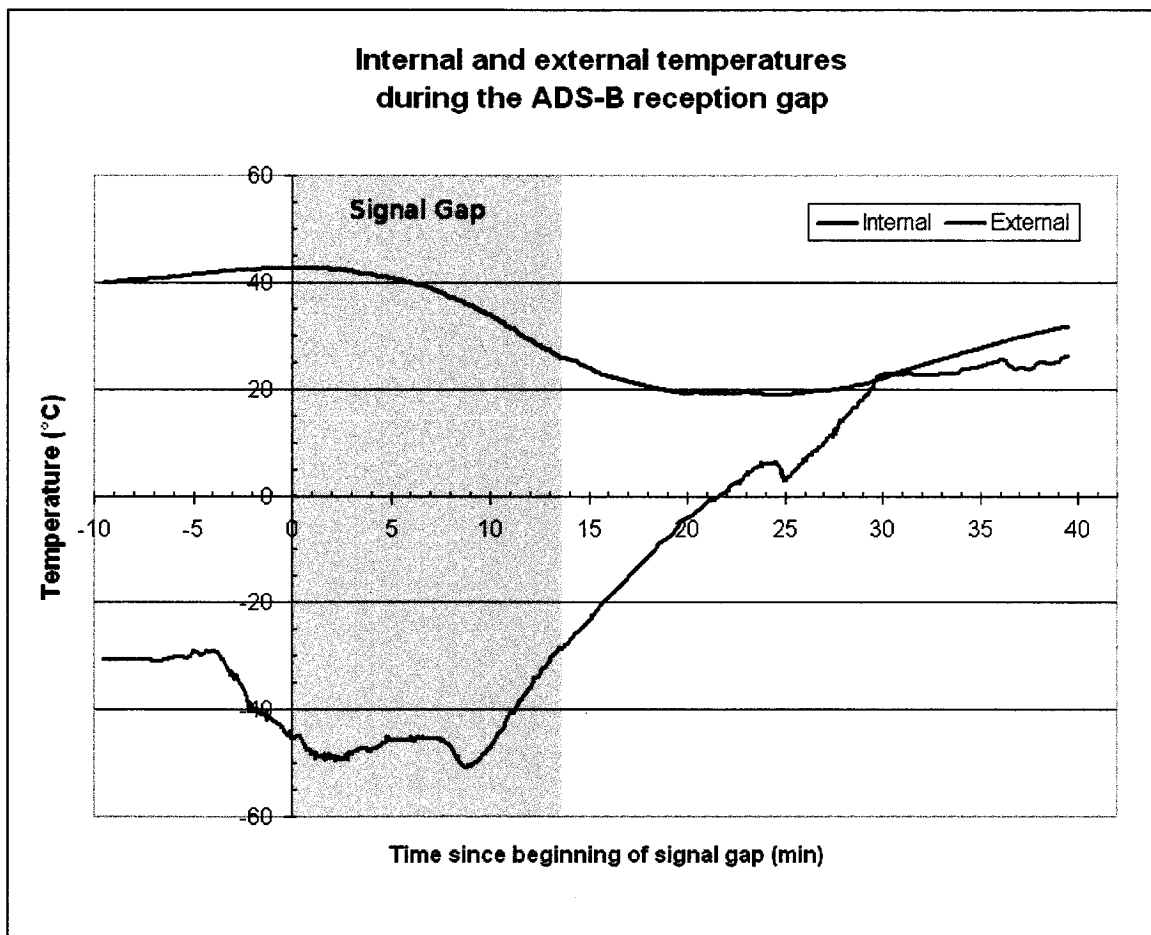


Figure 3.10: Evolution of external and internal temperatures during the ADS-B signal reception gap

During the entire flight, the internal temperature reached 40°C only once. This occurred ten minutes before the ADS-B reception gap begins. The internal temperature sensor hung freely inside the payload canister, measuring the temperature of the air between the payload components. The ADS-B receiver payload was a circuit board inside a metal enclosure surrounded by this air. Its temperature would be expected to lag behind that recorded by the sensor. A possible hypothesis, then, is that the receiver cannot operate reliably at temperatures of 40°C or more. However, following landing, the payload was exposed to external temperatures of 25-27°C, and this combined with continued power dissipation by the internal components caused the internal temperature to gradually rise to a steady value at 69°C. The post-landing detection of C-GJWS described in section 3.6.1, in which the payload successfully recorded several messages in short succession, occurred with an internal temperature of 66.5°C, indicating that the payload was able to operate at temperatures more than 20°C higher than those experienced during the signal gap. This casts doubt on the hypothesis of a limiting operation temperature for the ADS-B receiver.

An second hypothesis relates to the external air temperature. Four minutes before the beginning of the signal gap, the external temperature begins to fall rapidly from -29.3°C to its lowest point during the flight, -50.9°C. The signal gap begins at a temperature of -45.5°C, and normal operation does not resume until 13.6 minutes later, when the external temperature has risen to -28.3°C. A second hypothesis, then, is that the payload does not detect ADS-B signals reliably when the external temperature is very low. Although sustained temperatures of -44°C had been experienced earlier in the flight, the signal gap coincides with the coldest temperatures, and the first time temperatures colder than -47°C were sustained for longer than 60 seconds.

A possible mechanism to relate the external temperature to the performance of the ADS-B receiver is the design of the ADS-B antenna. This antenna was provided with the commercial ADS-B receiver carried aboard FLOAT, and takes the form of a full-wavelength monopole which is connected to the antenna mount by a threaded plastic fastener which butts the end of the antenna against the end of the antenna lead. No soldering or other fixed joint is used besides this slight compression contact. It is possible that, in very cold temperatures, the thermal contraction of the antenna and lead causes those two elements to lose contact with each other at this butt joint. In that event, the conduction of received signals from the antenna to the lead could become unreliable, though perhaps not consistently or completely interrupted, particularly as the components begin to warm. Such behaviour of the antenna becoming isolated from the lead in cold temperatures could explain the observed signal gap. Al-

though the post-landing reception of signals from C-GJWS establishes the possibility of receiving ADS-B data in the complete absence of the antenna, this was only possible at very short ranges on the order of 10-15 km, a condition not observed during the signal gap.

Poor connectivity of the ADS-B antenna caused by contraction in cold temperatures is therefore the suspected cause of the reception gap. This hypothesis is subject to further analysis.

3.6.3 Interruptions to temperature recording

The temperature sensor used in the analysis of the ADS-B signal gap was intended to record both internal and external temperatures continually throughout the flight. It was programmed to record both temperatures and the time, in the event that either reading changed by more than 0.5°C. In general, this sensor behaved as expected and provided frequent temperature recordings. However, two interruptions were observed in the recording of the temperature data. These occurred once on the ascent, at altitudes of approximately 7500 - 8700 m, and once on the descent, at altitudes of approximately 6100 - 4200 m. In both cases, the interruptions were approximately 3 minutes in duration.

On the ascent, the last temperature recorded before the gap was -9.6°C, with recording resuming 3 minutes, 11 seconds later at -20.0°C. On the descent, a similar event is observed: the temperature is recorded continually until -20.3°C, after which no record is made for 2 minutes, 46 seconds, followed by a resumption at -9.8°C. Inspection of the abbreviated data set from the first flight of the FLOAT payload revealed a third similar event: temperatures of -10°C to -19.9°C are not recorded, with the recording halted for a similar length of time.

The temperature lapse rate observed across this gap, 10°C across 1000 - 1900 metres, is consistent with that observed during the adjacent portions of the flight, suggesting that no sudden change in temperature occurred during the gaps to affect the recording. A possible explanation is a flaw in the implementation of the sensor, perhaps in the temperature logging function used, prevented data recording on the temperature range of -10°C to -19.9°C. The gap in recording does not appear to have affected the integrity of data from the rest of the flight, nor was there an adverse affect on the primary science data, the ADS-B messages. The behaviour of this sensor is nonetheless a candidate for further investigation.

Chapter 4

Orbital Detection of ADS-B Signals: Methodology

4.1 Introduction

In this chapter, a method is described to analyze the propagation of ADS-B signals from their transmission by an aircraft to a satellite receiver in Earth orbit. Necessary functional and regulatory background on the nature of the ADS-B signal to be detected is first laid out, in section 4.2. A model of signal detection from an orbital platform is then developed. First, the geometry of the problem is described, in section 4.3. Then, in section 4.4, the propagation of the electromagnetic waves carrying the ADS-B signal is modeled, and a link budget calculated. The result is an expression for the gain margin in the link, leaving out the gain or losses at the receiver. This allows estimation of the net gain needed at the receiver to reliably detect the signals, so that decisions can be made about the feasibility of the system and the necessary characteristics of the receiving antenna. An example of the sizing of such an antenna is given.

Following this discussion of signal strength, other factors which can affect the ability to detect the ADS-B signals are investigated. This begins with an analysis of the implications of the Doppler effect on the transmitted signal, given in section 4.5.

Lastly, in section 4.6, an analysis is carried out of the potential overload of traffic on the channel due to the abundance of aircraft in view from an orbital platform. The probability of unintelligible overlapping signals – signal collisions – is derived, and a function to allow key parameters of a surveillance system affected by these collisions to be designed and characterized is developed.

The results of the analysis described in this chapter are given in chapter 5.

4.2 Background

4.2.1 1090 MHz Extended Squitter

ADS-B surveillance information can be carried by any of several datalink technologies. In all cases, the same navigation and identification information is transmitted between aircraft and ground facilities, but each datalink technology uses a different set of frequencies, modulations, message formats, and other parameters relating to the radio broadcast and reception of the messages. The three datalink technologies in current use are the 1090 MHz Extended Squitter (ES), the Universal Access Transceiver (UAT), and VHF Data Link Mode 4 (VDL Mode 4).

Nav Canada's implementation of ADS-B surveillance in Canadian airspace uses the 1090 MHz ES as the datalink technology (Nav Canada, 2008). This same system is being adopted by EUROCONTROL (PSC ADS-B-NRA, 2008) and the FAA (FAA, 2003), the latter of which is implementing it for airlines and high performance aircraft, with UAT used for general aviation flights.

4.2.2 Signal modulation and message format

The 1090 MHz ES uses a 1 megabit per second (Mbps) signal encoded with binary Pulse Position Modulation (PPM) (EUROCONTROL, 2007), and is an extension of the Mode S transponder system. The message preamble contains a timing signal to allow the pulse positions to be synchronized. In the data block itself, each bit is represented by a $1 \mu\text{s}$ period. A signal pulse in the first half of a bit-period indicates a bit with value 1, in the second half, 0. This message format is diagrammed in Figure 4.1.

Each message contains either 56 or 112 bits of information, with various sub-components as shown in Figure 4.2. The 56-bit message is used only for response to interrogations by Air Traffic Control Radar Beacon System (ATCRBS) facilities, which form part of the Mode S transponder infrastructure over which the 1090 MHz ES datalink system operates. The greater length of the 112-bit messages give the 1090 MHz *Extended Squitter* system its name. These longer messages contain ADS-B data encoded in their message field, with prescribed encoding as defined in the reference document DO-260B (2009).

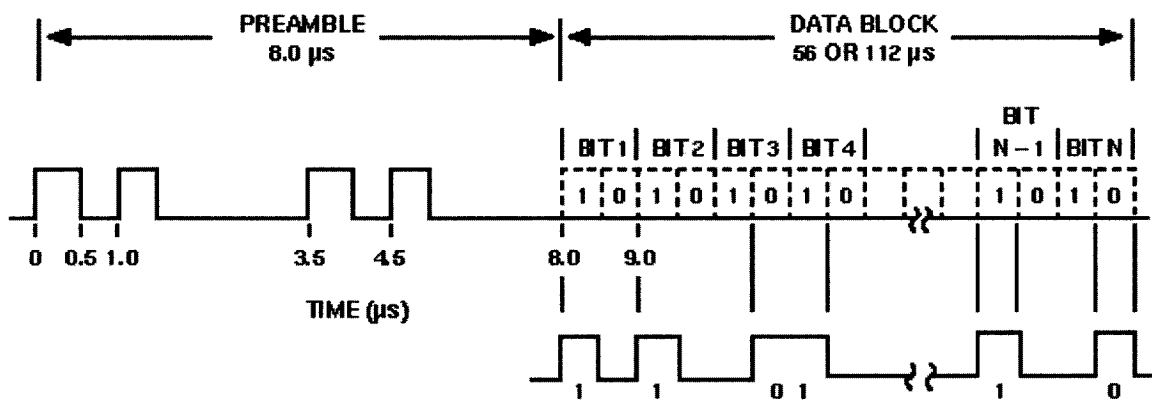


Figure 4.1: 1090 MHz ES message format. Image from Orlando (2001).

SURVEILLANCE INTERROGATION AND REPLY

FORMAT NO. (5 Bits)	SURV. & COMM. CONTROL (27 BITS)	ADDRESS/PARITY (24 BITS)	56 BITS

SURVEILLANCE/COMMUNICATION INTERROGATION AND REPLY - COMM-A AND COMM-B

FORMAT NO. (5 Bits)	SURV. & COMM. CONTROL (27 BITS)	MESSAGE FIELD (56 BITS)	ADDRESS/PARITY (24 BITS)	112 BITS

COMMUNICATION INTERROGATION AND REPLY - EXTENDED LENGTH MESSAGE (ELM)

FORMAT NO. (2 Bits)	COMM. CONTROL (6 BITS)	MESSAGE FIELD (80 BITS)	ADDRESS/PARITY (24 BITS)	112 BITS

Figure 4.2: 1090 MHz ES data block allocations. Image from Orlando (2001).

4.2.3 Transmission characteristics

The reference document for the 1090 MHz ES is DO-260B (2009), the *Minimum Operational Performance Standards for 1090 MHz Extended Squitter Automatic Dependent Surveillance – Broadcast (ADS-B) and Traffic Information Services – Broadcast (TIS-B)*. This document is published by RTCA, Inc., and is equivalent to standard ED-102A, published by the European Organization for Civil Aviation Equipment (EUROCAE) (EUROCONTROL, 2007). It sets out several requirements, with key aspects described below. References to section numbers are to DO-260B (2009), except where explicitly stated otherwise.

4.2.3.1 Transmitted power

Required transmitter power for the ADS-B signal varies with the aircraft or vehicle category. For the lowest classes, a minimum transmission power of 70 W is specified. For larger aircraft, a minimum power of 125 W or 200 W is specified (§2.1.12.1). The maximum output power for all classes is set at 500 W (§2.2.2.10.3).

Additional details are specified for each aircraft equipage category. In particular, the 70 W minimum transmission power only applies to ground vehicles, fixed obstacles, and aircraft in the A0 and B0 categories (§2.1.12.1). However, aircraft in these categories which are capable of operating at altitudes greater than 15000 feet (4570 m) above sea level, or with cruising speeds above 175 knots (324 km/h), are required to abide by the 125 W requirement (§2.2.2.10.1). This requirement effectively precludes large airliners and transoceanic flights from transmitting with power lower than 125 W.

4.2.3.2 Transmission frequency

The frequency is specified as 1090 ± 1 MHz (§2.2.2.1).

4.2.3.3 Timing of messages

The ADS-B message protocol includes several different specific messages (called squitters) that are transmitted at various intervals. Each contains the unique identification code of the aircraft assigned by ICAO or the national regulatory authority, as well as additional information that varies between message types. These messages are transmitted periodically, with the length of the period varying by message type. The transmission rates are summarized at §2.2.3.3.1.2 of DO-260B (2009), and are given in detail in DO-181D (2008) at §2.2.23.1.3.

For each message type, the message period varies randomly within a defined range. For example, the airborne position squitter is broadcast on a period which ranges randomly between 0.4 and 0.6 seconds. The randomization function assures even distribution over that period, with a time quantization no greater than 15 milliseconds. Effectively, this means that each airborne position squitter is transmitted 0.5 ± 0.1 sec after the preceding one, and that the average rate is once every 0.5 seconds. The purpose of this randomization is to prevent aircraft from having synchronized transmissions on the same frequency, and thus obscuring each other's transmissions.

Each squitter type has a transmission rate defined in this way, with a range of transmission interval and random variance within that range. The values vary by squitter type, and values for the key message types are given in table 4.1. The full list of values can be found in §2.2.3.3.1.2 of DO-260B (2009).

Table 4.1: ADS-B message broadcast rates by message type

ADS-B Message (Squitter type)	Interval between messages (seconds)		
	On the ground, not moving	On the ground, moving	Airborne
Airborne Position	N/A	N/A	0.4 – 0.6
Surface Position	4.8 – 5.2	0.4 – 0.6	N/A
Aircraft Identification and Category	9.8 – 10.2	4.8 – 5.2	4.8 – 5.2
Airborne Velocity	N/A	N/A	0.4 – 0.6

Most messages are transmitted routinely, but certain events aboard the aircraft or changes in the aircraft's state can trigger the transmission, for a period following the event, of an 'event-driven squitter' (DO-181D, 2008, §2.2.23.1.3). This can result in up to 2 additional messages per second (DO-260B, 2009, §2.2.3.3.1.2) being broadcast in addition to the routine messages being transmitted at the rates listed in table 4.1. However, in no case will the total rate of transmissions exceed 6.2 messages per second (DO-181D, 2008, §2.2.23.4), (DO-260B, 2009, Appendix R).

4.2.3.4 Transmitter antenna characteristics

The characteristics of the ADS-B transmitter antenna on the aircraft are described at §2.2.13.1. The antenna is required to closely emulate a quarter-wave monopole antenna for the operating frequency. Specifically, the antenna gain must not fall below a level 3 dB lower than that of the monopole, over 90% of the elevation range between 5° and 30° above the horizontal, in the complete range of azimuth. The performance of the antenna at 0° elevation, as installed on the aircraft, is compared to its performance on a ground plane, and must be no more than 1 dB lower within 45° of azimuth of aircraft forward, and 3 dB lower over the remainder of its azimuth range (§3.3.4.1.1). These requirements must be met for aircraft with higher-power transmitting requirements; aircraft with the 75 W transmission requirement must be equipped with antennas whose gain performance is at least that of a quarter-wave monopole (§3.3.1).

At §3.3.4 it is noted that, as expected of a monopole antenna, areas of reduced gain exist directly above (or below) the antenna.

Antennas are mounted so as to minimize obstruction in the horizontal plane due to airframe structures such as the vertical stabilizer and engine nacelles (§3.3.3), as well as interference from other transmitters (§3.3.3.1), or from aircraft manoeuvring under normal flight operations (§3.3.4.5.3).

4.2.3.5 Polarization

ADS-B signals are emitted as vertically polarized, as required at §2.2.13.5.

4.2.3.6 Transmitting diversity

Some ADS-B equipped aircraft implement a mode called “transmitting diversity”. In this mode, two antennas are used to transmit, installed on the top and bottom of the aircraft (§2.2.13.6). In this case, messages are transmitted alternately from the two antennas (§2.2.13.6.1). Diversity mode is required (in transmission) for the A1, A2, A3, and B1 equipage classes (§3.3.1).

4.2.3.7 Reception range

For equipment which complies with the standard set (in DO-260B (2009)) for ADS-B equipment installed aboard aircraft, ranges for reliable reception are specified at §3.3.4. These are specified according to equipage class, and range from 10 NM (18.52

km) for class A0, to 90-120 NM for class A3. These are specified for the aircraft-forward direction, with side and aft directions allowed to have reception ranges half and one third as far as specified. Additional details on practical range are given at appendix E to DO-260B (2009)

These distances are nominal for reception by other aircraft using standard-compliant equipment. It is possible to receive them at greater distances using more capable receivers (appendix D, §D.2.3.1.2).

Techniques to improve reception in cases of noise, interference, or other radio traffic are discussed in appendix I to DO-260B (2009). Techniques for extending the reception range are discussed at appendix M to the same document.

4.2.3.8 Transmission criteria

An ADS-B system becomes operational as soon as electrical power is supplied to the aircraft on the ground (§4.1.1). It begins transmitting position and navigation information as soon as its data inputs indicate a state of taxiing, or a state of the on-board mechanical systems indicating an imminent operational condition (such as simultaneous release of brakes and change in engine oil pressure while the doors are closed). The case is envisaged where regulations will require crew action to commence transmission on the ground. However, in general the system transmits the required messages without intervention from the crew (§4.2.2). An equipment manufacturer may optionally implement a feature which gives the crew the ability to disable ADS-B transmissions (§4.4.5).

4.2.3.9 Other information

Extensive details regarding the data content and encoding, transmitter and receiver operation, data handling, and other parameters are laid out in DO-260B (2009) §2.2.

4.3 Orbital geometry

To model the detection of ADS-B signals from orbital platforms, the case is considered of a receiver aboard an Earth-orbiting satellite at a known altitude above the Earth's surface, A_{Sat} . Also known is the horizontal range to the aircraft, which is expressed as the distance along the Earth's surface from the sub-satellite point. This distance, L , forms an arc of a great circle. The Earth is assumed to be a sphere of radius $R_{\oplus} = 6378\text{km}$. The aircraft is taken to be flying at an altitude above the spherical Earth at an altitude of A_{Air} . This geometry is shown in figure 4.3.

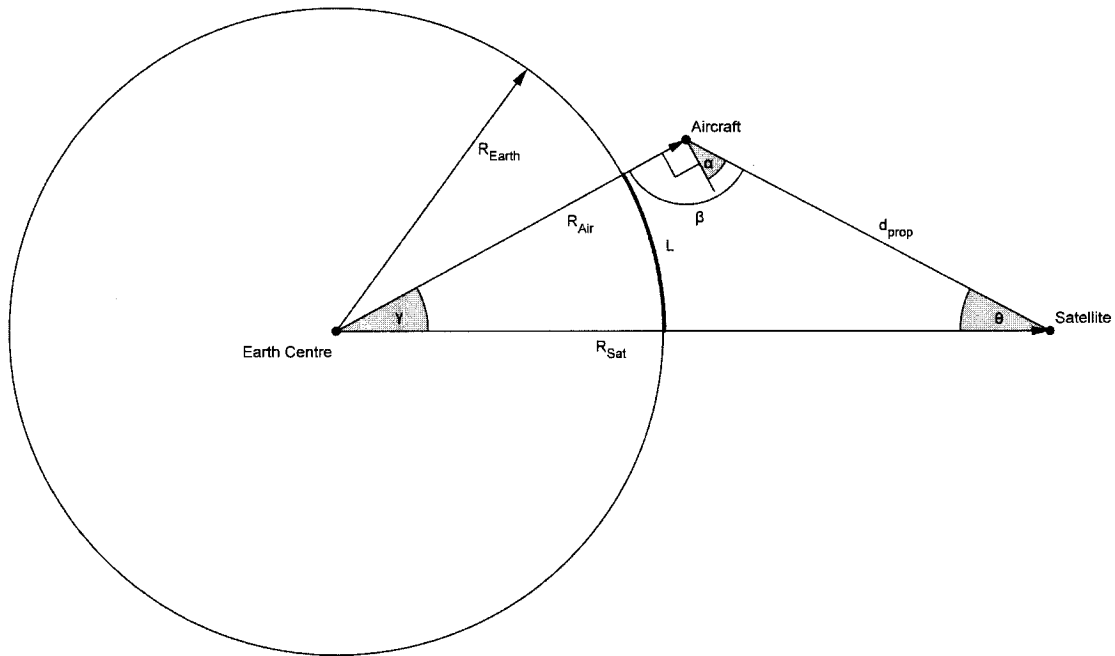


Figure 4.3: Orbital geometry

As shown in figure 4.3, γ is the angle between the satellite and the aircraft, viewed from the centre of the Earth. θ is the angle to the aircraft from nadir, as viewed from the satellite. α is the elevation angle of the satellite, as viewed from the aircraft.

Using L and R_{\oplus} , it is possible to calculate γ (in radians):

$$\gamma = \frac{L}{R_{\oplus}} \quad (4.1)$$

The radius from the Earth's centre is calculated by adding the altitude to the radius of the Earth, for both the aircraft and the satellite:

$$\begin{aligned} R_{Sat} &= A_{Sat} + R_{\oplus} \\ R_{Air} &= A_{Air} + R_{\oplus} \end{aligned} \quad (4.2)$$

The propagation distance of the signal is the distance from the aircraft to the satellite, d_{prop} . This is calculated using the law of cosines:

$$d_{prop} = \sqrt{R_{Sat}^2 + R_{Air}^2 - 2R_{Sat}R_{Air}\cos(\gamma)} \quad (4.3)$$

Knowing d_{prop} , γ , and R_{Air} , it is possible to calculate θ using the law of sines:

$$\theta = \arcsin\left(R_{Air} \frac{\sin(\gamma)}{d_{prop}}\right) \quad (4.4)$$

With θ and γ known, the angle β can be calculated by subtraction, since these three angles form a triangle whose angles must sum to π radians (180°):

$$\beta = \pi - \gamma - \theta \quad (4.5)$$

Since α is an angle above horizontal (at the aircraft, referenced to the Earth's surface), it can be found by subtracting a right angle from β :

$$\alpha = \beta - \frac{\pi}{2} \quad (4.6)$$

4.4 Link Budget

An aircraft-to-space link budget is next calculated, accounting for the transmitter characteristics, the propagation path, and the atmospheric effects encountered by the signal. The result is a signal power level for any position of an aircraft and satellite, which is used to determine the receiver-side gain needed to reliably receive the signal. The receiver characteristics are not considered; line losses, receiver noise, and receive antenna polarization mismatching will all affect the signal, and would need to be counteracted by increasing the gain at the receiver antenna. This analysis only addresses the physics of the propagation and aims to determine the feasibility of detecting the signals; the details of receiver design are left to follow-on work if the scenario is determined to be feasible. For this reason, the link budget determined is presented with the final result of a *net gain* needed at the receiver, including gain from the antenna and losses from other elements and receiver-specific effects. Similarly, the

discussion of received power refers to power available at the orbital position – that power level which is incident upon the antenna, not inside the circuits of any receiver which might be designed and employed there.

4.4.1 Gain of the ADS-B antenna

Following from the requirements described in section 4.2.3.4, the ADS-B antenna aboard the aircraft is modeled as a quarter-wavelength monopole at 1090 MHz, where the wavelength is 0.275 m. In the far field, this monopole is taken to have the same radiation pattern as its equivalent half-wavelength dipole (Orfanidis, 2008). The radiation pattern can be found using the following relation (Orfanidis, 2008):

$$g_t(\phi) = \frac{\cos^2(0.5\pi \cos(\phi))}{\sin^2(\phi)} \quad (4.7)$$

Seen from the side, this radiation pattern is as shown in Figure 4.4. This pattern is symmetrical in azimuth, about the antenna axis.

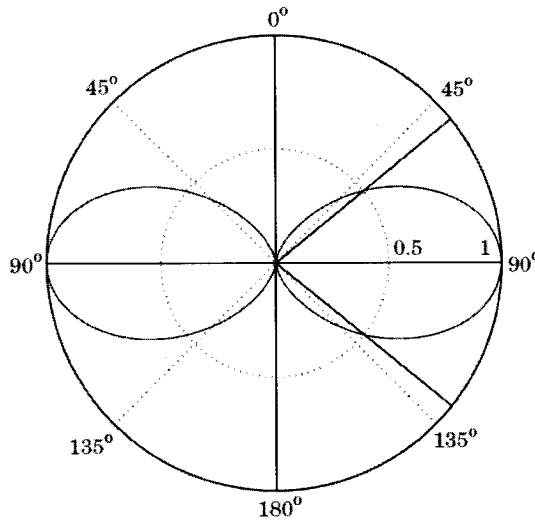


Figure 4.4: Quarter-wave monopole antenna radiation pattern. Figure from Orfanidis (2008)

This is a normalized antenna gain plot, with maximum value of gain equal to 1. To obtain the actual effective gain seen by an observer at a given angle, the result from equation 4.7 must be multiplied by the directivity of the antenna, which, for a quarter-wavelength monopole is 3.28 (Orfanidis, 2008). However, as noted in section 4.2.3.4, ADS-B antennas are permitted to have a gain 3dB lower than that of a monopole antenna. This is equivalent to a factor of 2 in directivity reduction, giving a gain

scaling factor of only 1.64. This lower scaling factor is used, to provide a conservative estimate of the signal power available on orbit.

For the antenna as installed on the top surface of an aircraft fuselage, the angle ϕ used in calculating the radiation pattern is the elevation angle measured from the vertical. ϕ and α sum to 90° , so ϕ as used in equation 4.7 can be found by

$$\phi = 90^\circ - \alpha \quad (4.8)$$

This relationship holds true for an aircraft in level flight. In the event of a pitch or roll manoeuvre by the aircraft, ϕ , an angle related to the antenna geometry, and α , related to the Earth's horizon, become decoupled. However, for large transport aircraft, most of the flight is conducted in level cruise, and pitch angles are limited. Roll occurs mainly during turns, and turns with steep bank angles are few and take up only a small portion of the total flight time. For this analysis, it is assumed that the transmitting aircraft is in level flight, so that equation 4.8 applies.

By converting in this way and applying the scaling factor and the function given in equation 4.7, the antenna gain seen by a satellite at an elevation angle α can be calculated. The meaningful range of α is $0^\circ \leq \alpha \leq 90^\circ$. At $\alpha = 0^\circ$, the satellite is on the horizon as viewed from the aircraft; at $\alpha = 90^\circ$, it is at zenith.

4.4.2 Free-space path loss

As the transmitted signal spreads outwards from its antenna, the signal power is progressively reduced by an inverse-square relation. This reduction in signal power is called the *free-space path loss*, L_f and is a function of the transmission wavelength and the propagation distance:

$$L_f = \left(\frac{4\pi d_{prop}}{\lambda} \right)^2 \quad (4.9)$$

This factor is a power reduction; that is, the signal power observed at a distance d_{prop} from the transmitter is equal to the transmitted power *divided* by L_f . To this idealized estimate of the propagation loss must be added losses due to atmospheric and other effects, discussed below.

4.4.3 Atmospheric propagation effects

The electromagnetic wave carrying the ADS-B signal propagates partly through the Earth's atmosphere, and partly through free space. The atmosphere has properties

which can affect this propagation, usually to the effect of reducing the received power.

4.4.3.1 Neutral atmosphere absorption

Some components of the gases which form the Earth's atmosphere absorb electromagnetic radiation as a function of wavelength. Rohan (1991) gives a technique for calculating this absorption. The significant contributions to the absorption are contributed by oxygen gas and water vapour. For frequencies below 57 GHz, Rohan (1991) gives the coefficient of absorption for oxygen as

$$\gamma_o = \left[\frac{6.6}{f^2 + 0.33} + \frac{9}{(f - 57)^2 + 1.96} \right] f^2 \cdot 10^{-4} \text{ dB/km} \quad (4.10)$$

where f is the frequency in GHz, and has a value of 1.090 for ADS-B over Mode S. The coefficient for water vapour is valid at frequencies below 350 GHz, and is given in Rohan (1991) as

$$\gamma_w = \left[0.0067 + \frac{2.4}{(f - 22.3)^2 + 6.6} + \frac{7.33}{(f - 183.5)^2 + 5} + \frac{4.4}{(f - 323.8)^2 + 10} \right] f^2 \rho \cdot 10^{-4} \text{ dB/km} \quad (4.11)$$

where ρ is the density of water vapour in g/m^3 . Taking a typical temperature of 15°C and relative humidity of 70%, we obtain $\rho = 9 \text{ g/m}^3$ (TIS, 2010), recognizing that this value varies on the surface of the Earth over space and time.

Using these two coefficients, the total atmospheric attenuation can be calculated (Rohan, 1991):

$$A_a = \frac{16\gamma_o}{\sqrt{\sin^2(\alpha) + 16/(kR_\oplus) + \sin(\alpha)}} + \frac{4\gamma_w}{\sqrt{\sin^2(\alpha) + 4/(kR_\oplus) + \sin(\alpha)}} \text{ dB} \quad (4.12)$$

where k is a geometric correction factor, given by Rohan (1991) as $\frac{4}{3}$ for a standard atmosphere.

The value of A_a calculated with equation 4.12 is in decibels. It can be converted to linear units if necessary, whereupon it becomes a reduction factor similar to L_f (from equation 4.9).

4.4.3.2 Attenuation by precipitation and clouds

Some electromagnetic signals are significantly attenuated by precipitation in the atmosphere, such as falling rain or snow. This attenuation is negligible at frequencies below 3 GHz (Rohan, 1991, p.248), so this effect is neglected. The same consideration applies to clouds and fog.

4.4.3.3 Atmospheric refraction

Because the Earth's atmosphere has an index of refraction, n , which is different than that of free space, electromagnetic waves passing into the atmosphere are refracted. The effect is small except at very shallow angles of incidence, since the difference in refractive indices is very slight: for air, $n = 1.0003$ (Tipler, 1999a, p.1041), while in free space $n = 1$. The effect of refraction on the ADS-B signal can be seen in figure 4.5. Rays departing from the transmitter pass from a medium of relatively high refractive index (the air) into one of lower refractive index (vacuum). This causes them to be deflected away from the normal – in this case, from the vertical. As a result, the satellite does not see the ray which was emitted at the elevation angle, α , but instead one from a slightly greater angle, $\alpha + \Delta\alpha$.

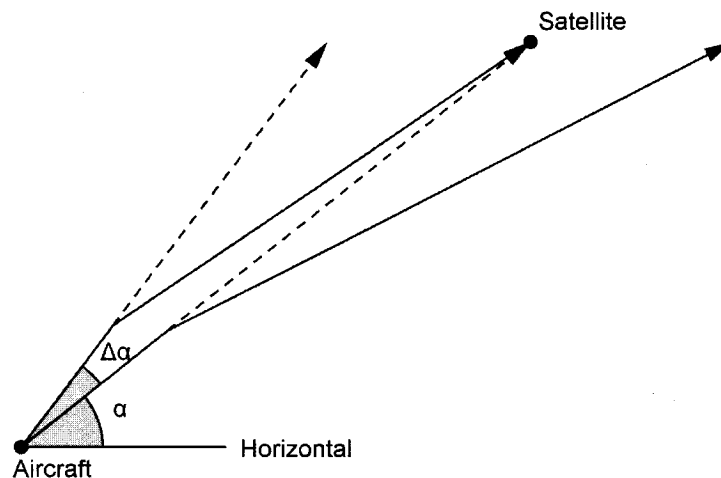


Figure 4.5: Effect of atmospheric refraction

The discontinuity in refractive index is not sudden, but gradual, as the composition and density of the atmosphere gradually change with altitude. Nonetheless, the effect is a difference between the perceived and actual angles of elevation from which the signal was emitted. This problem is also seen in the fine pointing of telescopes, where

the actual position of a star in the sky, and the position to which the telescope must be pointed to observe its emitted light, can be different due to this effect. Maddalena (2002) analyzed the problem for the Green Bank Telescope, a high-resolution radio telescope operating on a frequency band that includes 1090 MHz, and gives a general formula for calculating the angular offset caused by refraction:

$$\Delta\alpha = C_r(n - 1)\cot(\alpha) \quad (4.13)$$

with the coefficient C_r having a value of $2 \cdot 10^5$ arcseconds. Maddalena (2002) notes that this formula is of limited accuracy, but that further refinement requires knowledge of the ambient atmospheric conditions and to some extent of the receiving equipment.

The effect of this angular displacement is that the received signal is not emitted from the same point on the transmission antenna radiation pattern as assumed. In figure 4.4, it can be seen that as the angle of elevation increases from 0° to 90° , the antenna gain seen by the receiver decreases monotonically. To account for this effect, first the elevation angle α is converted to an angle from the antenna axis, ϕ , using equation 4.8. Equation 4.7 is then solved for $\phi - \Delta\alpha$ and for ϕ . The power reduction factor is the ratio of these two values:

$$L_r = \frac{g_t(\phi - \Delta\alpha)}{g_t(\phi)} \quad (4.14)$$

4.4.3.4 Atmospheric loss factor

The attenuation factor due to the atmospheric effects, L_a , is a combination of those calculated above. The factor for atmospheric absorption appears in the numerator, since A_a is greater than unity, and increases with larger attenuation effects. The refractive reduction factor, L_r , appears in the denominator, as a factor less than unity which decreases with increasing attenuation effect. This gives a combined factor which, like the free-space path loss factor L_f , is greater than unity and will be used as a quotient in calculating the signal power at the receiver. The combined factor for atmospheric effects is given in equation 4.15:

$$L_a = \frac{A_a}{L_r} \quad (4.15)$$

This equation uses the linear-unit form of A_a , which had been initially calculated in decibels (see section 4.4.3.1).

4.4.3.5 Ionospheric refraction

Electromagnetic waves passing through the Earth's ionosphere are refracted by the local change in the refractive index caused by the abundance of charged particles. Although overall atmospheric refraction was addressed in section 4.4.3.3, the effect caused by the ionosphere in particular is highly variable in time and space, and is of great importance in radio communication.

The refractive effect on electromagnetic waves is dependent on the conditions in the ionosphere and on the frequency of the incident signal. Lower frequency waves can be strongly refracted by the ionosphere, particularly during conditions of strong ionization in the layer or when transmitted at shallow angles of incidence. Rohan (1991, p.149) gives a formula for calculating the critical frequency, below which signals cannot penetrate the ionosphere:

$$f_c = \sqrt{80.5N_{max}} \quad (4.16)$$

where N_{max} is the ionization density in electrons per cubic metre in the ionosphere. In very strong ionization conditions, N_{max} can range as high as 10^{12} . f_c is the highest frequency, in Hz, which will be fully reflected by the ionization layer at normal incidence. To calculate the critical frequency for other angles of incidence, the following formula is used (Rohan, 1991):

$$f_v = f_c \sec(\phi) \quad (4.17)$$

where ϕ here is the angle of incidence at the ionospheric layer, and is related to the elevation angle by equation 4.8.

For any angle of elevation, if f_v does not reach the operating frequency of the ADS-B signals (1090 MHz), the signals will pass through the ionosphere instead of being reflected. The range of critical frequencies can be calculated across the range of α , to determine if any limit exists due to reflection by the ionosphere at shallow angles. The presence of such a limit is the suspected cause of the very long range detections made by the FLOAT-2 balloon payload (see section 3.5.1).

4.4.3.6 Ionospheric attenuation

In addition to refraction, the ionosphere also acts to attenuate signals passing through it. Rohan (1991) gives a formula for calculating the attenuation factor:

$$A_i = \frac{60\pi N e^2 \nu}{\sqrt{\epsilon'}(\nu^2 + \omega^2)m} \quad (4.18)$$

where:

A_i is the attenuation factor per kilometre

N is the electron density in the ionosphere, in electrons per cubic metre

e is the elementary charge, 1.60×10^{-19} coulombs

m is the mass of the electron, 9.11×10^{-31} kg

ν is the collision frequency, related to the dynamics of the electrons in the ionosphere

ω is the angular frequency of the transiting wave, equal to 2π times the frequency in Hertz, and

ϵ' is the relative permittivity of the ionosphere, calculated by

$$\epsilon' = 1 - \frac{N\omega^2}{\epsilon_0 m(\nu^2 + \omega^2)} \quad (4.19)$$

with ϵ_0 the permittivity of free space, which Rohan (1991) expresses as $10^{-9}/36\pi$ F/m.

The attenuation factor, A_i , takes the form of a fractional power reduction, per kilometer of the ionosphere traversed. Multiplying it by the thickness of the ionosphere gives the total fraction of the transmitted power lost in the transit. If the effect is significant, it is included in the atmospheric loss factor calculated in section 4.4.3.4.

4.4.3.7 Scintillation fading

Fluctuations in the physical state of the atmosphere, due to bulk motion, winds and currents, temperature and pressure gradients, ionization, and other effects, can cause transient attenuation and refraction of propagating signals. While this scintillation is difficult to predict and can only be quantized statistically, the importance of the effect is related to the fraction of time the radio link is active (Rohan, 1991). A system which is transferring data 100% of the time is guaranteed to eventually experience fading due to scintillation, while such events will be much more rare for a link which is only active a fraction of the time. For a single aircraft, transmitting several squitters of $120\mu\text{s}$ each second, the link fraction is low. But for a sensor monitoring large numbers of aircraft, the fading effect may lead to failed reception of squitters in numbers high enough to affect system performance. Since the effect is statistical and transient, rather than one which provides a predicatable and consistent reduction in power, and

since it is dependent on the number of aircraft in the field of view, fading will be neglected in the present analysis. Allowance will however have to be made for this effect in the design of receivers, with reference to the aircraft population expected.

4.4.4 Received power

The signal power received, P_r , at the satellite's position is calculated by applying the gain of the transmitting antenna, g_t , and the reduction factors for free-space path loss and atmospheric losses to the transmitted power, P_t :

$$P_r = P_t \cdot g_t \cdot \frac{1}{L_f L_a} \quad (4.20)$$

This is the total power level available at the satellite, but does not account for any directivity or radiation pattern of the receiving antenna.

4.4.5 Signal-to-noise ratio

The normalized signal-to-noise ratio can be calculated with equation 4.21 (Wertz & Larson, 1999):

$$\frac{E_b}{N_o} = \frac{P_t g_t L_f^{-1} L_a^{-1} g_r}{k T_s R} \quad (4.21)$$

where P_t transmitted power, g_t is the transmitter gain seen by the receiver (equation 4.7), L_f is the free-space path loss (equation 4.9), L_a is the loss due to atmospheric effects (equation 4.15), and g_r is the gain of the receiving antenna. This last parameter has the value of 1 for an isotropic receiver, but a different factor can be included if a specific antenna is to be modeled. k is the Boltzmann constant, $1.380658 \cdot 10^{-23}$ J/K, T_s is the system noise temperature, and R is the data rate in bits per second.

For the 1.090 GHz signal used in this ADS-B application, a system noise temperature of 600 K is used, after Wertz & Larson (1999, p.558). The data rate in this application is 1 Mbps.

E_b/N_o is the ratio of energy received per bit to noise density (Wertz & Larson, 1999). In designing link budgets for communication with spacecraft, this value is used as a metric of the adequacy of a data communication channel; a sufficiently high E_b/N_o ratio indicates that the bit energy dominates the noise, and allows successful reception of data over the channel. Wertz & Larson (1999, p.551) give a ratio of E_b/N_o of 5 to 10 as a guideline value for a sufficient margin. This metric is often expressed in decibels, where the corresponding values are 7 to 10 dB.

An additional margin may need to be applied to account for bit-error rate limitations of the digital modulation scheme. The values are available for commonly-used digital modulation schemes (Wertz & Larson, 1999), but the development and application of such a margin, if needed, for the pulse-position modulation used in the 1090 MHz ES is left to future analysis.

Should the value of E_b/N_o be less than 1 (or negative on the decibel scale), it can be raised by adjusting several of the factors in equation 4.21. The transmitter gain and atmospheric losses are functions of the elevation angle (α , as viewed from the aircraft) or off-nadir angle (θ , as viewed by the satellite). The free-space path loss is a function of distance, which is driven by altitude and elevation angle (see figure 4.3). The system noise temperature is largely a function of the transmitter environment, and cannot be significantly adjusted, nor can the fixed data rate of the 1090 MHz ES. As a result, the main adjustments that can be made to improve the E_b/N_o ratio are to adjust the altitude of the satellite's orbit, to accept restrictions on the angle from nadir at which it will detect ADS-B signals, or to improve the gain of the reception antenna.

4.4.6 Parabolic receiver antenna

In some cases, it is useful to investigate the characteristics of an antenna having sufficient gain to raise the ratio of E_b/N_o to an adequate value for transmission. Parabolic reflector antennas are routinely used on spacecraft to boost receiver gain, for example on geostationary communication satellites.

The gain of a parabolic reflector antenna is calculated from the following formula (Orfanidis, 2008):

$$G = \eta \left(\frac{\pi D}{\lambda} \right)^2 \quad (4.22)$$

where λ is the wavelength, D is the antenna diameter, and η is the antenna efficiency, typically ranging 0.55 to 0.65 (Orfanidis, 2008). As in the case of the monopole antenna, the gain, G , is used to scale the normalized radiation pattern.

Compared to the monopole antennas which are the baseline for the 1090 MHz ES, parabolic antennas are highly directive, giving the highest gain along the axis of the parabola. The radiation pattern has some secondary side lobes of generally much smaller gain. An example of this radiation pattern is shown in figure 4.6 (Orfanidis, 2008)

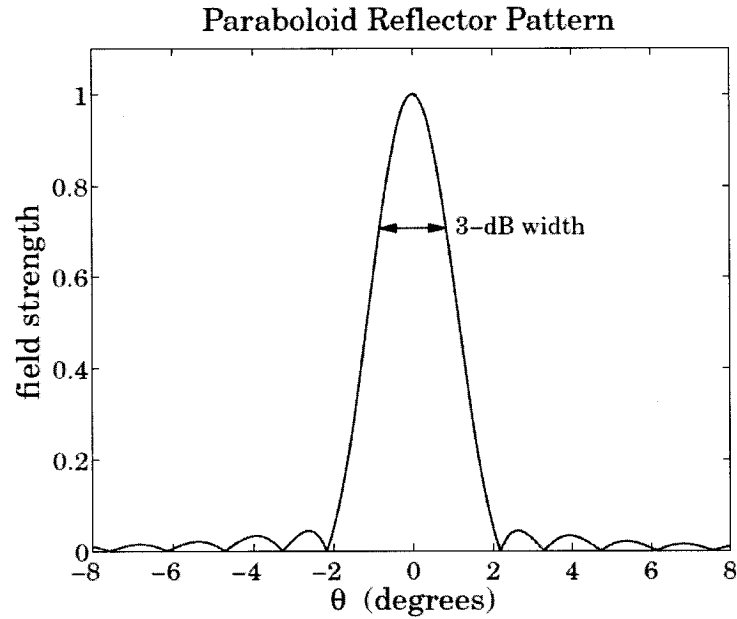


Figure 4.6: Radiation pattern of a typical parabolic reflector antenna. Image from Orfanidis (2008)

The calculation of the radiation pattern of the parabolic antenna is significantly more complex than that of the monopole. Orfanidis (2008) gives a procedure for calculating it:

$$\begin{aligned}
 E_{\theta} &= -j \frac{e^{-jkr}}{\lambda r} \frac{1 + \cos\theta}{2} [f_A(\theta) + f_B(\theta)] \sin\phi \\
 E_{\phi} &= -j \frac{e^{-jkr}}{\lambda r} \frac{1 + \cos\theta}{2} [f_A(\theta) + f_B(\theta)] \cos\phi
 \end{aligned} \tag{4.23}$$

where θ and ϕ are angles from the axis of the parabola in two mutually perpendicular planes, k is the wavenumber ($2\pi/\lambda$), and f_A and f_B are functions of the parameter ψ which depend on the nature of the feed antenna used with the reflector. ψ is the angular extent of the reflector as viewed from its feed, with ψ_o , its maximum value, calculated by (Orfanidis, 2008):

$$\psi_o = 2 \arctan \left(\frac{D}{4F} \right) \tag{4.24}$$

where D is the antenna diameter and F the focal length of the parabola. F is determined by design requirements and by relationship to D ; practical ratios of F/D are from 0.25 to 0.5 (Orfanidis, 2008, p.748).

Orfanidis (2008) develops the functions f_A and f_B in detail, using Gauss-Legendre quadrature integration to numerically evaluate them, and also provides MATLAB algorithms to use them to calculate the radiation pattern of the parabolic antenna with a dipole feed (a basic and generic design) for given values of frequency and antenna diameter. This MATLAB code is used in this analysis, with permission.

If a parabolic antenna is chosen to improve the gain of the receiver, a value for the gain can be chosen which is sufficient to bring the ratio of E_b/N_o to the desired value (equation 4.21). By rearrangement of equation 4.22, a necessary diameter can be determined. This diameter is used in calculating the geometry of the radiation pattern (equation 4.24). The radiation pattern can then be scaled by the gain factor, and applied to the incoming signal as a function of the angle from the antenna axis (which may be at nadir, or otherwise) to obtain the angular distribution of the received power.

4.5 Doppler effect

The receiver on the satellite will be in motion relative to the surface of the Earth in all but the geostationary case. As well, the aircraft is in motion. As a result, the Doppler effect may in some cases be important, shifting the received frequency away from the nominal frequency, $f_0 = 1090$ MHz. The frequency shift can be calculated by (Tipler, 1999b, p.467):

$$\Delta f = \pm \frac{u_{sat} \pm u_{air}}{c} f_0 \quad (4.25)$$

where u_{sat} and u_{air} are respectively the velocities of the satellite and aircraft relative to the surface of the Earth, and c is the speed of light. The equation is solved in vector form. The rotational speed of the Earth contributes to the effect; the orbital velocity of the satellite is relative to the geometric centre of the Earth, and does not account for the planet's rotation, which carries the aircraft with it. The Earth's velocity will add to the effect to a sinusoidally-varying degree with the position of a satellite in an inclined orbit, and with the magnitude of the inclination. An equatorial orbit carries the greatest effect, with a prograde orbit giving a reduction proportional to the Earth's equatorial rotational velocity, and a retrograde orbit giving an increase of the same magnitude. The effective aircraft velocity is the aircraft's groundspeed, added vectorially to the Earth's rotational velocity, which is calculated by:

$$v_g = R_{\oplus} \cdot \omega_{\oplus} \cdot \cos(\phi_{lat}) \quad (4.26)$$

where ϕ_{lat} is the latitude.

Additionally, the angular motion of the satellite at a large radius is constant to observers at all altitudes, but its apparent linear motion is not. The equivalent satellite velocity to be used is thus the equivalent linear velocity which, at the aircraft's altitude, would give the same radial velocity as that of the satellite. Since

$$v_{sat} = R_{sat} \cdot \omega_{sat} \quad (4.27)$$

then for an object at the aircraft's radius having the same angular velocity, the linear velocity would be

$$v_{equiv} = R_{air} \cdot \omega_{sat} \quad (4.28)$$

and, combining these, we obtain:

$$v_{equiv} = \frac{R_{air}}{R_{sat}} v_{sat} \quad (4.29)$$

The equivalent velocity, and thus the Doppler effect, will be greatest for satellites having low altitude or high orbital velocity.

In the LEO case an upper boundary for the shift can be found in the case when the satellite and aircraft pass directly over each other heading in opposite directions, with the satellite in an equatorial orbit. In the GEO case the Doppler effect is greatly reduced, since the orbital speed of the satellite relative to the surface of the Earth is zero and only the groundspeed of the aircraft contributes to the effect. In all cases, the greatest effect will occur when the aircraft is at its farthest range, when the relative velocity is very close to the transverse velocity due to the small angle of approach. Additionally, due to the curvature of the Earth, at the range limit the aircraft will see the satellite at or near an elevation angle of 0° , meaning that its relative motion will in fact be, in some cases, directly toward or away from the satellite.

4.6 Signal collisions from simultaneously observed aircraft

As discussed in section 4.2.3.3, ADS-B signals on the 1090 MHz ES system are broadcast at rates which vary randomly about a mean, regular interval. This is to prevent the possibility of two nearby aircraft having synchronized signals which interfere with each other on each transmission, preventing reception of the encoded information by a third aircraft or a ground station. An additional rule is that the transmitter of an

aircraft delays sending a message if it is in the process of receiving an incoming one (DO-181D, 2008, §2.2.18.2.2).

These randomization and delay processes produce a form of self-organizing time-division multiple access (TDMA) allocation of the 1090 MHz frequency, and allow aircraft using the 1090 MHz ES system to effectively share the frequency with each other, as well as with other systems active at or near 1090 MHz, including Mode A and C transponder systems, Distance Measuring Equipment (DME) and Tactical Air Navigation (TACAN).

A signal collision is an event in which squitters transmitted by two aircraft overlap in time, and are therefore unintelligible to a third-party receiver. When a single aircraft operates in isolation, this does not occur, but as the number of aircraft within reception range of each other increases, the likelihood of such collisions increases, and they therefore become more frequent. A satellite-based receiver will possibly be able to receive signals from a very large geographic area, with a correspondingly large number of aircraft being monitored simultaneously. This will result in an increased occurrence of signal collisions compared to the case of a ground-based receiver. The rate of these signal collisions will vary based on the number of aircraft in view, which is variable both in time and space across the surface of the Earth.

4.6.1 Probability of signal collision

To characterize the rate of occurrence of signal collisions, a model is developed of their probability.

Squitters are transmitted at intervals which vary in an equal random distribution about a prescribed mean. Overall, then, they are transmitted on average m times per period T . The total length of time, out of the period T , which is occupied by the squitters of a single transmitter is equal to l , where

$$l = m \cdot d \tag{4.30}$$

with d being the duration of a squitter. All squitters are of equal duration.

One squitter will collide with another if the two overlap in time to any degree. This occurs if the transmission of the second squitter begins anytime during the duration, d , of the first squitter.

The beginning of transmission of a squitter varies randomly about its average mean, but the synchronization of this time is random. That is, the mean component of the cycles of two transponders will be out of phase by a random amount, even

before the random variability about the mean is added for each. This is because the transponders begin transmitting squitters when they are powered on and have sufficient navigational data, rather than having their cycles synchronized to an external reference. The effect of this is to add a second randomization to the variation of the timing of a squitter transmission, and it means that a squitter may be transmitted beginning at any time during the period T , lasting for a duration d . Since the phase variability of the mean component of the cycle is effectively random, it can be taken that the probability of beginning at each time in the period T is equal.

Since the transmission of the second squitter may begin at any point of time within the period T with an equal likelihood, the probability of that second squitter beginning during the transmission of the first squitter is equal to

$$\frac{l}{T} \quad (4.31)$$

The probability of such an overlap *not* occurring is

$$P_{no,2} = 1 - \frac{l}{T} = \frac{T-l}{T} \quad (4.32)$$

This is the probability of no collision occurring the period T , for two aircraft. As more aircraft are added to the system, each additional aircraft carries the same probability of interfering with the first. The probability of that first aircraft *not* experiencing a signal collision with *any* of the other aircraft is multiplied for each additional aircraft, giving a general formula of

$$P_{no,n} = \left(\frac{T-l}{T} \right)^{n-1} \quad (4.33)$$

where n is the number of aircraft in view of the receiver, *including* the first. Each aircraft has this same probability of experiencing no signal collisions during a given period T . This is, therefore, the probability that, during a period T , an intelligible squitter is received (leaving out other components of the system which reduce the possibility of correct reception such as system noise, interference, or operational aspects). In a multi-aircraft environment, equation 4.33 gives the probability that surveillance information is successfully obtained from a given aircraft during a single period, T . It applies equally to all aircraft in the area, meaning that during that period, it is expected that, on average, surveillance data will be obtained from a number of aircraft equal to $R_{no,n}$, where

$$R_{no,n} = n \cdot P_{no,n} \quad (4.34)$$

4.6.2 Allowed detection time and probability

Equation 4.33 gives the probability that a given aircraft will experience *no* signal collisions during the period T . The probability that it *will* experience a signal collision during T is given, then, by

$$1 - \left(\frac{T-l}{T} \right)^{n-1} \quad (4.35)$$

This probability is the same for each successive period of T . Over t periods, the probability that a given aircraft will experience a signal collision in every period is

$$\left[1 - \left(\frac{T-l}{T} \right)^{n-1} \right]^t \quad (4.36)$$

Therefore, the probability that a signal collision does *not* occur in *every* one of those t periods is

$$P_{no,t} = 1 - \left[1 - \left(\frac{T-l}{T} \right)^{n-1} \right]^t \quad (4.37)$$

Otherwise stated, equation 4.37 gives the probability that, over t periods (each of length T), surveillance information will be successfully obtained from a given aircraft at least once.

The undesirable event is calculated in equation 4.36; that of failing to detect a given aircraft over the course of t periods. For surveillance purposes, it is desirable that such a failure to track an aircraft be very unlikely. The probability of such a failure to track, P_f , should be very low, and its value may be a driver for the design of a surveillance system. Here, equation 4.36 is reproduced, but with the bracketed expression replaced by the value A , which since T and l are constant, is a function only of n :

$$P_f = A^t \quad (4.38)$$

The two key parameters here are t , the length of time surveillance is conducted, and P_f , the chance of a failing to detect any individual aircraft during that length of time. In the system design, these two parameters may be chosen, and, using equation 4.36, the corresponding value of n determined, which is the maximum number of

aircraft that can be in view of the satellite receiver such that sufficient surveillance reliability is achieved.

Chapter 5

Orbital Detection of ADS-B Signals: Theoretical results

5.1 Introduction

In this chapter, the results of the analysis described in Chapter 4 are presented, describing the propagation of ADS-B signals from aircraft to orbital sensors, and other considerations for their detection and for the development of an operational system to support ATS provision.

In section 5.2, the characteristics of the orbital geometry are described, including their variation across a range of potential cases and orbits. This geometry is used as the basis for the propagation problem, whose output is the link budget for the transmission. The results of this link budget analysis are given in section 5.3, including the description of the free-space path loss (5.3.1), the neutral atmosphere absorption (5.3.2), overall atmospheric refraction (5.3.3) and ionospheric refraction in particular (5.3.4), as well as a discussion of the overall implications of these atmospheric effects (5.3.6).

Using these aspects of the propagation, the power level of the ADS-B signals received by the orbital sensor are calculated, and presented in section 5.3.7. This is then used to derive the ratio of bit energy to noise density, which, as a normalized signal-to-noise ratio, gives an estimation of the detectability of the signal, expressed as the link margin. This result is given at section 5.3.8. This result for link margin as a function of orbital geometry, and accounting for propagation effects including the Earth's atmosphere, is the key tool to be used in analyzing the feasibility of an air traffic monitoring system using orbital ADS-B sensors.

In subsequent sections, this analytical result is applied to specific scenarios of in-

terest to developing a space mission to implement ADS-B surveillance. The low Earth orbit (LEO) case is addressed in section 5.4, including a description of the satellite coverage area and its detection implications, for several orbits of particular interest. The case of a satellite in geostationary orbit (GEO) is next addressed, in section 5.5, including preliminary sizing and selection of a suitable antenna, and selection of an orbital longitude slot suitable for coverage of Canada and its delegated North Atlantic airspace, as well as the neighboring United States, and the oceanic approaches to both countries. Section 5.6 extends the discussion to constellations of satellites and hybrid systems composed of spacecraft in multiple, and different, orbits, along with the implications for system reliability and coverage area. Finally, in section 5.7, the possibility of using high-altitude stratospheric platforms for ADS-B monitoring is explored, extending the concept demonstrated in the FLOAT experiment to a component of an operational system.

The discussion then turns to the implications for the receivability of signals, investigating two effects which can interfere with reception of signals which nonetheless have sufficient power to be detected. First, the implications of the Doppler effect are explored, in section 5.8. The probability of message losses due to signal collisions is then derived, in section 5.9, including a description of the expected system performance as a function of the number of aircraft in the field of view. The chapter concludes with a description of the design methodology for an orbital ADS-B detection system, in light of the signal collision effect, and a discussion of strategies to further improve the performance of the system.

5.2 Orbital geometry

The model of orbital geometry is implemented in MATLAB, using the techniques discussed in section 4.3. Results presented use an aircraft at an altitude of 10 km, and satellites at a range of altitudes.

As an aircraft's distance from the sub-satellite point (L) increases, the nadir angle (θ) increases from zero to its maximum value, which is equal to the angular radius of the Earth as viewed by the satellite. This relationship varies with satellite altitude, and the maximum value of θ decreases as the satellite moves farther from the Earth. The relationship is shown for a variety of orbital altitudes in Figure 5.1.

The graph shows the variation of L with θ for several orbital altitudes, ranging from LEO to GEO and slightly beyond. Among the lower orbits included are 400 km, the approximate altitude of the ISS and typical range for numerous satellites,

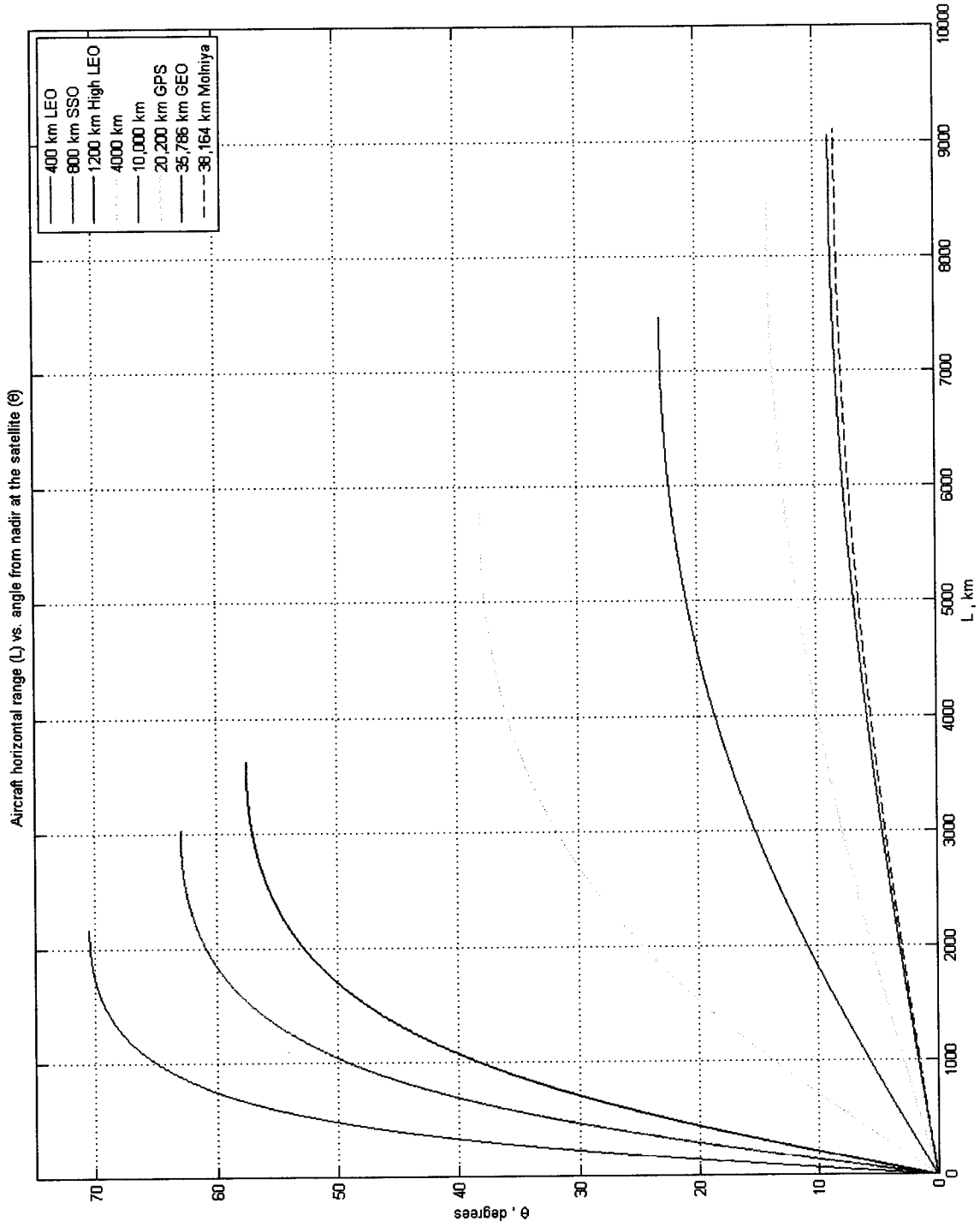


Figure 5.1: Aircraft horizontal range (L) vs. nadir angle (θ)

800 km, the typical altitude of Earth-observing satellites in sun-synchronous orbits (SSO), and 1200 km, near the upper range of LEO altitudes. Several other orbits above these altitudes are also considered, including three particular cases. The lowest of these is at 20,200 km, the altitude of GPS navigation satellites. The geosynchronous case is included, as well as the highly eccentric molniya orbit, for which the apogee altitude is used. Molniya orbits are used mainly for communications satellites to service high latitude regions, and are the planned destination of the proposed Polar Communications and Weather (PCW) mission of the Canadian Space Agency (CSA).

In Figure 5.1, the gradual reduction in the maximum value of θ with increasing altitude can be seen. At LEO altitudes, the aircraft's angle from nadir can range to slightly beyond 70° , while at GEO the angular radius of the Earth is 8.7° (Wertz & Larson, 1999), limiting the value of θ to this amount. Noted is the similarity between the curves for GEO and molniya orbits; the angular change between these two positions is very small.

As the aircraft moves towards the sub-nadir point, the elevation angle to the satellite, α , will increase from 0° (as the satellite comes into view over the horizon) to 90° . Simultaneously, the nadir angle, θ , will decrease from its maximum value to 0° . This relationship is shown in Figure 5.2.

Again visible is the maximum value of θ , which decreases with increasing satellite altitude. The variation of α across the satellite's field of view is an important parameter, since this angle determines which part of the transmitting antenna's radiation pattern (Figure 4.4) is seen by the satellite. The relationship between θ and α is inverse, and not linear; for all altitudes, as θ increases, α decreases. When α is 0° , the detector sees the highest gain; as α approaches 90° , the antenna null is seen, and the gain approaches 0. As shown in the plot, for all altitudes, this antenna null will be seen when the aircraft is closest to nadir.

As θ increases, so does the distance to the aircraft. The propagation distance, d_{prop} , is another parameter affecting the strength of the signal available to the orbital detector. Its increase results in a weaker signal. However, this distance is shortest when the aircraft is directly below (at $\theta = 0$). This is also the point at which the transmitting antenna gain is lowest. The contribution to the signal strength of distance and transmitter gain pattern are therefore inversely related – the implications of this will be explored in later sections. Figure 5.3 shows how the propagation distance (d_{prop}) varies together with α . Because of the large variation in distance between LEO and Molniya orbits, a logarithmic scale is used to show the range of d_{prop} .

The increasing distance with decreasing elevation angle is apparent. Also notable

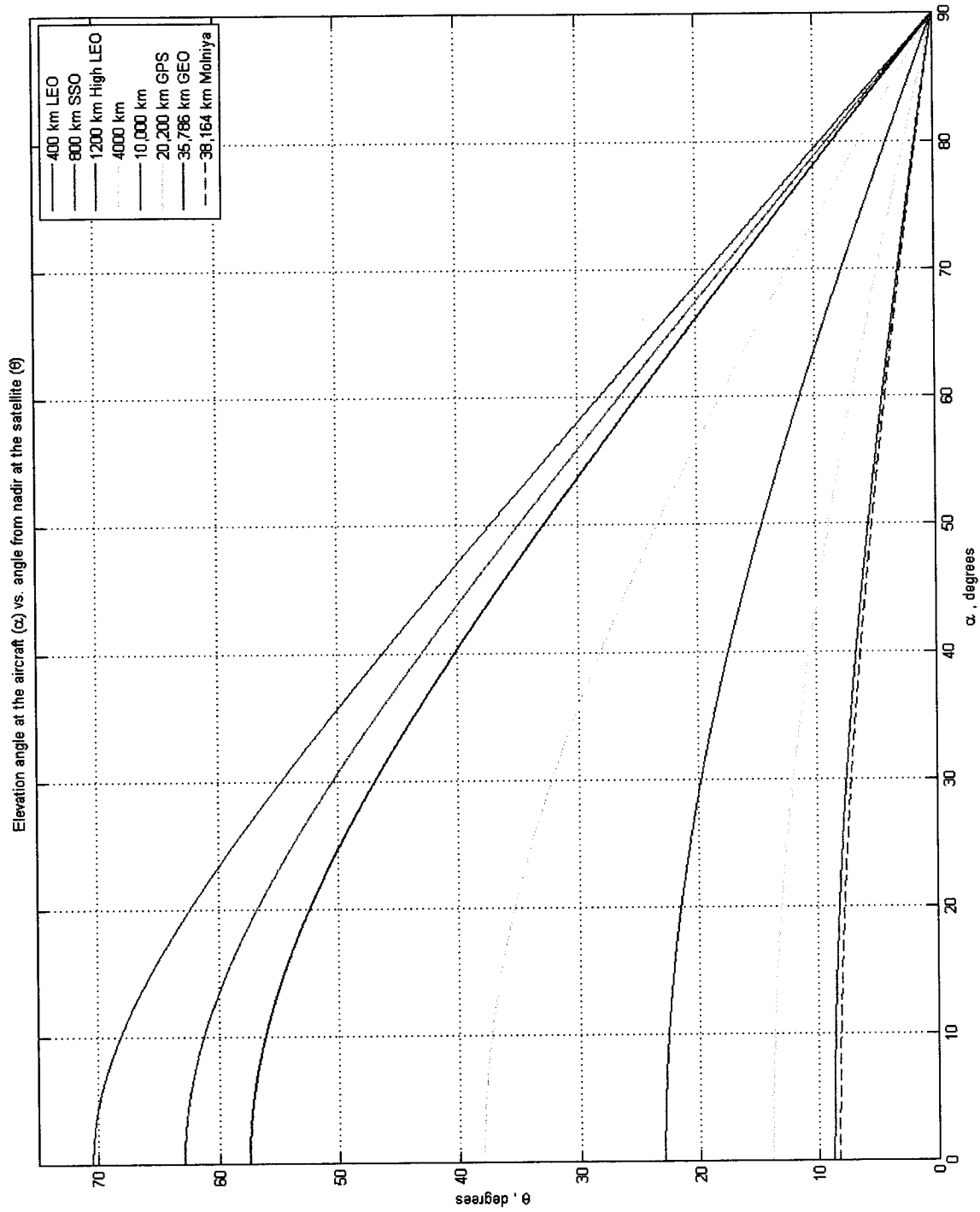


Figure 5.2: Elevation angle (α) vs. nadir angle (θ)

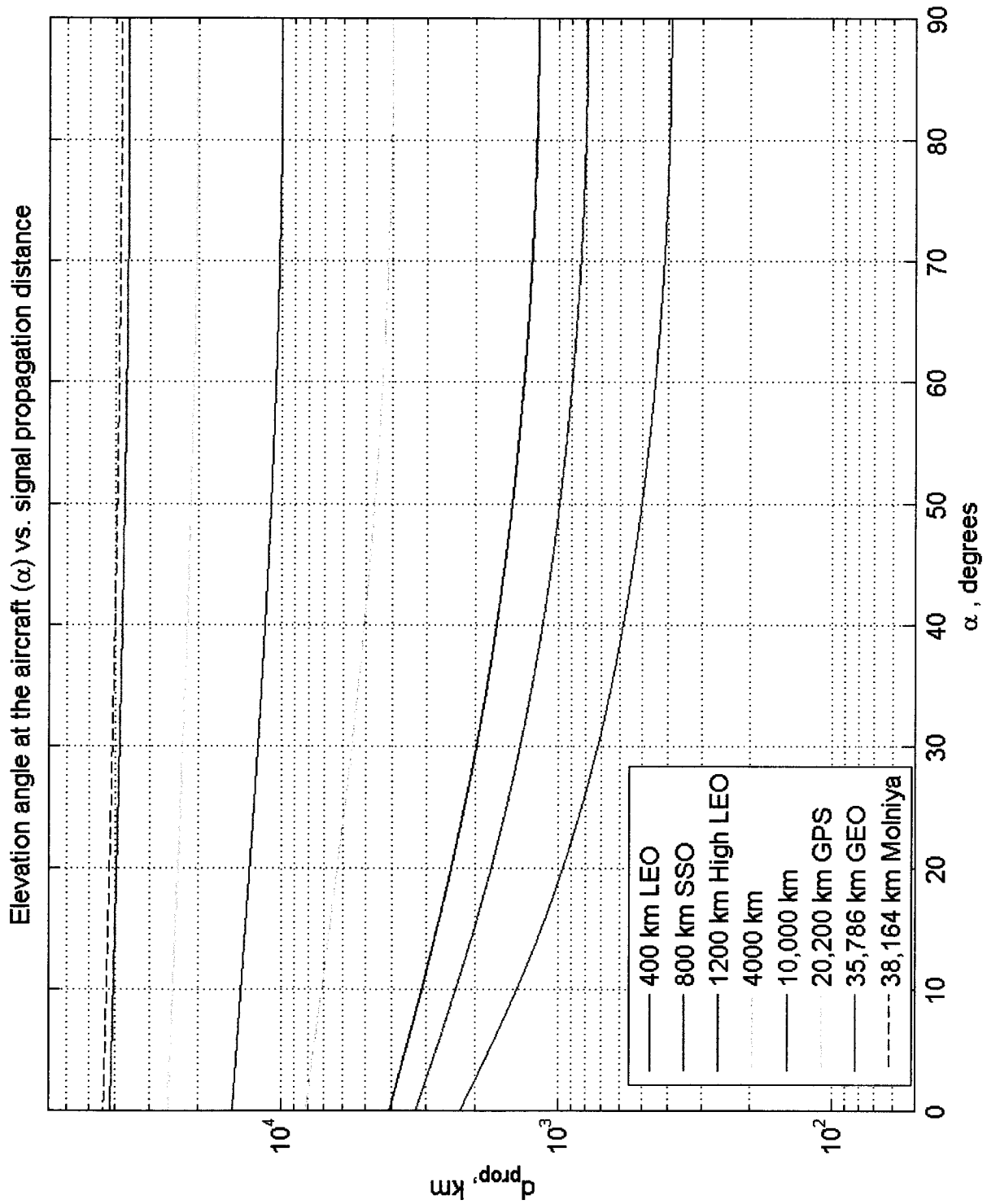


Figure 5.3: Propagation distance (d_{prop}) vs. nadir angle (θ)

is the lessening of this effect as the satellite increases in altitude. This is to be expected, since with increasing distance from the Earth, lengths along its surface become increasingly small relative to the satellite altitude.

5.3 Link Budget

5.3.1 Free-space path loss

With a fixed wavelength of 0.275 m (corresponding to the transmission frequency of 1090 MHz), the free-space path loss calculated in equation 4.9 depends only on the propagation distance, d_{prop} . The loss increases with the square of this distance. For the same set of cases shown in the previous graphs, Figure 5.4 shows the variation of the free-space path loss, L_s .

The great variation in the losses with range necessitates a logarithmic axis for L_s . Due the much larger distances, the losses are 3 to 4 orders of magnitude higher at GEO and molniya than in the LEO range. As aircraft move away from nadir, they follow the curvature of the Earth and move farther from the satellite. As a result, the losses increase with θ . The lessening of this effect with increasing altitude is also apparent, caused by the same lessening in the effect on d_{prop} discussed above. Also visible, again, is the increasingly restricted range of θ with altitude.

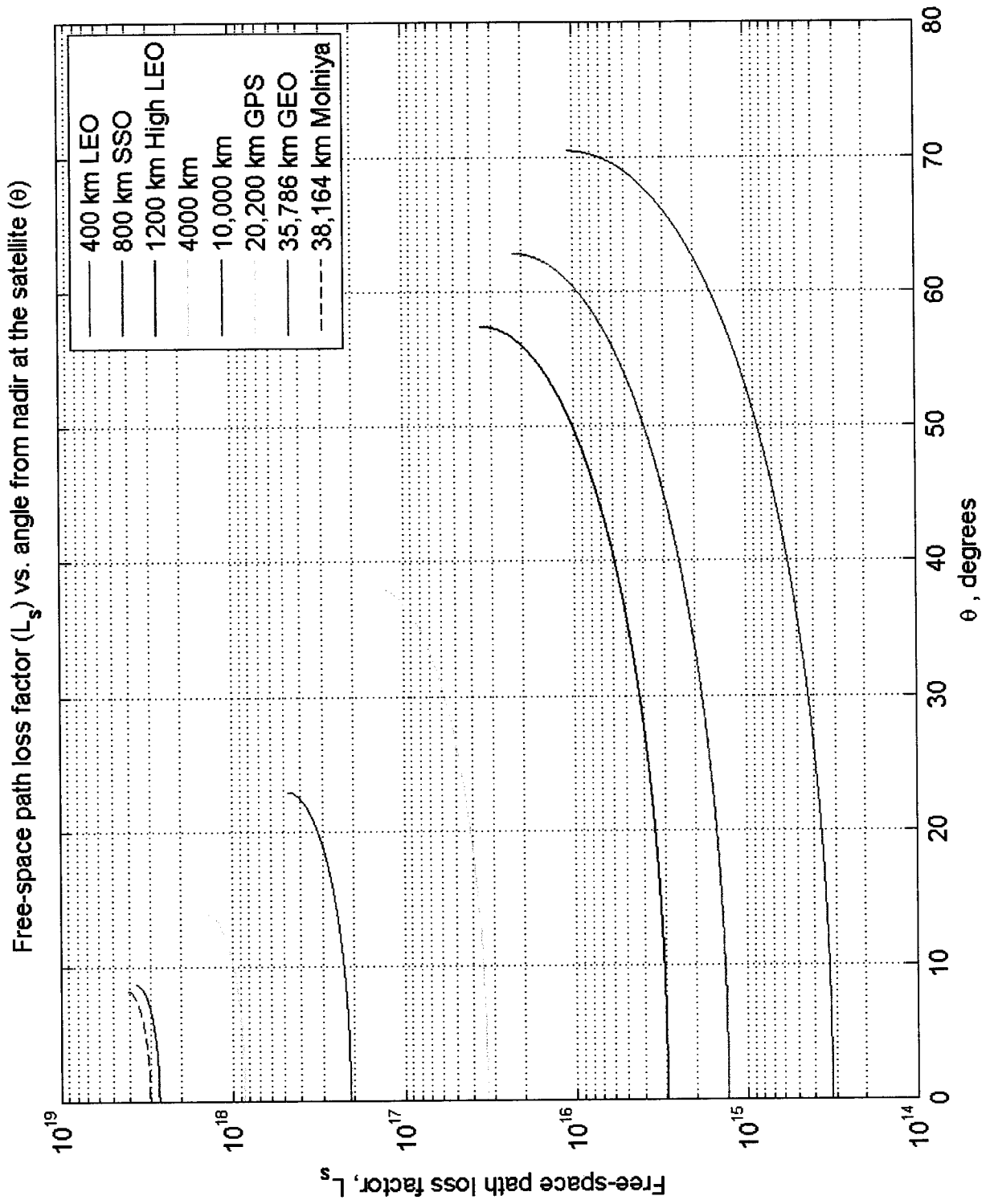


Figure 5.4: Free-space path loss (L_s) vs. nadir angle (θ)

5.3.2 Neutral atmosphere absorption

The attenuation of the ADS-B signal due to absorption by the neutral atmosphere is modeled using the technique described in section 4.4.3.1. Its value, as a function of the angle of elevation at the aircraft, is plotted in Figure 5.5.

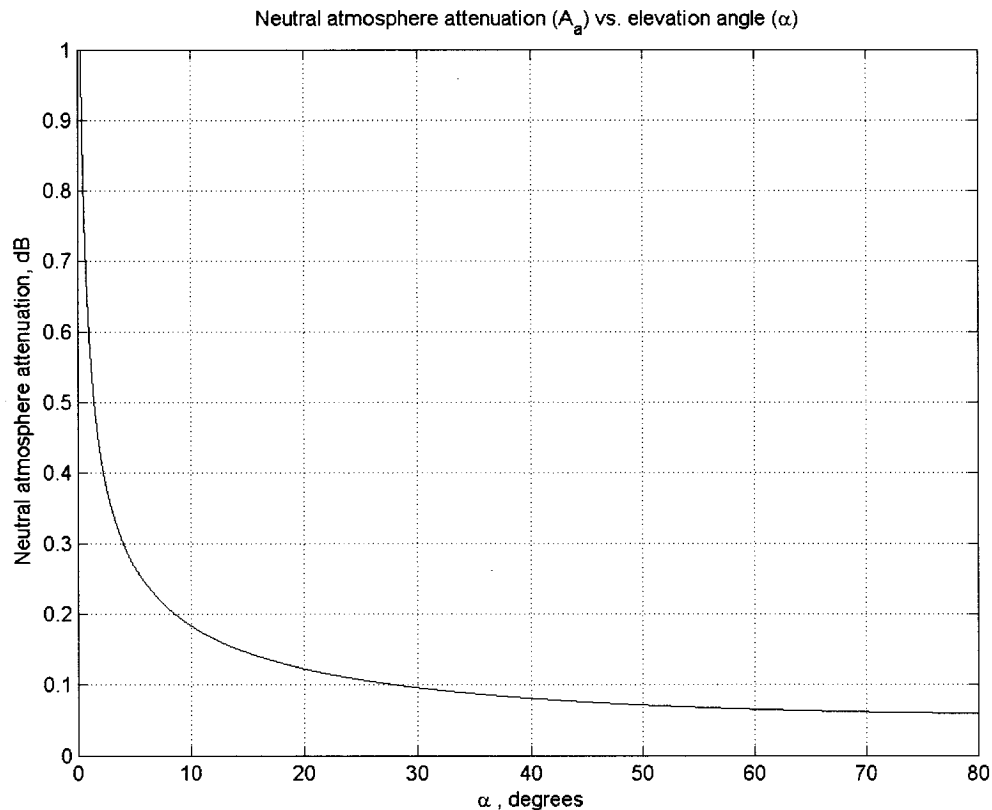


Figure 5.5: Neutral atmosphere attenuation (A_a) vs. elevation angle at the aircraft (α)

The absorption is very low for most values of α . As the satellite approaches the horizon, the absorption rises asymptotically, reaching and surpassing a full decibel of attenuation only within the last degree before α reaches zero. The asymptotic behaviour of the absorption is due to the increasing thickness of the atmosphere through which the signal passes. Over most of the range of elevation angles, the view from the satellite to the aircraft is through a thin layer of the Earth's atmosphere. But, as the aircraft nears the horizon, the length of the signal's path through the atmosphere rapidly increases, and the signal is greatly attenuated. The total effect is much less than one decibel of attenuation except at extremely shallow angles of elevation. The effect is independent of satellite altitude, and depends only on the elevation angle of the satellite as viewed from the aircraft (α). Figure 5.6 shows how

the effect maps to nadir angle (θ) as a result of the relationship between α and θ shown in Figure 5.2.

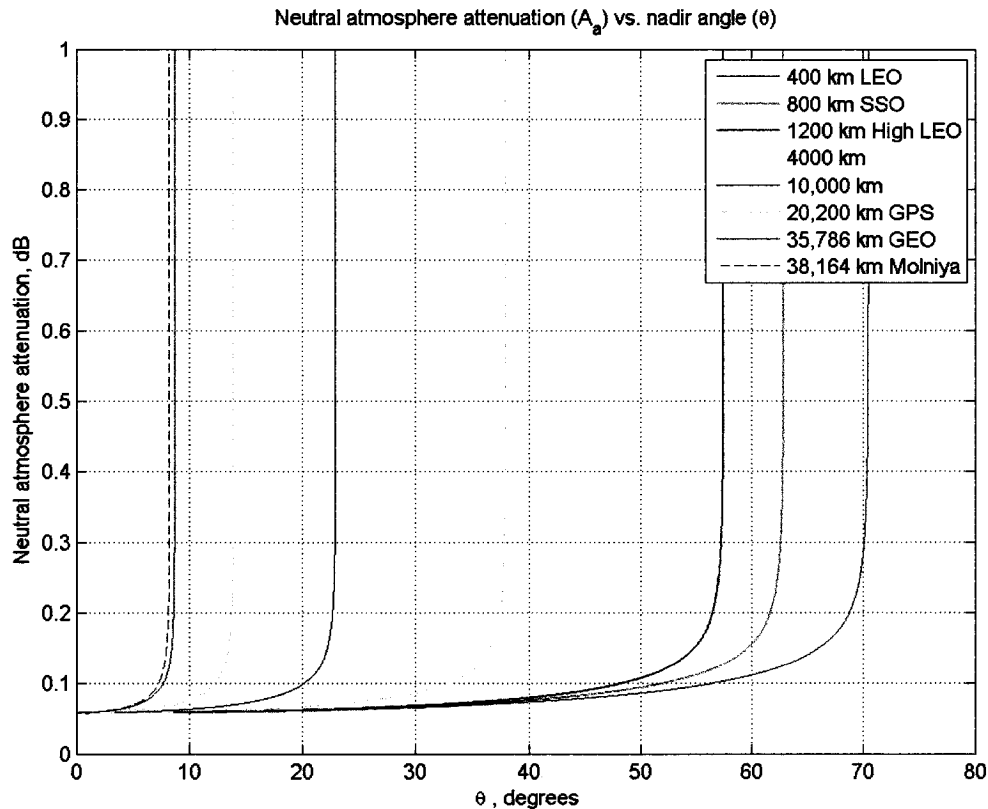


Figure 5.6: Attenuation due to neutral atmosphere absorption (A_a) vs. nadir angle (θ)

5.3.3 Atmospheric refraction

The effect of atmospheric refraction is calculated using the technique described in section 4.4.3.3. The value of the resulting power reduction factor is plotted in Figure 5.7.

As with the neutral atmosphere absorption, the effect of refraction is dependent only on the elevation angle of the satellite as viewed from the aircraft, (α). It can be seen that due to the cotangent function used in the calculation, the attenuation is nearly absent (reduction factor of ~ 1) over nearly the whole range, and asymptotic in the fraction of a degree above the horizon. To show the behaviour of the function more closely, a detail of the graph is given in Figure 5.8.

The effect of atmospheric refraction is only important for very shallow angles

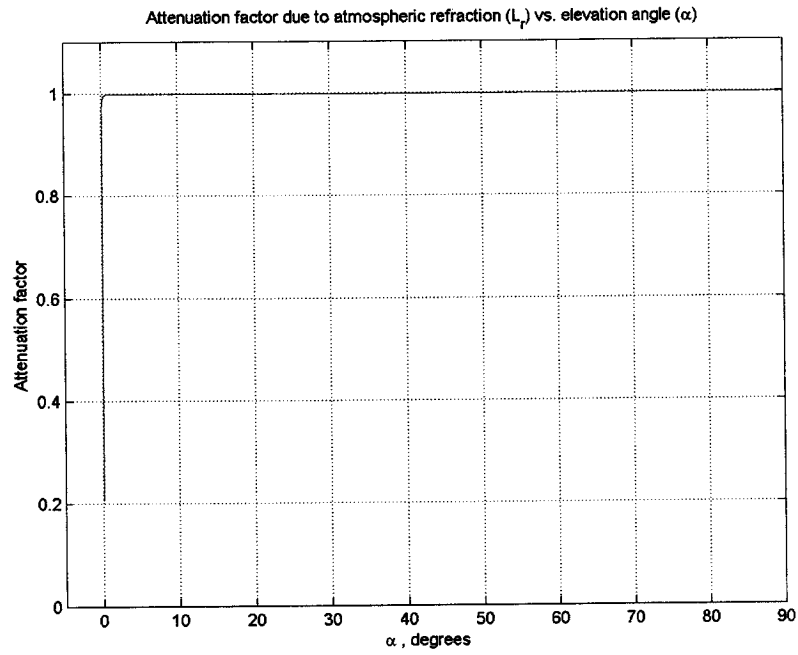


Figure 5.7: Attenuation factor due to atmospheric refraction (L_r) vs. elevation angle (α)

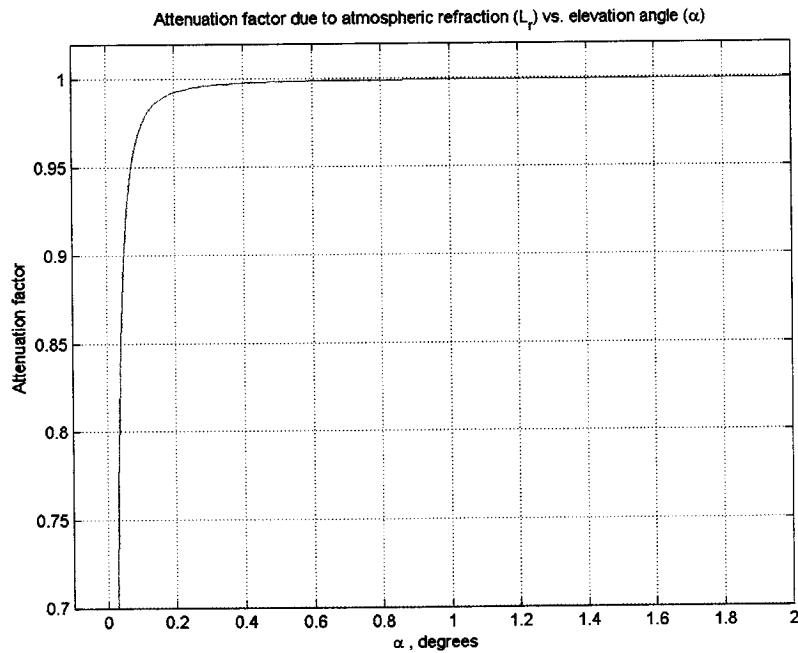


Figure 5.8: Attenuation factor due to atmospheric refraction (L_r) vs. elevation angle (α), detail

of elevation. At angles very close to 0° , the effect can be very significant. The sudden amplification of atmospheric refraction very close to the horizon is expected and familiar; this effect is responsible for the visual notability of sunsets, and the resultant angular offset effect is the cause of the distortion of the sun's disc often observed during this event.

5.3.4 Ionospheric refraction

The critical frequency for ionospheric transmission is calculated using the technique described in section 4.4.3.5. As with the more general case of atmospheric refraction, this effect depends only on the elevation angle α (or the incidence angle, ϕ , which is its complement). The critical frequency, below which signals cannot reliably penetrate the ionosphere, is shown as a function of α in Figure 5.9

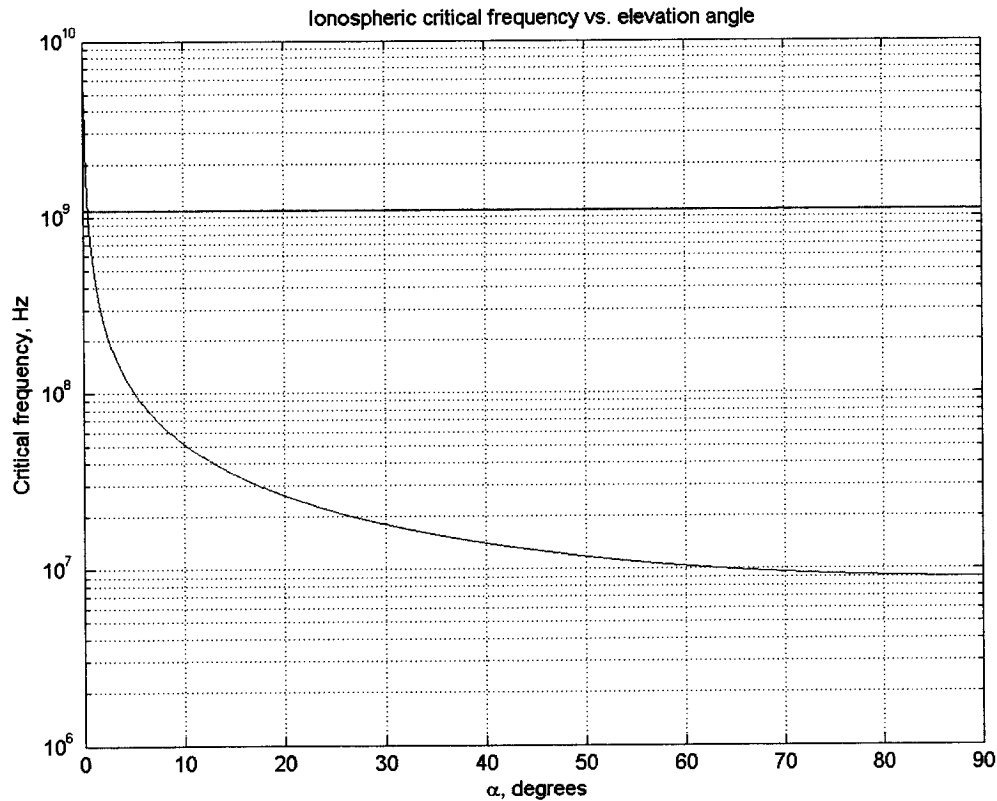


Figure 5.9: Critical frequency for ionospheric transmission vs. elevation angle

The axis for critical frequency is logarithmic. A red line indicates a frequency of 1090 MHz, used for the ADS-B signals. To show the behaviour of the function more

closely, a detail of the graph is given in Figure 5.10.

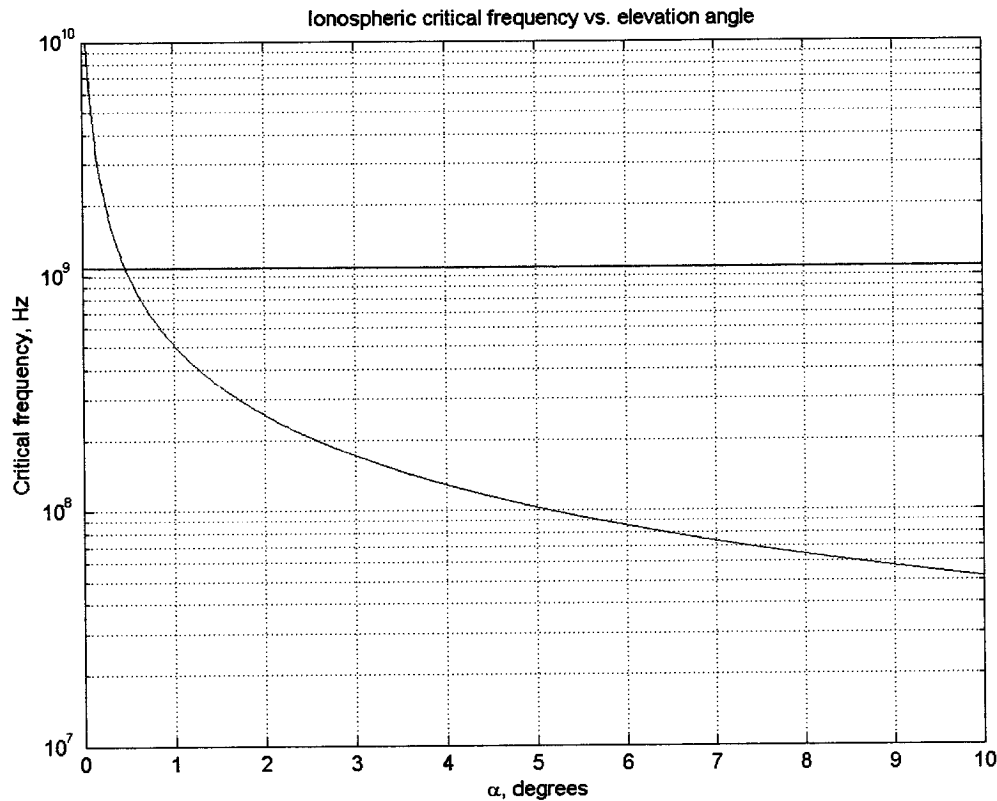


Figure 5.10: Critical frequency for ionospheric transmission vs. elevation angle, detail

At normal incidence ($\alpha = 90^\circ$), the critical frequency is 8.97 MHz. As α decreases towards 0° , the critical frequency increases. It does not reach 1090 MHz until $\alpha = 0.47^\circ$. At these very shallow elevation angles of less than half a degree, the other atmospheric effects are also significant, and, from the view of the aircraft, the satellite is nearly on the horizon. It is also at such very shallow angles that the long-range detections observed in the FLOAT-2 experiment were made, reinforcing the conclusion that reception of these signals was due to atmospheric refraction, very possibly from the ionosphere.

5.3.5 Ionospheric attenuation

To determine the effect of ionospheric attenuation, a worst-case value is determined by application of Equation 4.18, using the F layer of the ionosphere. This layer has the lowest collision frequency, at $10^3/\text{s}$. The maximum possible electron density, $10^{12}/\text{m}^3$,

is also used. Applying these values and the operating frequency of 1090 MHz gives a value of ionospheric attenuation of 1.11×10^{-10} /km. This low value is unsurprising; as Rohan (1991) notes, the attenuation falls off rapidly with increasing frequency. With this attenuation value, the signal would have to travel through an ionosphere with a thickness of 89.6 million km – nearly the radius of the Earth’s orbit about the Sun – to be attenuated by 1%. The effect of ionospheric attenuation will therefore be neglected in the analysis.

5.3.6 Overall implication of atmospheric effects

Taken collectively, these atmospheric effects indicate that the reception of ADS-B signals within approximately 0.5° of the horizon may be difficult or unreliable. It is typical of satellite communication systems that signals are very difficult to obtain very close to the horizon, and this effect is reproduced here.

However, because of the relationship between α and θ , the resulting reduction in the detection range has limited implications for the detectability. In Figure 5.2, this relationship was plotted for various altitudes. If the atmospheric effects limit α to the range $0.5^\circ \leq \alpha \leq 90^\circ$, a corresponding reduction in the maximum value of θ will occur. But for all altitudes, it can be seen that this reduction is very small – much less than one degree. In the GEO case, for example, for a reduction in the range of α by 0.5 degrees, the corresponding reduction in θ is 0.00033° . For a LEO altitude of 400 km, the same reduction in α gives a reduction in θ of 0.0061° . The resulting reductions in maximum aircraft detection ranges (L) are 54.75 and 54.12 km, respectively.

The result is that while signals from the aircraft cannot reliably propagate to the satellite in the last half degree above the horizon, the satellite can still detect signals from aircraft until virtually the limit of possible nadir angles.

5.3.7 Received power

The signal power level available at the position of the satellite is calculated as per equation 4.20 and is plotted as a function of nadir angle in Figure 5.11, for each of the orbital cases studied. This figure shows the curves for a transmitted power of 500 W. For 125 W transmitters, the received power is lower by a factor of 4.

The power is shown with a logarithmic axis. The plot includes the effects of free-space path loss, the radiation pattern of the transmitting antenna, and the atmospheric losses.

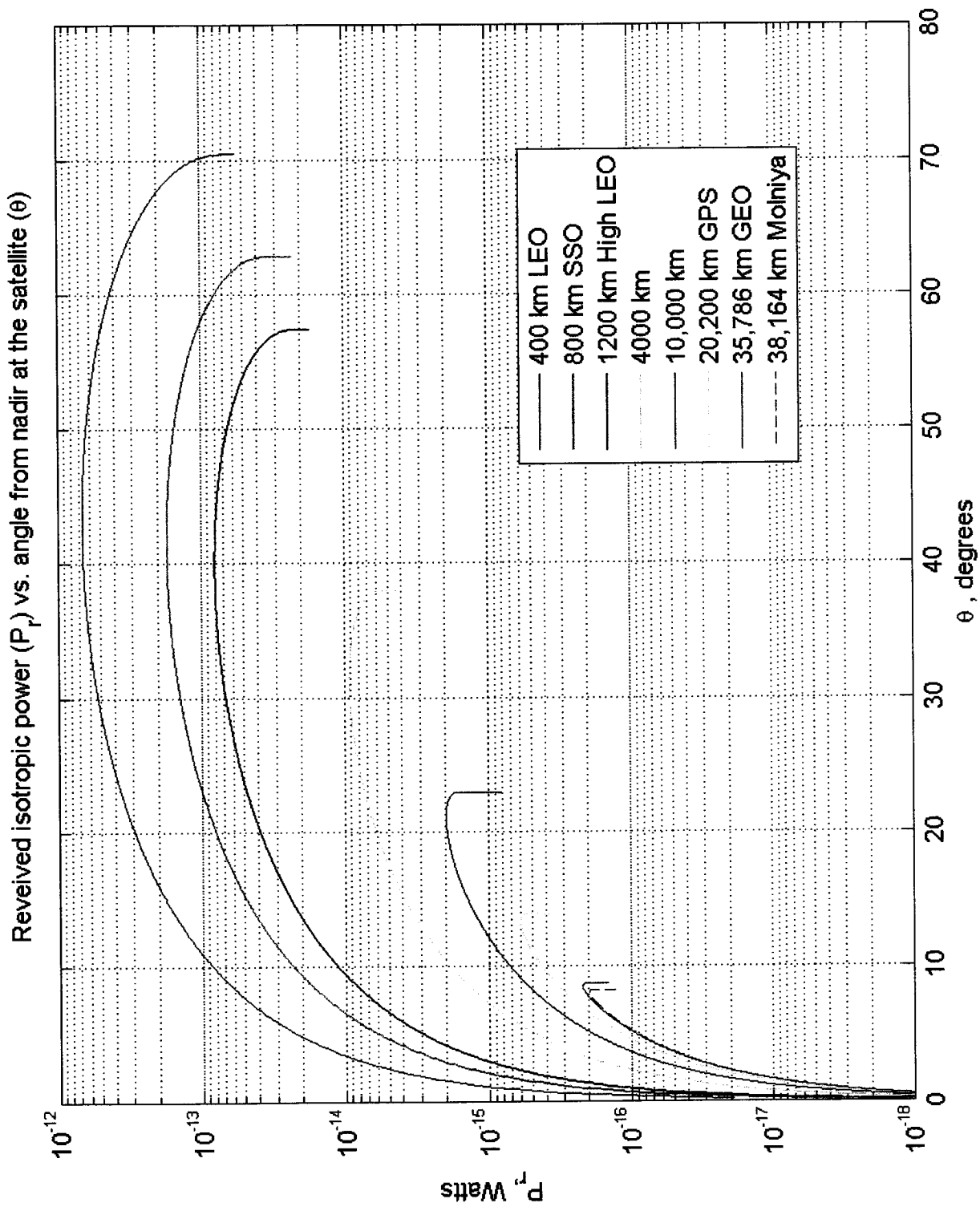


Figure 5.11: Received isotropic power vs. nadir angle θ

The power level decreases with increasing altitude, as expected. As before, the maximum nadir angle narrows with altitude as the angular radius of the Earth is reduced. In all cases, the power falls off rapidly just before the maximum angle, which is expected due to the rapid increase in atmospheric attenuation effects at these angles.

The angle at which peak power is received occurs well away from nadir in all cases. This is due to the radiation pattern of the transmitting antenna, modeled as a quarter-wave monopole with 3 dB loss (see section 4.4.1). This monopole has a null along the antenna axis, vertically above the aircraft. As a result, very little power is received from aircraft which are directly below the satellite, or nearly so. The strongest radiation from the antenna is in the horizontal (per Figure 4.7), corresponding to $\alpha = 0^\circ$, and thus to the maximum value of θ (per Figure 5.2). The peak signal power is not received at maximum angle from nadir, however, due to two effects. Firstly, as θ increases, so does the propagation distance (Figure 5.1), and thus the free-space path loss (Figure 5.4). This results in lower power at high angles from nadir. Secondly, the atmospheric effects are very minor until the elevation angle (α) becomes very low (see section 5.3.6), causing the power to fall off rapidly just before the maximum angle from nadir. These two effects, which reduce power at high values of θ , combine with the effect of the transmitter radiation pattern, which gives low power at low θ , to give a net peak power angle at a point between nadir and maximum θ for the altitude.

This point moves closer to the maximum nadir angle with increasing altitude. This results from the decreasing importance with altitude of the propagation length difference, discussed at section 5.2 and below.

With θ replaced by L , the power received as a function of aircraft range from the sub-nadir point can be inspected. A graph of this is shown in Figure 5.12.

For low altitudes, the power peaks strongly, and at relatively short ranges, falling off by roughly an order of magnitude by the maximum range. Again, this is due to the great effect the horizontal range has on the total propagation distance, when the vertical range (the altitude) is very small. Where the altitude is much larger in comparison to the horizontal range, this effect is reduced, and at higher altitudes, the peak is much weaker, with the range of received power levels smaller over large ranges of L .

In comparison to AIS signals, which are transmitted at 12.5 W on 162 MHz, the 500 W ADS-B signal is slightly weaker, having 88.3% of the received power, assuming the same antenna radiation pattern, and using equations 4.20 and 4.9. The value holds true at all altitudes, neglecting atmospheric effects which apply only at shallow

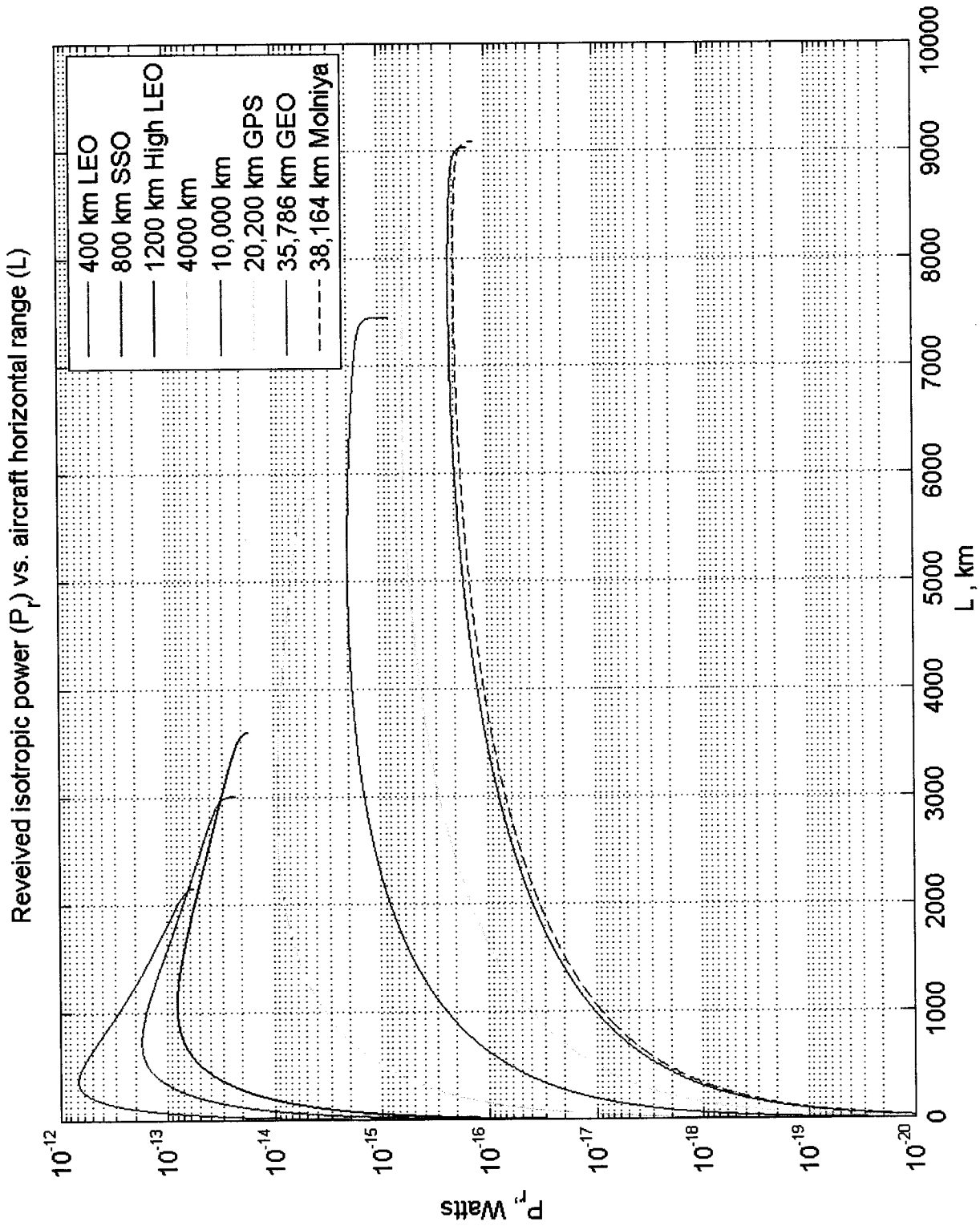


Figure 5.12: Received isotropic power (P_r) vs. aircraft horizontal range (L)

elevation angles. The lower received power despite higher-power transmission is due to the increased free-space path loss caused by the shorter wavelength.

5.3.8 Signal-to-noise ratio

The normalized signal-to-noise ratio, E_b/N_o , is a key metric for designing radio communication systems. As discussed in section 4.4.5, values of E_b/N_o of 7 to 10 dB are considered the minimum for reliable data transfer over radio channels, and the key variables which can be adjusted to affect E_b/N_o are the receiving antenna gain, the altitude of the satellite, and range of nadir angles observed. For the several altitude cases studied, the value of E_b/N_o , in decibels, is plotted as a function of nadir angle in Figure 5.13, using an ideal receiver with an isotropic gain of 1. Once again the transmitter power is set to 500 W; for the 125 W case the curves are identical, but 6 dB lower. As before, the presented result does not account for losses within the receiver. Instead, the curves give a value for the net gain needed at the receiver; gains or losses from the antenna, the antenna lead, or components internal to the receiver must be accounted for in the design of any system to receive these signals, using the link margins presented in this section as the design point.

The pattern of the plots in Figure 5.13 follow that seen in the graph of received power (Figure 5.11). This similarity is expected; with a gain of 1, the form of equation 4.21 follows that of the formula for received power (equation 4.20), with only constant factors in the denominator that act to scale the function vertically.

A horizontal line is included at $E_b/N_o = 7$ dB, and the level of 10 dB is also indicated. Using these as the guideline for minimum values of E_b/N_o , it can be immediately seen that for an altitude of 400 km, the ADS-B signal should be easily received with an antenna gain of only 1, at all nadir angles greater than 8.8° (using the 10 dB line). The performance is almost as broad at 800 km, beginning at 17.8° (again for the 10 dB criterion). At 1200 km, the case is marginal for the 10 dB criterion, but the 7 dB criterion is met over a broad range. For higher altitudes, a receiver antenna with an increasingly large gain is needed; the GEO and molniya cases fall, at their best, some 25 dB below the 10 dB criterion, necessitating a gain of at least this much on the receiver antenna.

The plot is given again in Figure 5.14, this time against aircraft horizontal range. The wide gain margin of the LEO cases is again visible, but the behaviour of the higher-altitude cases is now more readily seen. Over a broad run of aircraft ranges (L), the E_b/N_o curve at higher altitudes is comparatively flat; it does not experience large spikes, meaning that an antenna of a single gain value will have similar performance

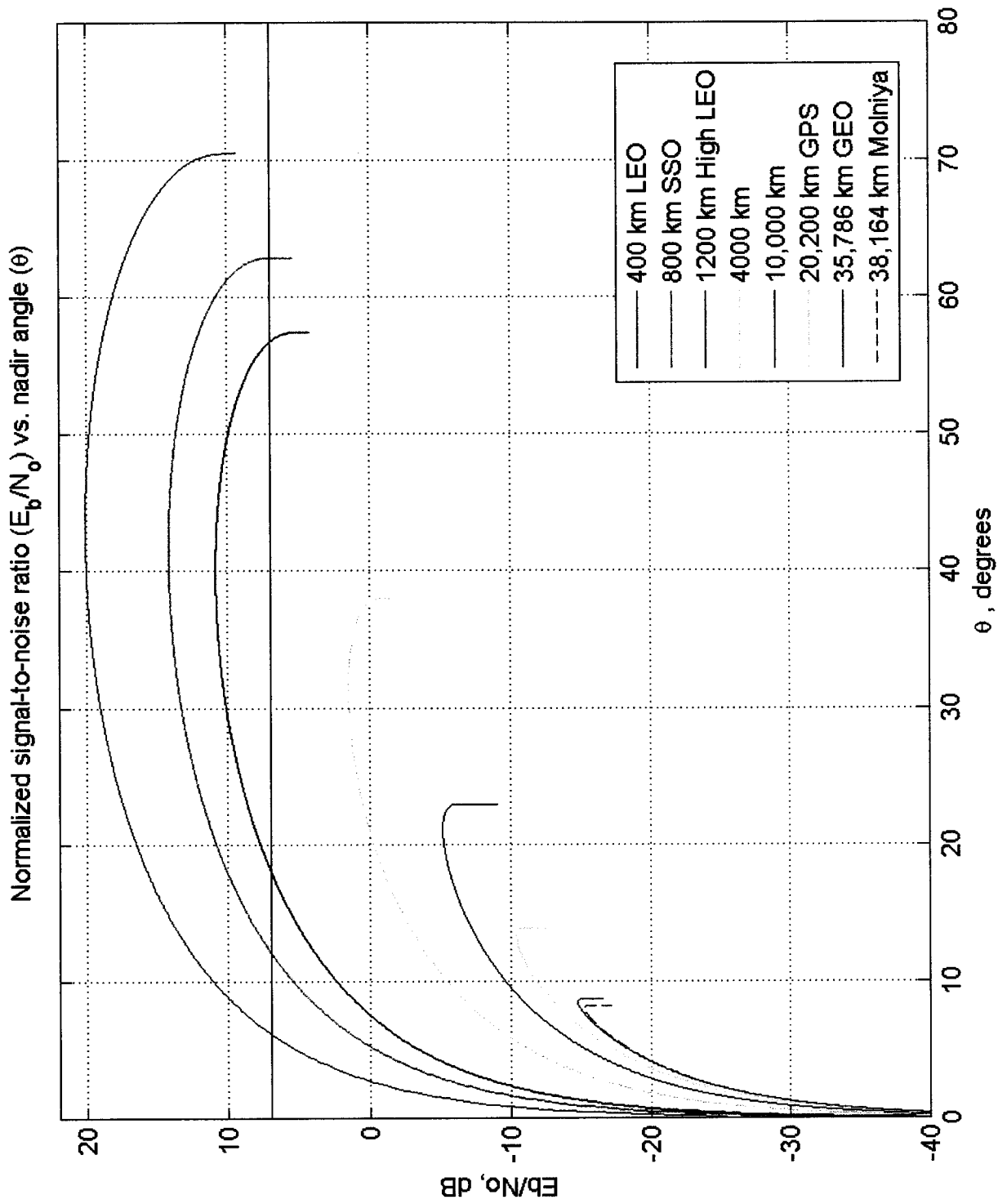
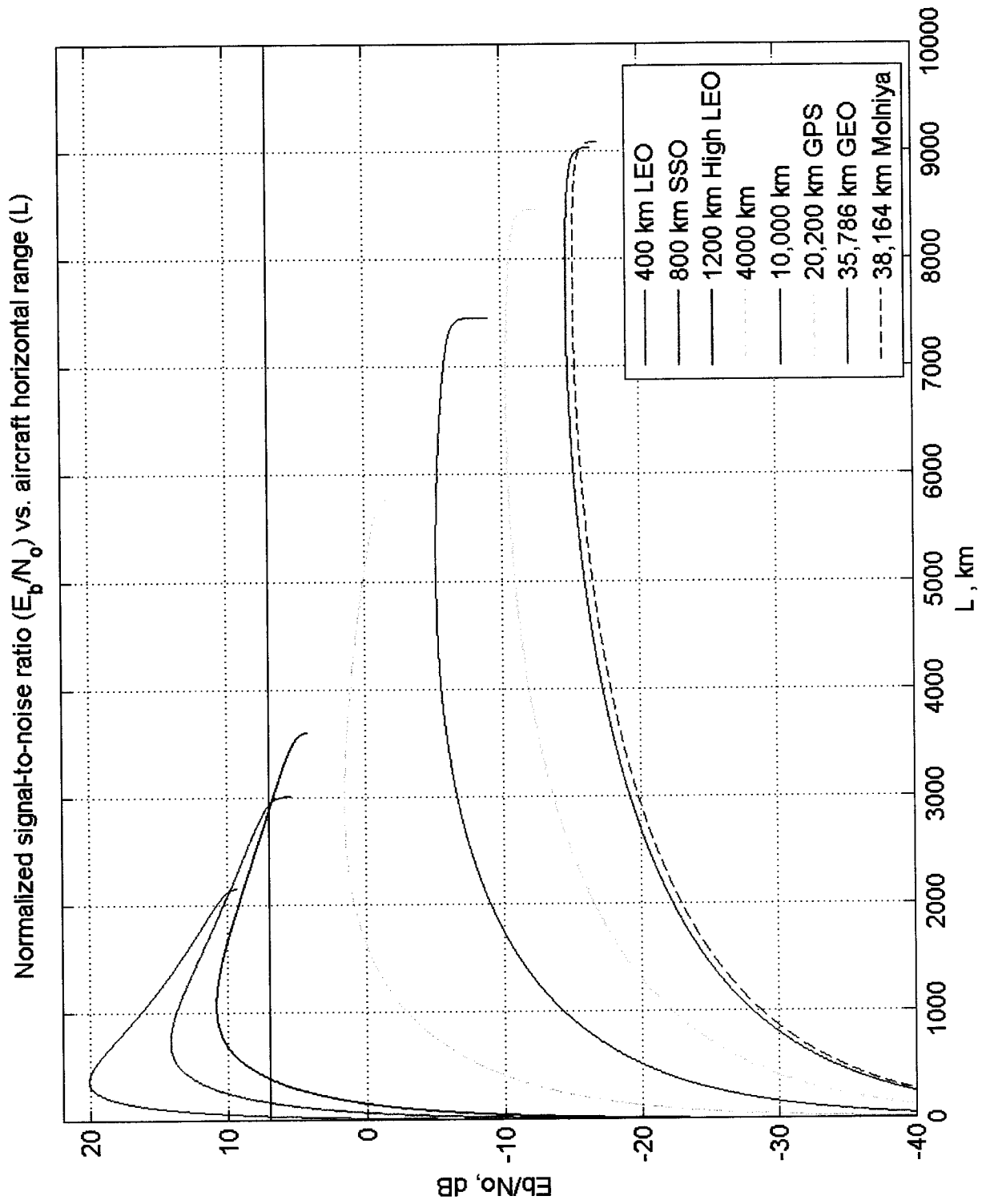


Figure 5.13: E_b/N_0 vs. nadir angle

Figure 5.14: E_b/N_0 vs. aircraft horizontal range

over a wide range of L . Thus, at high altitudes, while a high-gain antenna is needed, few restrictions on the detection range of the aircraft would exist due to compromises in antenna design. As usual, of course, aircraft directly below the satellite, or nearly so, are most difficult to detect, and this applies at all altitudes.

Nonetheless, the strength of the signal, before any receiver gain is assumed, is promising. The results are suggestive that a satellite mission to detect such signals from orbit is feasible. To further investigate that possibility, certain specific cases are discussed in the sections which follow.

5.4 The LEO case

At LEO altitudes, the detection range and the receiver antenna gain needed to detect the signal vary significantly with altitude. The central null due to the radiation pattern of the transmitting antenna is present, as always, but its width varies with altitude, and with the link margin criterion used. The parameters for the three altitude cases studied are given in Tables 5.1 and 5.3, for the case of an isotropic antenna with gain of 1 and a 500 W transmission power. These cases are plotted for E_b/N_o and detection range in Figure 5.15.

Table 5.1: Parameters for LEO orbits, 10 dB link margin criterion

Altitude (km)	Maximum detection radius (km)	Central null radius (km)	Central null diameter (km)	Orbital speed (km/s)	Time to cross null diameter (s)
400	2125	60	120	7.67	16
800	2100	256	512	7.45	68.7
1200	1685	689	1378	7.25	190

Table 5.3: Parameters for LEO orbits, 7 dB link margin criterion

Altitude (km)	Maximum detection radius (km)	Central null radius (km)	Central null diameter (km)	Orbital speed (km/s)	Time to cross null diameter (s)
400	2171	42	84	7.67	11
800	2938	170	340	7.45	45.6
1200	2883	393	786	7.25	108.4

Using the 10 dB criterion, the 400 km case gives the smallest null and largest detection range. But as can be seen from Figure 5.15, the higher-altitude cases give detections at much larger ranges, for lower signal strength. Addition of a gain of 3 to 5 dB at the receiver would significantly change the ranking of the altitude cases. As shown in Table 5.3, if the 7 dB link margin criterion is used, the greatest detection range is found at the 800 km case. This 7 dB margin would become 10 dB with the addition of a receiving antenna having 3 dB of gain over the isotropic case. With

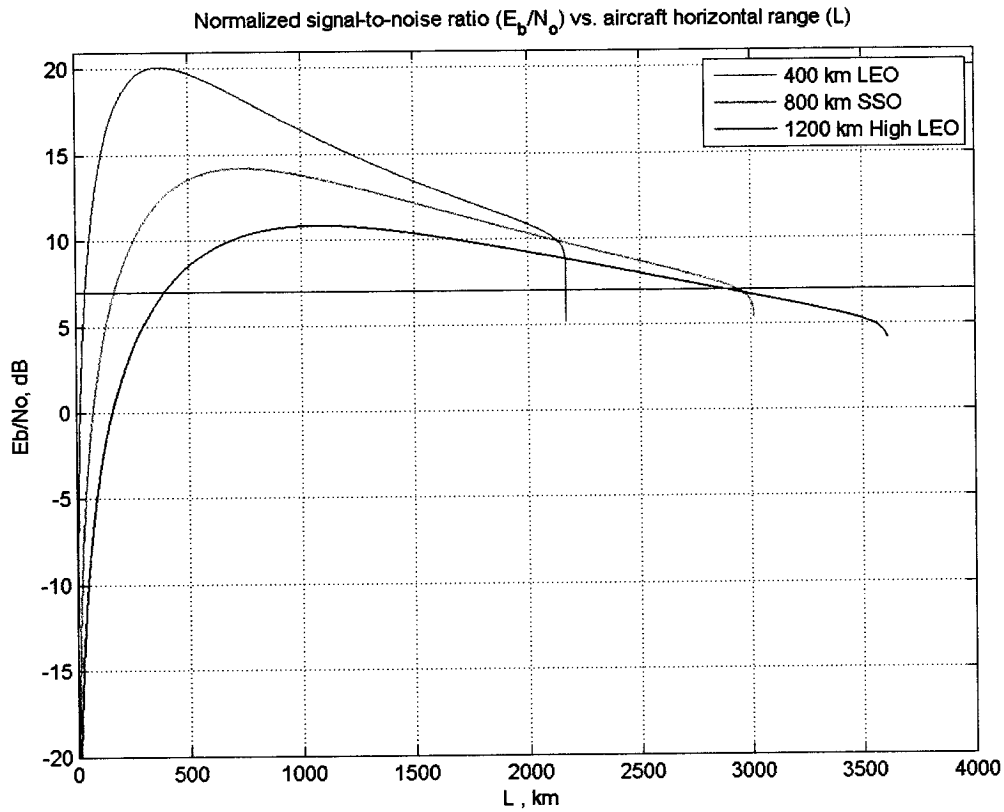


Figure 5.15: Range and signal strength comparison for LEO orbits

a uniform gain of 5 dB at the receiver, the greatest range is found with the highest orbit.

Of course, truly isotropic gain is difficult to achieve, so any real antenna will affect the shape of these curves. It may enhance reception at some nadir angles and ranges, while reducing it in others. For example, in Figure 5.16, the link margin for a satellite altitude of 400 km is shown, for both the isotropic case, and for a quarter-wavelength monopole with an efficiency of 0.5. In this case, because the receiving monopole has a null at nadir, reception performance at nadir is reduced, so the minimum detection range has increased. For the 10 dB criterion, the gap radius has expanded from 60 to 161 km. At large aircraft ranges, however, the performance has improved compared to the isotropic case. These characteristics will vary with the antenna type selected and with the altitude, making antenna design and selection a key element of designing an ADS-B detection space mission. The prospect of polarization losses will be an additional consideration in the selection and design of the antenna for such a mission.

Another feature of the LEO case is that, due to the orbital motion of the satellite

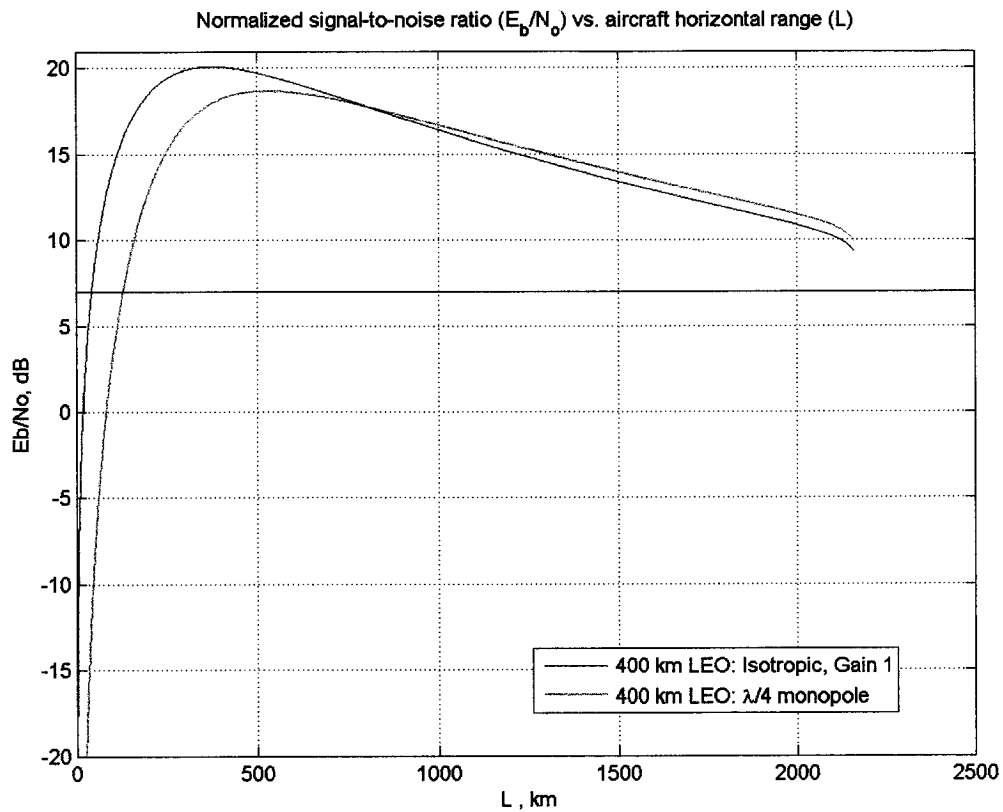


Figure 5.16: Comparison of antenna cases at LEO

with respect to the Earth, the position of the central null, where aircraft cannot be detected, is constantly in motion. The actual motion of this zone, as projected on the surface of the Earth, is due to the orbital velocity as well as the rotation of the Earth. The vector sum of these will depend on the altitude and inclination, and, within an inclined orbit, on the true anomaly. However, the orbital velocity, as found in Tables 5.1 and 5.3 (Wertz & Larson, 1999) is the dominant factor, since the contribution from the Earth's rotation is no more than 0.46 km/s, the rotational velocity of the Earth at the equator.

At the orbital speed of a satellite in LEO, the satellite will travel a distance equal to the diameter of the detection null in the corresponding time given in Tables 5.1 and 5.3. This means that, neglecting the much slower motion of the aircraft, the gap in detection for any individual aircraft will be no longer than that time, and will only reach this duration when the satellite passes directly overhead. While an operational air traffic surveillance system may require near-continuous surveillance, it is possible that occasional gaps in position information of a few seconds would be acceptable in

the system design. The length and frequency of these gaps is strongly affected by altitude and receiver antenna radiation pattern, and may be a significant driver for the design of an orbital ADS-B detection mission.

A visualization of the relative size of the detection area and central null is given in Figure 5.17. The image shows the geometry of the detection area for a satellite at 400 km altitude and with an isotropic antenna. The area shaded in blue is the detection field, in which ADS-B signals are detected with a link margin of 10 dB or greater. The area shaded in red is the central null, in which signals are not detected.



Figure 5.17: Detection region (blue) and central null (red) for a satellite at 400 km. Receiver gain 1.

5.5 The GEO case

The E_b/N_o curve for the case of geostationary orbit shown in Figure 5.14 falls, at all points, more than 20 dB below the 10 dB level. The signal, therefore, fails the 10 dB (and the 7 dB) criterion for reliable detectability, at 500 W and a gain of 1 (0 dB). To detect this signal, a highly directive antenna having a gain on the order of 30 dB is needed. Several choices of antenna design are possible; one example is a parabolic reflector. Such antennas are frequently carried on geostationary communications satellites. Using equation 4.22, with a conservative antenna efficiency of 0.5, the necessary diameter of a parabolic antenna for a 30 dB gain is found as 1.96 metres.

Parabolic antennas of 2 metres in diameter are frequent features of geostationary satellites. For example, the Canadian commercial telecommunications satellite Anik F2, launched in July 2004, carries two 2.16 m antennas, along with several other reflectors with diameters ranging from 0.51 to 1.40 m (Rao, 2003). Such antennas can be accommodated in conventional launch vehicles serving geostationary orbits, such as Ariane 5. The usable volume of that launcher's payload fairing has a diameter of 4.57 m (Arianespace, 2008).

Using the procedure given by Orfanidis (2008) (see section 4.4.6), a parabolic antenna of 1.96 m diameter and an F/D ratio of 0.25 has a radiation pattern with a central lobe as shown in Figure 5.18. The plot is shown only across the portion of the central lobe which is oriented towards the Earth, limiting it to an angular radius of 8.7° . The gain is normalized, with a value of 1 assigned to the point of highest gain.

With this antenna pattern and a gain of 30 applied to the receiver, a new plot of E_b/N_o is prepared, and shown in Figure 5.19 alongside the original plot with a 0 dB gain and isotropic receiver, and showing the 7- and 10-dB cutoff lines. The antenna orientation is with the axis of the central lobe at nadir.

The effect of the antenna is threefold. The link margin is increased, such that it peaks as high as 11.0 dB, occurring at a range of 6119 km. Because the strongest receiver gain is at nadir, and the strongest received signals are far from nadir, the curve is also flattened, giving a more constant gain across a large range of L . This also has the effect of reducing the minimum range for detection. With the 10 dB criterion, this occurs at 3821 km; for 7 dB, at 2237 km. Signals at smaller ranges from the sub-nadir point cannot be reliably detected due to the vertical null of the transmitting antenna, despite the strong receiver gain at nadir.

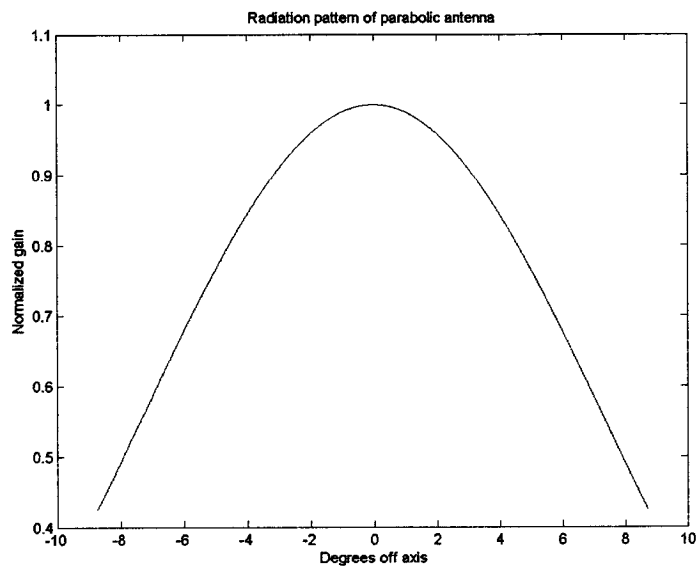


Figure 5.18: Central lobe of parabolic antenna radiation pattern

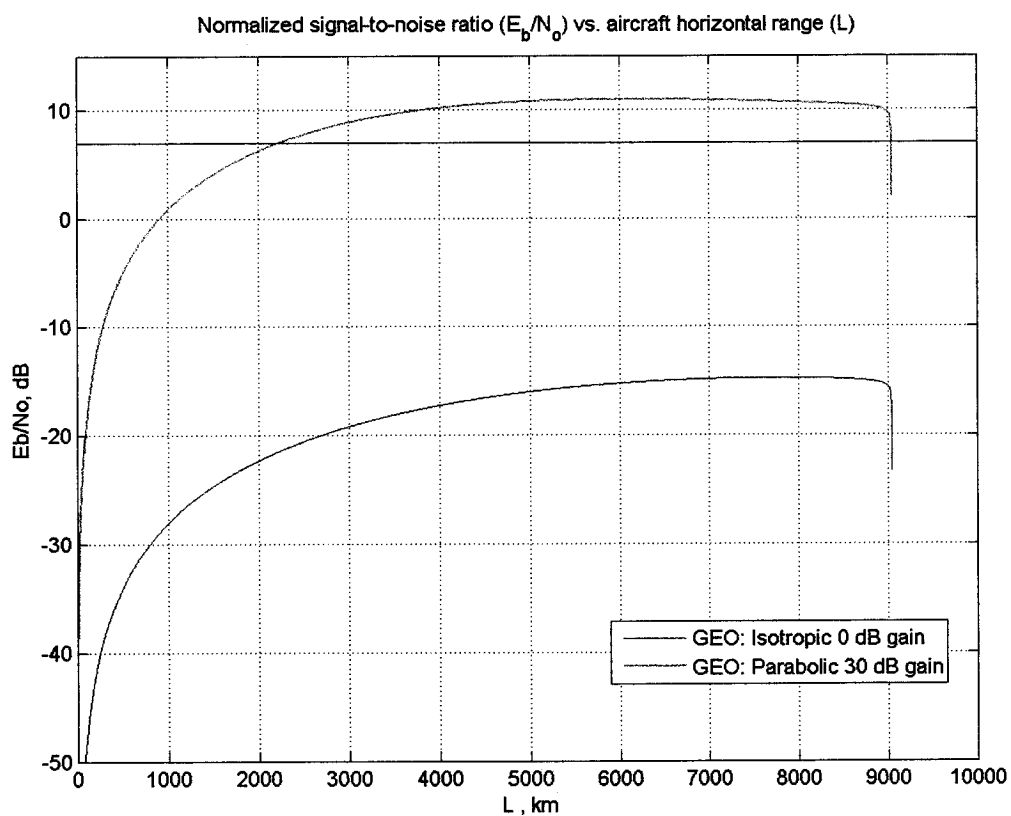


Figure 5.19: Performance of 1.96 m parabolic antenna at geostationary altitude

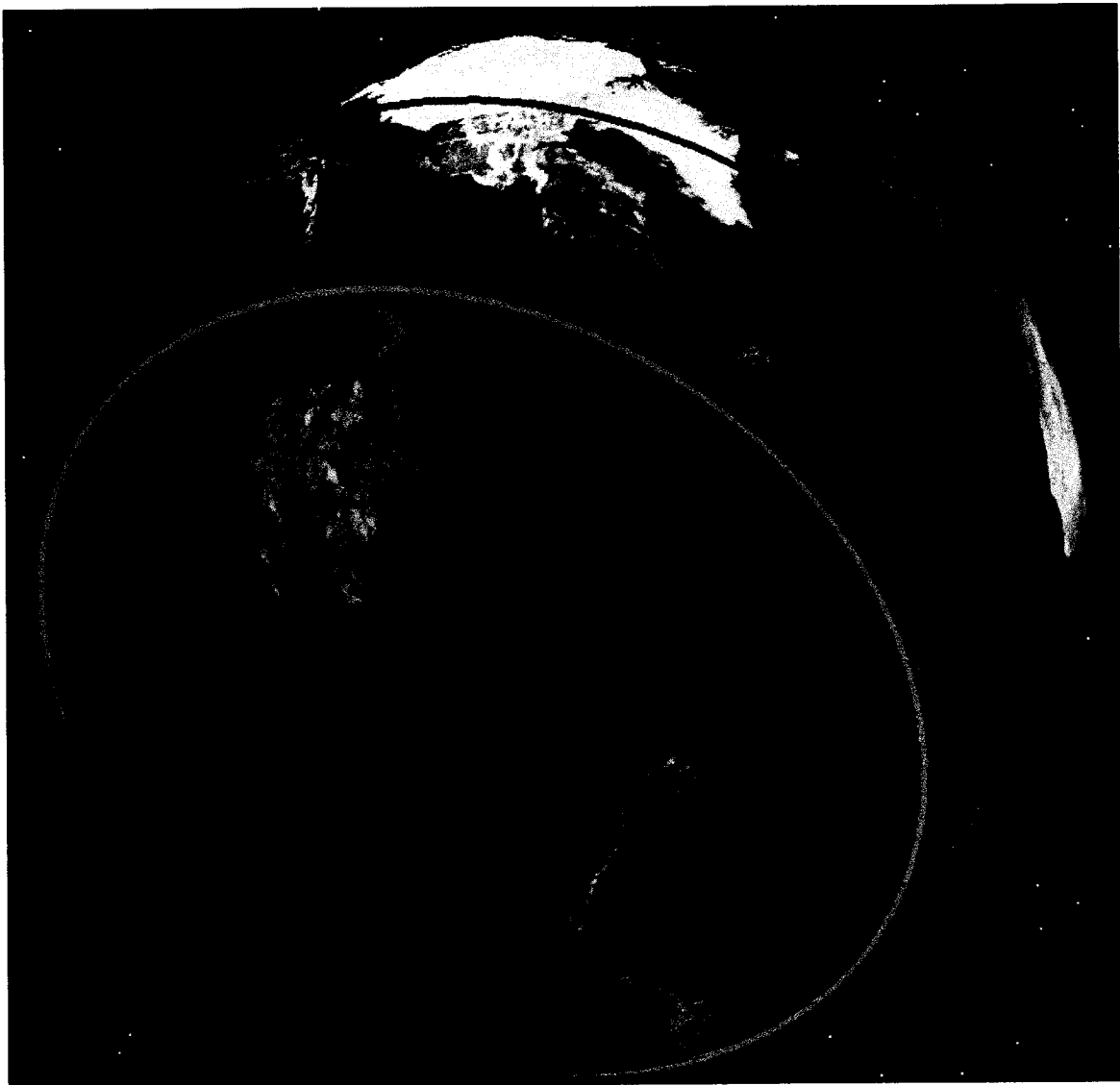


Figure 5.20: Detection area for GEO case: 100°W longitude

For a geostationary satellite at a longitude of 100° west, this geometry is shown in Figure 5.20. In this figure, the red boundary indicates the minimum range for detection; the solid line for the 7 dB case, the dashed line for 10 dB link margin. The green boundary indicates the maximum range for detection, for which the 7 and 10 dB cases are too close together to show separately in this image. The blue line indicates the range for maximum signal strength. The given values are for a signal power of 500 W. A 250 W signal is 3 dB weaker at the receiver, and thus the 10 dB line shown is also the 7 dB line for 250 W transmitters. Signals transmitted at 125 W have, at the peak, a 5 dB link margin; these do not meet the link margin criteria with the selected antenna.

It can be seen from Figure 5.20 that the area of coverage is suited to monitoring air traffic in Canadian domestic airspace and on the oceanic approaches to Canada. Virtually all of Canada falls within the detection area, with the exception of the most northerly portions of Ellesmere and Axel Heiberg islands. The locus of peak signal power passes through the Canadian landmass, and near several key areas. It crosses the Maritime provinces, and passes a few degrees north of Quebec, Montreal, and Ottawa. It crosses the James Bay, placing it close to the current ADS-B service region in Hudson Bay. Passing a few degrees north of Winnipeg, it lies almost directly over Edmonton, and crosses Vancouver Island. Most of Canada's major airports, therefore, including Calgary, lie within 5 degrees of arc of the peak reception locus. Notably, Toronto and its nearby airports are somewhat farther from the peak, but well within the 10 dB margin. A single satellite in this orbit, then, could receive signals from ADS-B-equipped aircraft virtually anywhere in Canada, with the most reliable reception in areas very close to the concentration of Canadian air traffic.

While control of air traffic rests at the national level with Nav Canada, airspace monitoring and continental aerospace defence are conducted jointly by Canada and the United States through the North American Aerospace Defense Command (NORAD). Nearly all of the United States lies within the 10-dB detection area, with the exception of portions of the most southerly states and extreme points of Alaska. Even the Hawaiian Islands (see Figure 5.25) are within the coverage area, as is the airspace between them and the continental states. The southern states are well inside the 7-dB detection area, as is nearly the entire Gulf of Mexico, where the FAA has begun deploying ADS-B ground stations on oil platforms (FAA, 2007). With regards to air defence in particular, the entire Canadian Air Defence Identification Zone (ADIZ), shown in Figure 5.21, lies within the detection region.

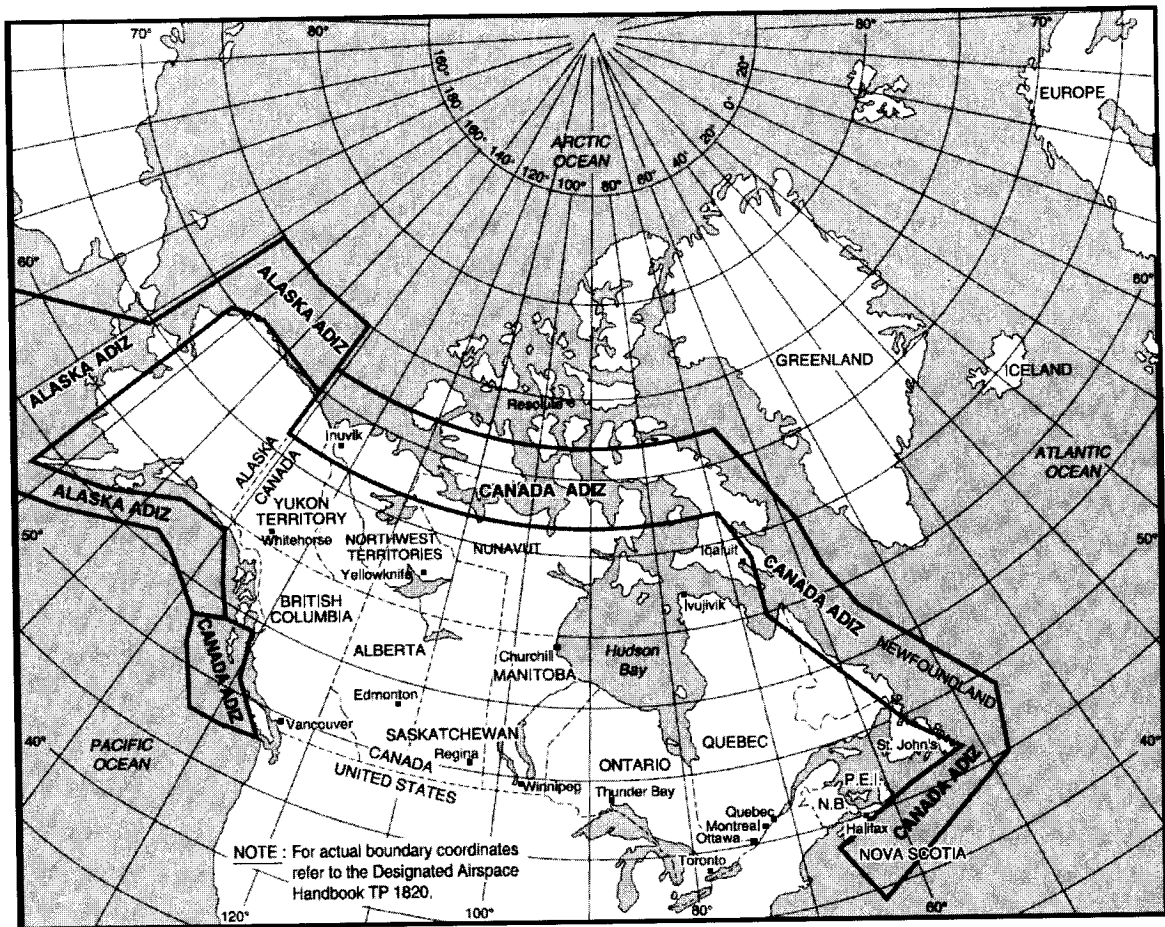


Figure 5.21: Canadian Air Defence Identification Zone. Figure from TC AIM (2009). Reproduced with permission of the Minister of Public Works and Government Services Canada, 2010.

Beyond North America, ICAO has delegated control of a portion of the airspace over the North Atlantic ocean to Canada. This region, the Gander Oceanic Control Area (CTA), is shown in Figure 5.22.

The boundaries of the Gander Oceanic CTA and its associated Flight Information Region (FIR) are given in the Designated Airspace Handbook (DAH) (DAH, 2010). Using these, the region is plotted on the surface of the Earth, with the result shown in Figure 5.23. The entire Gander Oceanic CTA lies within the area of coverage for the 10 dB link margin criterion, with the satellite at 100° W.

A geostationary satellite does not only have visibility of the northern hemisphere. In Figures 5.24 and 5.25, the coverage of South America and of the Pacific Ocean are shown. In these images, as before, the green boundary shows the maximum range for detection, the blue line the locus of peak signal strength, and the red boundary the minimum range for detection at 10 dB link margin (dashed) and 7 dB (solid).

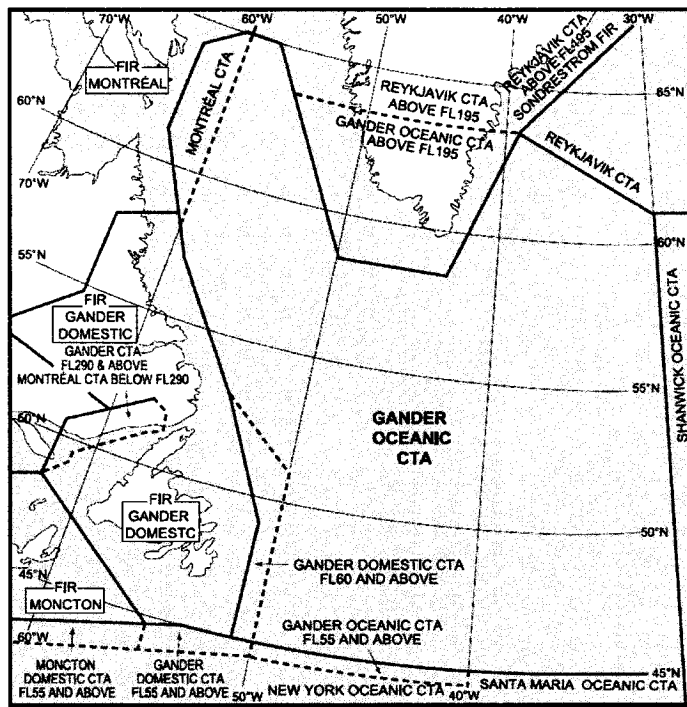


Figure 5.22: Gander Oceanic Control Area. Figure from TC AIM (2009). Reproduced with permission of the Minister of Public Works and Government Services Canada, 2010.



Figure 5.23: Position of the Gander Oceanic CTA within the area of coverage

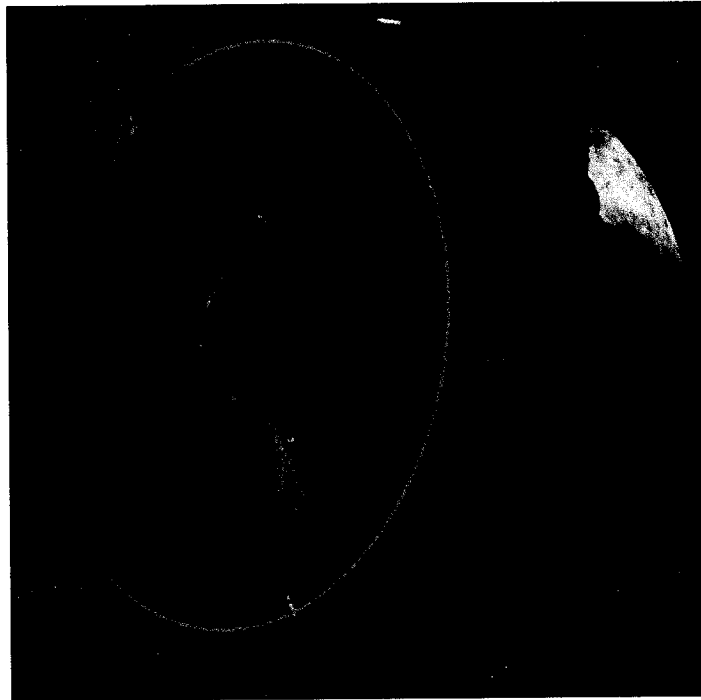


Figure 5.24: ADS-B coverage over South America for a geostationary satellite at 100°W

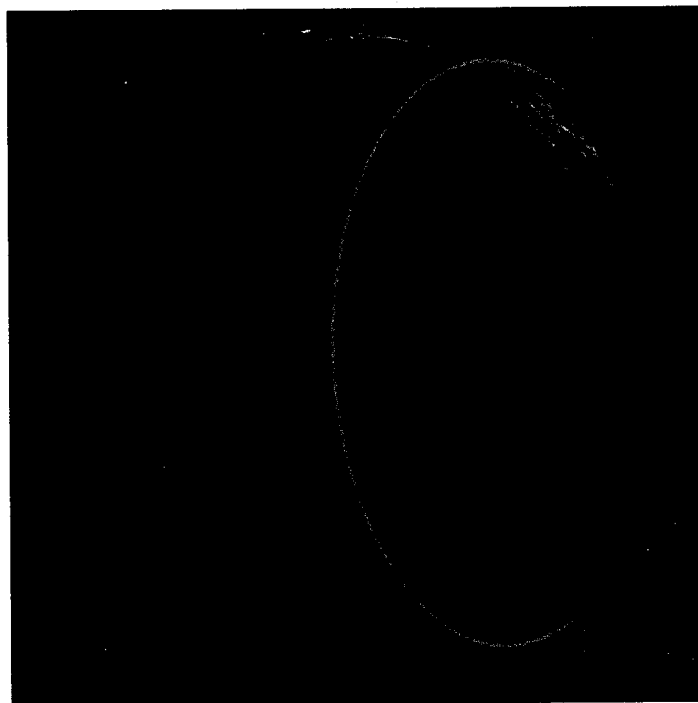


Figure 5.25: ADS-B coverage over the Pacific Ocean for a geostationary satellite at 100°W

5.6 Constellations and hybrid systems

While a satellite in GEO at 100° W provides very good coverage of Canada and other regions, there are limits to the coverage offered by a single spacecraft. To provide coverage with a larger extent, or to provide continuous coverage of a defined area over time, it may be necessary to deploy a system of several satellites, or to combine orbital sensors with other assets. Continuous temporal coverage is desirable for air traffic monitoring, allowing aircraft to be reliably tracked without fear that position information will suddenly become unavailable. Continuous spatial coverage is useful for monitoring large areas, and ensuring that aircraft remain under surveillance for the whole duration of their flight.

A satellite in any chosen orbit has limitations. For example, in LEO, any single satellite has a field of view with a radius ranging from approximately 2000 - 3000 km (see section 5.4, in particular Figure 5.14). The actual detection area will depend on the receiver antenna design, the altitude, and the link margin necessary. These factors can be variously balanced to come to a design of a constellation to cover, continuously, any chosen area on the surface of the Earth. Due to the motion of the satellites, no area can have continuous coverage without the availability of multiple satellites.

At GEO, a single satellite can provide continuous temporal coverage, but a much larger antenna is needed, and even for a parabolic reflector with a diameter of 2 m, weaker signals may not be detectable. The coverage for a satellite at 100° W is very good for Canada and the western North Atlantic airspace, but to provide continuous tracking of a flight which takes off in North America and lands in Europe, either the satellite must be relocated to a position better favouring the Atlantic, or coverage must be extended with a second satellite positioned over longitudes suitable to cover Europe. In the former case, coverage over the Pacific and western North America will be reduced, and a coverage gap will exist over the equatorial latitudes of the Atlantic ocean. In the latter case, sufficient overlap of the detection areas will be needed to ensure that the full area traversed by aircraft on intercontinental flights is covered.

The GEO constellation can be extended from two satellites to a larger number, to provide extended or even near-global coverage. The coverage gaps at satellite nadir, near the equator, can be eliminated by overlapping the coverage of adjacent satellites in the constellation. The angular width of these gaps is shown in Figure 5.26, in terms of γ , the Earth central angle between the satellite and aircraft (see Figure 4.3). Along the equator, γ is equivalent to longitude.

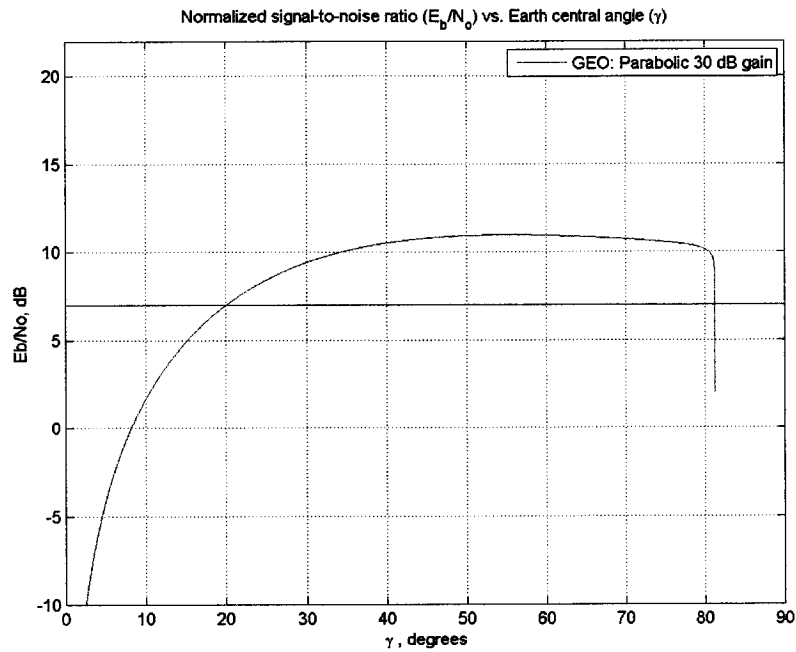


Figure 5.26: Variation in received signal strength with angular separation

To completely eliminate gaps near the equator, the coverage must be overlapped such that the furthest extent of the coverage of a satellite extends beyond the extent of the gap of the adjacent one, as shown in Figure 5.27.

This places a limitation on the longitudinal separation of the satellites, which in turn gives a lower limit for the number of satellites needed for continuous coverage across all longitudes. These values are shown in Table 5.5.

Table 5.5: Parameters for GEO constellation, with elimination of low-latitude coverage gaps

Link Margin	Max γ for detection	Min γ for detection	Max satellite longitudinal separation	Satellites for coverage across all longitudes
10 dB	80.5°	34.3°	46.2°	8
7 dB	81.2°	20.1°	61.1°	6

While such a system of satellites would provide continuous coverage at equatorial and mid-latitudes, no GEO constellation can provide coverage at the poles. At the

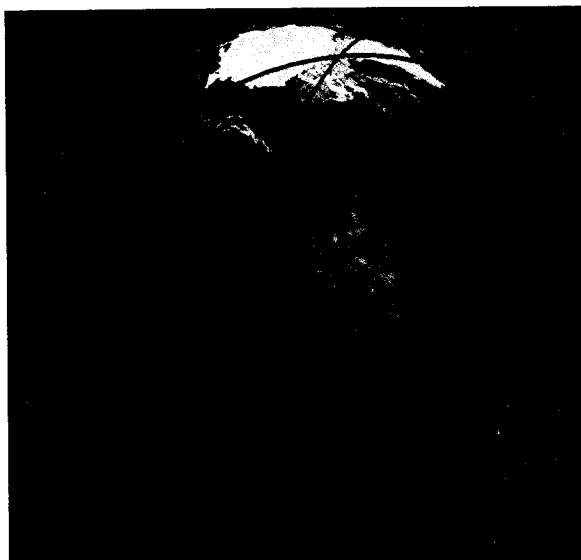


Figure 5.27: GEO constellation arrangement strategy

longitude of each satellite, the maximum latitude for detection is equal to the maximum value of γ . This latitudinal range is diminished at longitudes other than that of the satellite, and even at the satellite longitude the coverage does not reach the pole. As a result, gaps exist near the poles, of the form shown in Figure 5.28. The southern boundary of the gap region varies between 80.5° N and 79.7° N (for the 10 dB case); an equivalent gap exists at the south pole.



Figure 5.28: Polar detection gap in the GEO constellation with 10 dB link margin

If it is necessary to provide air traffic surveillance within ten degrees of the pole, the GEO constellation could be augmented with satellites in other orbits. A satellite in molniya orbit requires a similar antenna to that in GEO; two such satellites could provide continuous coverage of the pole, including an area much larger than the gap shown. Alternately, sensors could be deployed on highly-inclined LEO satellites, or at higher altitudes below GEO. Such satellites might augment a GEO constellation which has full longitudinal coverage, to give a complete global network, or one which has only limited coverage, if it is desirable to provide surveillance over only a certain portion of the Earth's surface. These lower-orbiting satellites could transmit their data directly to ground stations, or relay it via the GEO satellite, or by another data relay system.

A further option is to mix satellite coverage with deployment of ground stations, in areas where this is possible. Depending on the area of interest, such a mixed deployment may reduce the cost and complexity of the constellation needed.

5.7 The stratospheric balloon case revisited

The same methodology used to analyze the signal propagation to a sensor at orbital altitudes can be used for the propagation to lower altitudes. Figure 5.29 gives the link margin as a function of aircraft range for a balloon-borne sensor at 30 km altitude. A quarter-wave monopole with an efficiency of 0.5 is used at the receiver. As usual the aircraft is assumed to be at an altitude of 10 km.

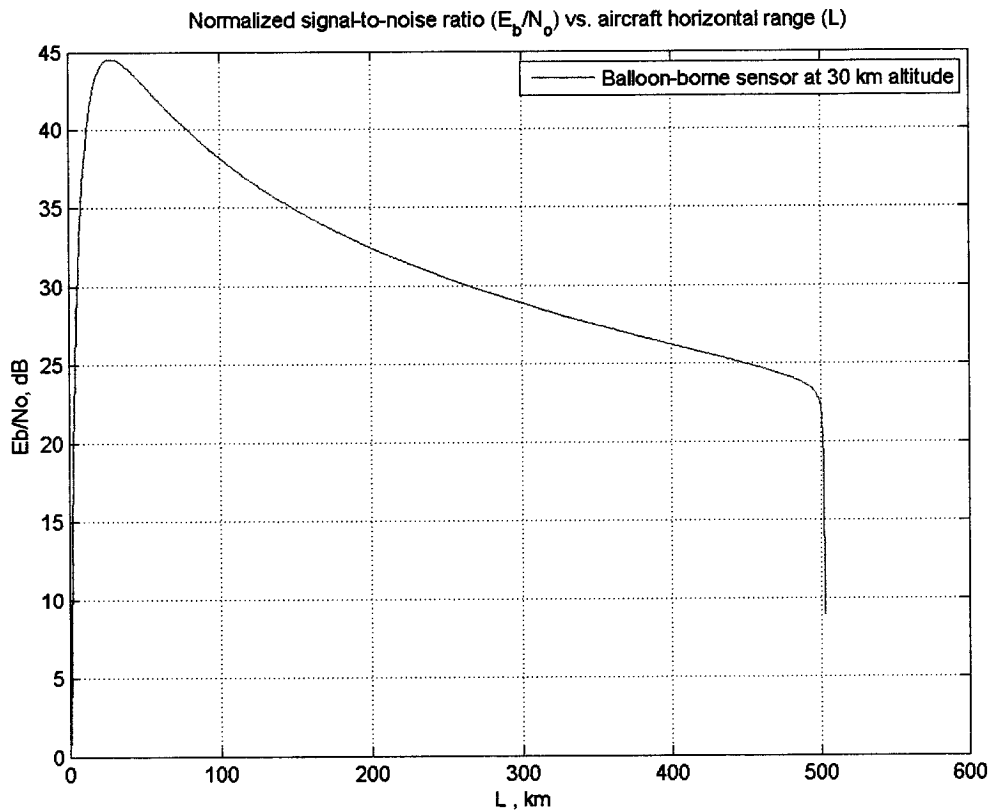


Figure 5.29: Link margin vs. range for a balloon-borne sensor at 30 km

Across ranges from 0 to 503 km, there is no question of having sufficient link margin, with values ranging from 20 to nearly 45 dB. The limiting factor is only the limb of the Earth – aircraft behind it are not in view. As with the satellite cases discussed in previous sections, atmospheric effects are seen in the very farthest ranges before the Earth's limb.

The result is a maximum detection range of approximately 500 km. As a comparison, the FLOAT-2 balloon reached a maximum altitude of 28.3 km, slightly lower than this example. It however did not remain steadily at that altitude, reaching it

only briefly at the end of the balloon's ascent, followed by the burst and descent by parachute. Most of the flight, therefore, was spent at much lower altitudes, and correspondingly smaller detection ranges were achieved, with typical maximum distances on the order of 200 km, and some detections beyond this range. FLOAT also used a full-wave monopole antenna, which has gain lobes directed away from the horizontal (Orfanidis, 2008), emphasizing reception at smaller ranges than with the quarter-wave antenna in this example. The 500 km limit, for a 30 km altitude, reinforces the conclusion that atmospheric (likely ionospheric) refraction was responsible for the longest-range detections observed by FLOAT-2, one of which was beyond 500 km, at an altitude of 12.3 km. (See details at section 3.5.1.)

The result for 30 km is extended in Figure 5.30 to two higher altitudes. The highest of these, 53 km, is the highest altitude ever reached by a stratospheric balloon (Yamagami, 2003). The plot shows that maximum aircraft detection range for a balloon at 40 km is 615 km; at 53 km, this is extended to 736 km. Sensors at these altitudes have large gain margins; they do not require large or directional antennas. And, since they cover a smaller area, the risk of signal collisions is reduced compared to satellites with large coverage areas.

It is possible, then, that balloon-borne sensors – realized as long-duration aerostats – might serve a role in monitoring air traffic. To compare them to the satellite cases, Figure 5.31 shows the 53-km balloon case, with a monopole antenna, alongside a satellite in an 800 km sun-synchronous orbit (SSO) with an isotropic antenna of 0 dB gain, and a GEO case with the previously-analyzed 2-metre parabolic antenna.

Sensors on each of these platforms have different fields of view. Depending on the application, one or the other may be chosen to give the needed performance, in light of the signal power, area of coverage, and traffic density for the given application. It may well be that a complete operational system for ADS-B-based air traffic monitoring will make use of the complementary performance of satellites in various orbits, and of aerostats, in addition to ground stations.

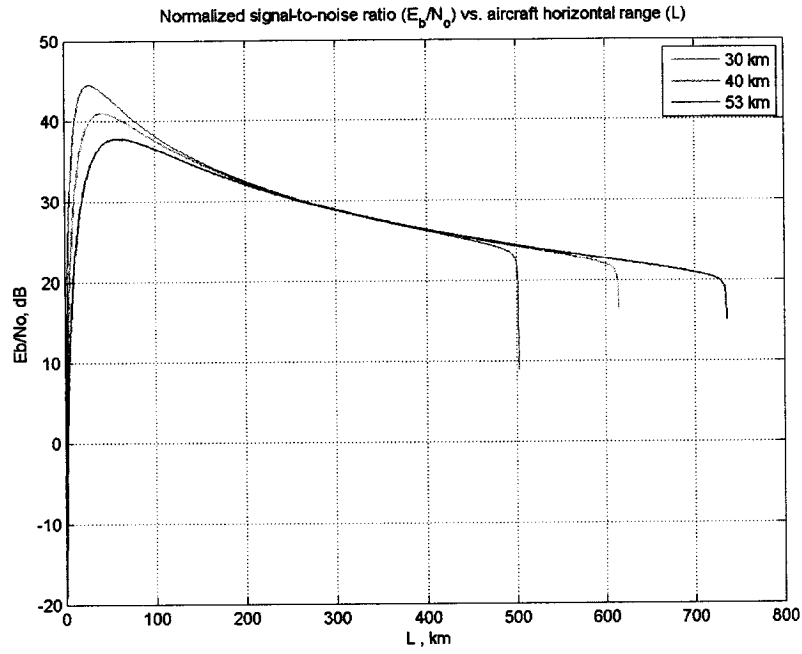


Figure 5.30: Comparison of reception ranges for various balloon altitudes

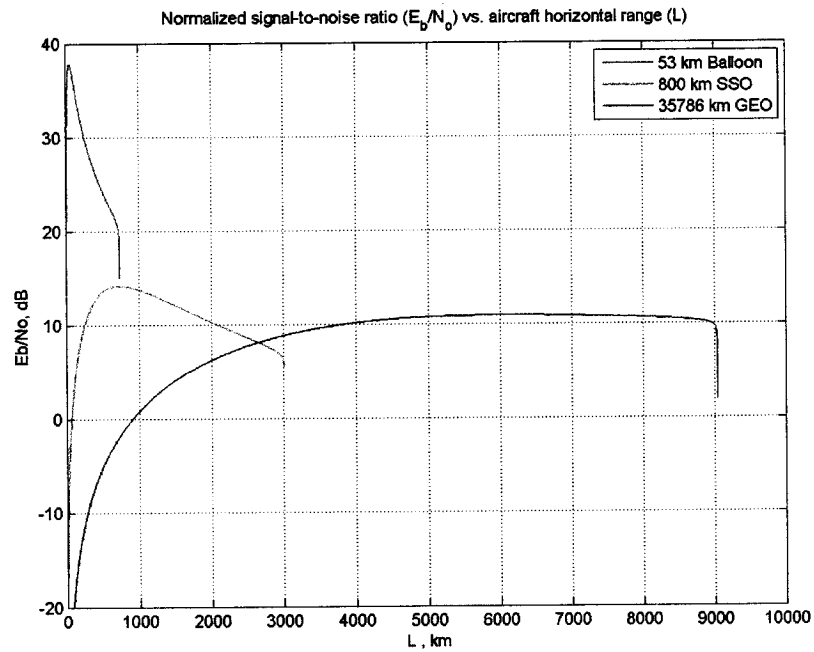


Figure 5.31: Comparison of link margin and range for stratospheric and orbital platforms

5.8 Doppler effect

For a satellite in a circular Earth orbit at 400 km altitude, the orbital velocity is 7.669 km/s (Wertz & Larson, 1999). For an aircraft at 10 km altitude, and a spherical Earth of radius 6378 km, equation 4.29 gives an equivalent satellite velocity of 7.227 km/s (v_{equiv}).

The Earth's rotational velocity at the equator, using the same radius and an angular velocity of 2π radians per day, is 0.464 km/s (v_g at the equator). This value can be multiplied by the cosine of the latitude to obtain the rotational speed at other positions on the Earth's surface.

A typical cruising speed for a common intercontinental airliner, the Boeing 777-300, is Mach 0.84 at 35,000 ft (Boeing, 2007), or 896 km/h (Air Canada, 2009), equivalent to 0.249 km/s. Neglecting the motion of the atmosphere relative to the Earth, this airspeed can be taken as a groundspeed, and thus as v_{air} .

The greatest possible velocity difference, and thus Doppler shift, occurs when the relative velocity between the aircraft and the satellite are greatest. This case occurs when Earth's motion and that of the aircraft are aligned, and the satellite is traveling in exactly the opposite direction. This geometry is possible for an aircraft flying eastbound along the equator, and a satellite in a retrograde equatorial orbit. This improbable arrangement provides the maximum possible Doppler shift. The minimum possible Doppler shift will occur in the converse case, when the motion vectors of the Earth's surface, the aircraft, and the satellite are all aligned and traveling in the same direction to minimize the relative motion velocity. This occurs for a satellite in a prograde equatorial orbit observing an aircraft flying eastbound on the equator. All other geometries reduce one or more components of the contributing velocities, and result in a relative velocity (and Doppler shift) which lies between these two extremes. Solving the equation using these extreme cases, with all vectors aligned, not only places boundaries on the problem, but also eliminates the need to solve the equation vectorially.

With a satellite at 400 km, for the case of maximum possible Doppler shift, using equation 4.25 with $u_{sat} = v_{equiv}$ and $u_{air} = v_g + v_{air}$, gives a frequency shift of 28.9 kHz. For the case of minimum shift, the result is 21.7 kHz.

In the GEO case, the satellite equivalent velocity is equal to the Earth's rotational velocity, since the Earth and the satellite have the same rotational period. As a result, the only contribution to the velocity difference (and thus to the Doppler shift) is from the motion of the aircraft relative to the Earth. Using the same value for v_{air} results

in a frequency shift ± 0.905 Hz.

The transmission requirements for ADS-B over the 1090 MHz ES are specified in DO-260B (2009), and noted in section 4.2.3.2 above, as requiring signals to be transmitted on a frequency of 1090 ± 1 MHz. Potentially, the variation in the frequency of transmitted signals will be 5 orders of magnitude greater than the maximum Doppler shift observed on orbit, and 9 orders of magnitude greater than that observed from a geostationary platform. It is possible that real equipment, as built and operated, operates with a greater precision in frequency than the standard (or less), but the signal shift from the Doppler effect remains very small. Even absent transmitter variability, a shift of 0.9 Hz to 29 kHz may be difficult to discern in a 1.09 GHz signal.

As a result, Doppler shifting of the ADS-B signal is unlikely to present a difficulty in receiver design.

5.9 Signal collisions

Squitters have a duration of $120 \mu\text{s}$ (see section 4.2.2). The maximum number of messages transmitted per second is 6.2 (see section 4.2.3.3). Thus, within a single second, the total duration of time occupied by transmissions from a single aircraft is

$$6.2 \times 120\mu\text{s} = 744\mu\text{s} \quad (5.1)$$

This time is spread out across several individual messages, spanning the duration of one second, including at least two position messages and two velocity messages, if the aircraft is airborne (see table 4.1), with the balance being aircraft identification messages and event-driven squitters.

Complete information about a previously-untracked aircraft requires reception of one of each type of message, and regular reception of the airborne position and velocity messages thereafter. The position and velocity messages carry the ICAO 24-bit address unique to the aircraft, allowing them to be assigned to the aircraft after reception, even in the absence of new aircraft identification messages.

Since bit errors are possible in the transmission, and since external factors may cause a single message to be missed, it is useful that two of each critical message (position and velocity) are included in the fundamental analysis period, for redundancy. To additionally take, as the analysis baseline, that all messages from a given aircraft are received in a given analysis period, permits a conservative case with regards to the probability of lost signals.

Therefore, the analysis described in section 4.6.1 is undertaken with the values of the basic parameters (given in equation 4.30), as follows:

$$\begin{aligned}d &= 120\mu s \\m &= 6.2 \\l &= 744\mu s\end{aligned}\tag{5.2}$$

The analysis period, T , is one second, or:

$$T = 10^6\mu s\tag{5.3}$$

It follows then that for the purpose of this analysis, a no-collision event is one in which, for a period of 1 second, a given aircraft has all of its messages, totaling 744 μs in duration, received by the sensor without overlap by signals from another aircraft.

Using equation 4.33, the probability of such a no-collision event is, for each of n aircraft observed by the sensor,

$$P_{no,n} = (0.999256)^{n-1}\tag{5.4}$$

The variation of $P_{no,n}$ as the number of aircraft in view (n) increases from 2 to 6000 aircraft is shown in Figure 5.32. The probability of avoiding collisions decreases monotonically as more aircraft enter the field of view.

The expected number of aircraft successfully tracked is $R_{no,n}$, calculated by equation 4.34. The variation of $R_{no,n}$ with increasing n is shown in Figure 5.33. As n increases, so does the expected number of aircraft detections, initially. But while the number of aircraft rises arithmetically, the probability of avoiding collisions falls exponentially. The latter effect soon overwhelms the former, and $R_{no,n}$ reaches a peak before falling off. The maximum number of aircraft expected to be detected within each period ($T = 1s$) is 494.6, when there are $n = 1344$ aircraft in the field of view. The expected rate of successful detections falls off asymptotically to zero as the number of aircraft in the field becomes very large.

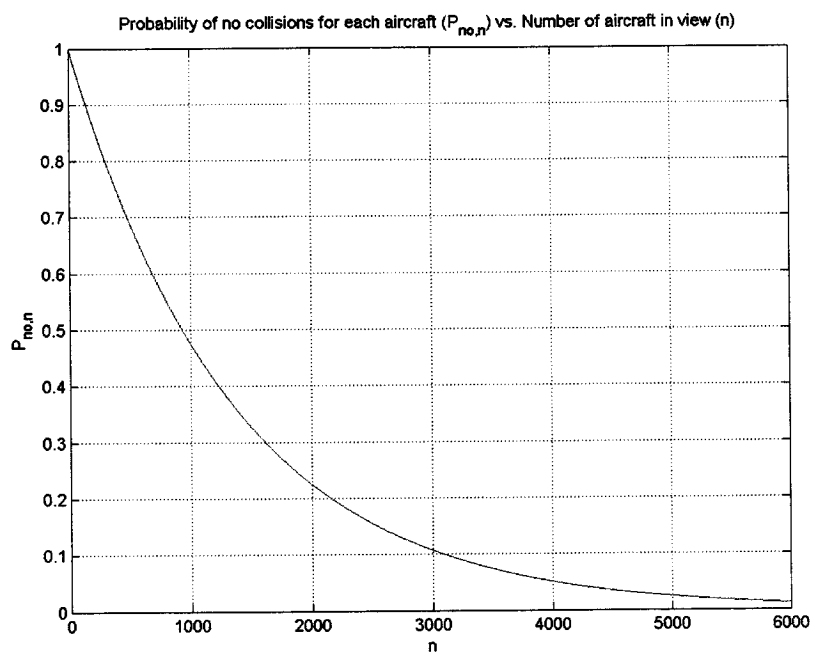


Figure 5.32: Probability of no collisions vs. Number of aircraft in view

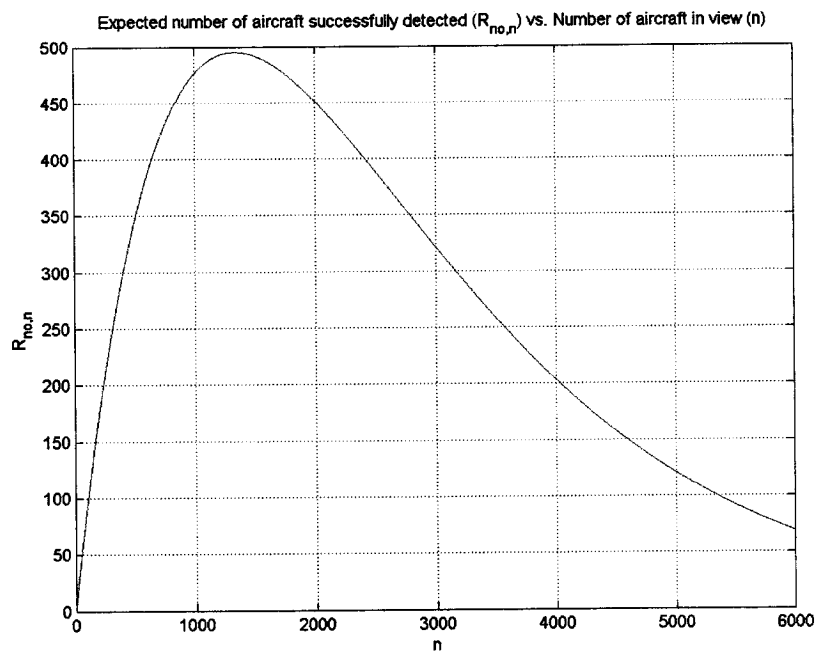


Figure 5.33: Expected number of aircraft successfully detected vs. Number of aircraft in view

To improve the detection probability as the number of aircraft increases, it is necessary to integrate over several periods. The probability of successful detection (no collisions) for a given aircraft over t seconds is $P_{no,t}$, given by equation 4.37. $P_{no,t}$ is plotted for various values of t in Figure 5.34. As the duration of the integration increases, so does the probability of detection, for any number of aircraft in the field of view.

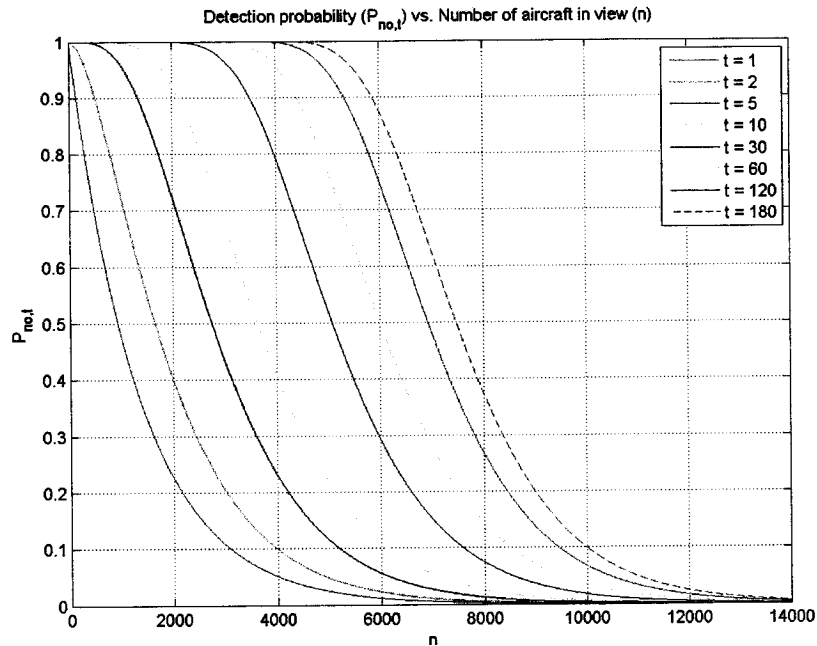


Figure 5.34: Detection Probability by number of aircraft and integration time

The result can be expressed alternately by the probability of detection failure for a given aircraft, P_f , whose value is $1 - P_{no,t}$. P_f is plotted in Figure 5.35, for varying integration times. Horizontal lines are included at the levels $P_f = 10^{-6}$, 10^{-9} , and 10^{-12} . These show the combinations of n and t for which the probability of failing to detect any individual aircraft are one in a million, one in a billion, and one in a trillion, respectively.

The result can be expressed as in equation 4.38:

$$P_f = A^t$$

where A is equal to

$$A(n) = \left[1 - \left(\frac{T-l}{T} \right)^{n-1} \right] \quad (5.5)$$

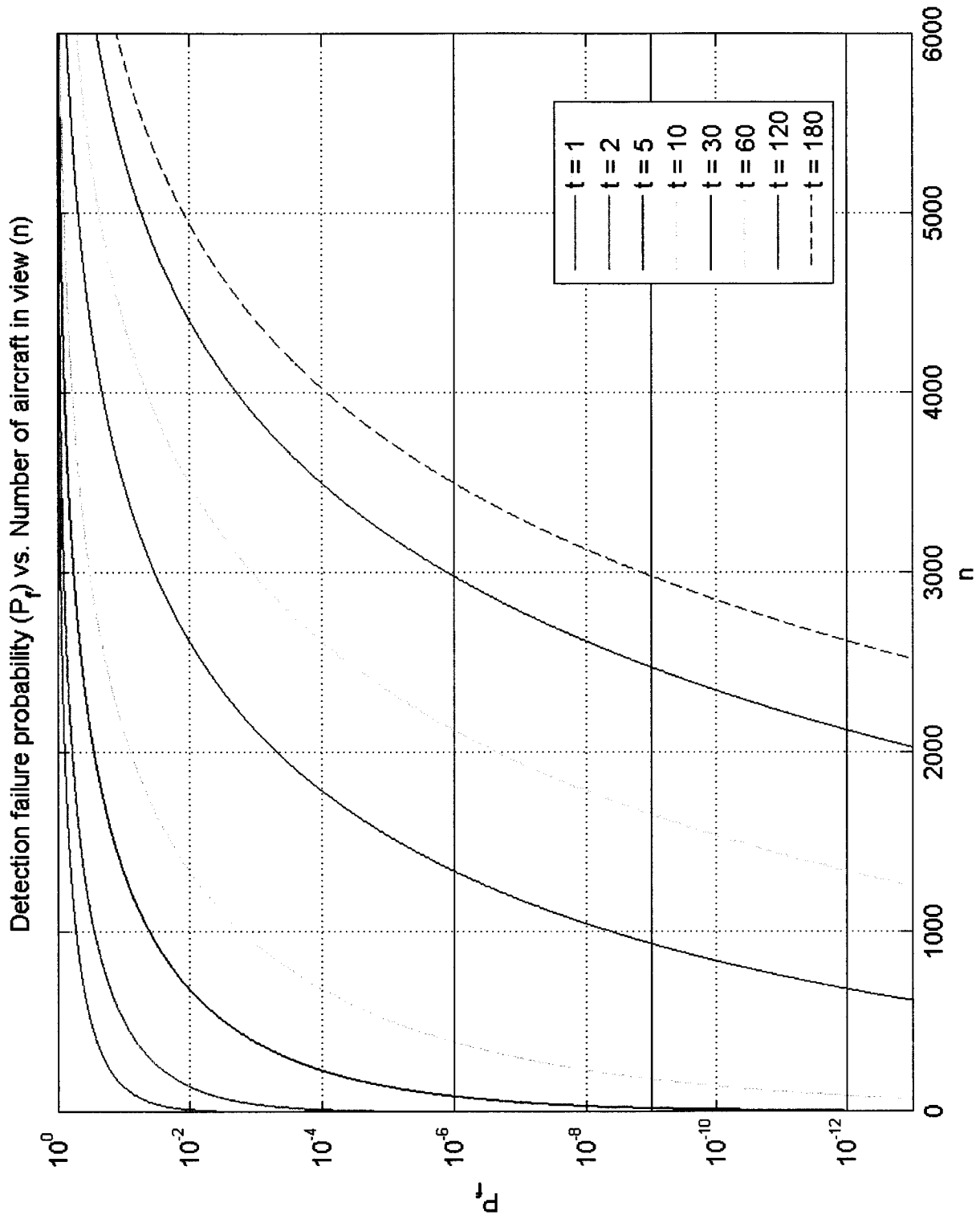


Figure 5.35: Detection failure probability by number of aircraft and integration time

Using this relationship, it is possible to plot the integration time t needed as a function of the number of aircraft in view, n , given a chosen value of the detection failure probability, P_f . This is given for several values of P_f in Figure 5.36.

Table 5.7 contains values for the number of aircraft allowed in the field of view for various integration times and failure probabilities. These will be key parameters for the design of a system to monitor ADS-B signals from orbit. While counts of aircraft airborne in a given area vary widely with both time and geographical region, a comparison can be made to the total number of aircraft which were reported in the FLOAT reference data provided by Nav Canada (Burrige, pers. comm., 2009). For the 24 hours of June 12th, 2009, Nav Canada's Area Control Centres handled 1673 flights, in an circular area of approximately 450 km radius centred on southwestern Ontario and including the Toronto Pearson airport. The count includes all Instrument Flight Rules (IFR) and Controlled Visual Flight Rules (CVFR) traffic; low-speed, low-altitude general aviation aircraft on uncontrolled VFR flights were not counted in this list, but are in general not the targets of planned ADS-B surveillance.

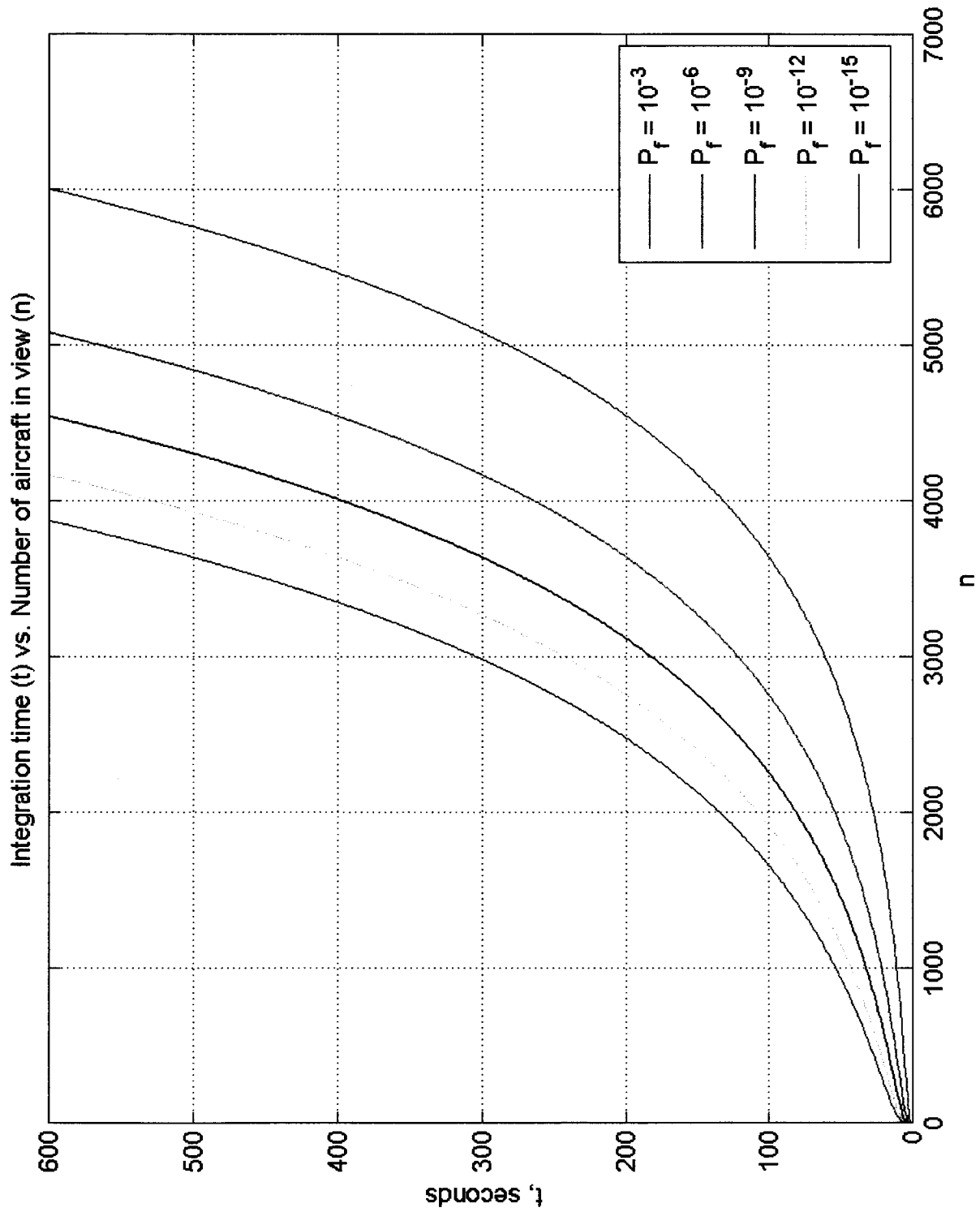


Figure 5.36: Relationship between key signal collision parameters

Table 5.7: Number of aircraft allowed in the field of view for detection failure probability and integration time

Integration time (t, seconds)	Probability of failing to detect an aircraft (Pf)			
	10^{-3}	10^{-6}	10^{-9}	10^{-12}
1	2	1	1	1
2	44	2	1	1
5	389	88	22	6
10	935	389	181	88
30	2125	1340	935	683
60	2982	2125	1654	1340
120	3875	2982	2475	2125
180	4407	3501	2982	2620
300	5083	4167	3637	3266
600	6006	5083	4546	4167

5.9.1 System design parameters and strategy

The first step in designing an orbital ADS-B monitoring system to provide operational surveillance information to support ATS is to fix the two key parameters P_f and t . No system will ever provide complete certainty of constant detection of all aircraft, so, in consultation with the needs of the ATS provider, it must be determined what is a sufficient level of certainty for detecting aircraft to support operations and to satisfy the operational safety concept. While very high certainty is desired, it is noted that the ADS-B system itself is designed to accept an undetected error rate of 1 error per 10^{-6} messages (DO-260B, 2009, section 2.2.4.4.3.1). If the orbital monitoring system provides a similar (or better) level of reliability in tracking these messages, then the overall fidelity of the tracking system is not degraded, and the information provided to ATS will be of the same quality as to an aircraft equipped for ADS-B In flying in the same airspace.

Having decided on an acceptable level of detection failures, the next key parameter is the tracking delivery time. In order to record messages from all aircraft in view (with probability of missing one P_f), it is necessary to listen for a period t . In air traffic monitoring, it is desirable to have timely and accurate data on the positions of all aircraft in the region of responsibility. Currently, radars provide updated position every few seconds, but over the ocean position updates must be sent by radio to the control centre, and typically these are only available every 30-50 minutes (NAT SPG, 1999). An orbital system to monitor traffic using ADS-B signals could monitor thousands of aircraft over an ocean simultaneously, and provide timeliness nearly to the level of radar, with a single sensor. If the system uses multiple discrete sensors covering portions of the ocean, the number of aircraft that can be tracked increases with the number of sensors.

The present analysis addresses the case of interference from other aircraft. The performance will be reduced in the event of interfering signals from other sources. The PPM signal modulation of the 1090 MHz ES is, fortunately, resistant to random pulse noise on nearby channels (DO-181D, 2008, section 1.2.2). Nonetheless, any system design will require a survey of these potential sources, including terrestrial air navigation beacons such as DME and terminal radars, which operate near 1090 MHz, as well as other Mode S traffic which is not part of the ADS-B system. The performance will also be affected if other phenomena, such as atmospheric scintillation, cause the occasional loss of messages. In the particular case of scintillation, there is an advantage that should a fading event attenuate one of two overlapping signals, the other will become detectable, where both would have been lost in the absence of

scintillation. Non-overlapped messages which are faded by scintillation offer no such recovery, of course, as is the case with multiply-overlapped messages.

5.9.2 Addressing the aircraft population limit

If the number of aircraft in the region of interest exceeds the no-collision limits, it is possible to improve reception by dividing these aircraft into groups by various methods. The simplest is geographic; rather than having a single antenna which covers the entire area, several sensors can be used, each with an antenna covering a portion of the total area. The number of sensors can be selected to ensure that, with expected traffic levels for the area of interest, the number of aircraft in view of each antenna will remain below the threshold for acceptable detection probability. If appropriate, these sensors can be housed on the same spacecraft, or alternately, deployed as a constellation of discrete satellites. The limit on the number of observed aircraft may thus be a driver of antenna and constellation design.

Other techniques can be used to sort signals in the same geographic area. Received ADS-B signals will vary in signal power, due to varying transmitter power and distance from the receiver. It may be possible to first filter the received signal by power level, processing the strongest signals and the weakest ones in two (or more) separate groups. Within each subgroup, the collision probability will be as for an aircraft population of that subgroup's size, and thus lower than for all of the subgroups combined.

Such a discrimination might instead be effected using the frequency of the incoming signal, relying on variation of transmitted frequency within the allowed limit (see section 4.2.3.2), or on the Doppler effect. Such an implementation may have practical difficulties due to the small frequency spread imparted by both effects (see section 5.8).

A further option is to effect this division by discrimination on the polarization of the incoming signal. Although the transmitted signals all have vertical polarization, the transmitting antennas will be at varying orientations as viewed by a receiving antenna with a large field of view. In the GEO case, for example, aircraft will be visible around the entire circumference of the Earth's limb, each emitting signals from a monopole antenna oriented to the local vertical. If this variability in relative polarization is not reduced during propagation to the receiver – for example by Faraday rotation or the effects of precipitation – then received polarization might be used to divide the incoming signals into groups for separate processing.

All of these techniques attempt to produce discrete populations of signals within which non-colliding signals can be found at the rates calculated above. A further

possibility is to develop advanced signal processing algorithms capable of deconflicting two or more overlapping squitters. In this, inspiration may be drawn from current and planned orbital AIS detection missions, which use such techniques to address a similar problem of signal decollision (Bonin, 2008). Were such techniques used, the number of aircraft detected would be greatly increased, though the probability remains less than 100%. Depending on the capability of the algorithms, it is possible that collisions of order 2, where only two signals overlap, are detectable, while collisions of some higher order remain unavailable. As a result, the probability analysis used above would need to be extended to address higher-order collisions. Nonetheless, such techniques, appropriate to the ADS-B case, would greatly increase the number of aircraft that can be simultaneously monitored for given values of P_f and t , improving the performance of an orbital monitoring system greatly.

Chapter 6

Considerations for implementation of space-based ADS-B surveillance

6.1 Introduction

Following the scientific and technical results presented previously, this chapter explores the programmatic considerations for the implementation of an operational surveillance system using orbital ADS-B sensors. Section 6.2 reviews the motivation for implementing such a system. Section 6.3 examines the prospects and potential form of international co-ordination in the development of such a system to serve the safety and efficiency of civil aviation. Section 6.4 considers the agencies and groups which might have an interest in discussions surrounding the development of the system. In section 6.5, the characteristics of a space-based surveillance system to support air traffic management are briefly introduced, followed by notes on the nature of the space segment in section 6.6. Finally, section 6.7 notes briefly the long-range implications of an orbital ADS-B surveillance system.

6.2 Motivation

The prospect of orbital monitoring of ADS-B signals may have broad interest. A reliable, operational – as opposed to experimental – system providing spatially- and temporally-continuous surveillance of air traffic would provide an alternate or redundant source of surveillance information to air traffic authorities. Countries with large, sparsely-settled land areas, such as Canada, Australia, and Russia, could use it to supplement or replace arrays of ground stations which would need to be expensively

deployed in remote and sometimes inhospitable territory. Large areas of Canada, for example, currently have no surveillance at all (Cochrane, 2007), though deployment of ground stations is planned to reduce this coverage gap (Nav Canada, 2008).

Over the ocean, however, ground stations cannot provide a solution. With growing traffic levels, such as over the North Atlantic, the need for accurate and timely surveillance information will increase. Current practices to provide oceanic separation, such as the need pass through designated reporting points and to relay position reports by radio (TC AIM, 2009), cause longer flight times, increased fuel consumption, and increased air pollution compared to more direct great-circle routes between airports on separate continents. As well, while full adoption of ADS-B Out and In technology would eventually provide pilots of transoceanic flights with information on the aircraft in their vicinity, oceanic controllers would continue to lack information about the positions of aircraft over the ocean. They would instead continue to rely on assignment of time slots and vertical separation minima, which have already been reduced to accommodate increased traffic levels (TC AIM, 2009). A space-based system could monitor oceanic airspace and provide oceanic controllers with timely and accurate information to help monitor and separate the growing numbers of aircraft in their responsibility. Clear advantages for aviation safety, fuel conservation, and the efficiency and security of transportation networks would result from such a system.

6.3 International co-ordination

Because of the wide fields of view available to satellites, the co-operative nature of oceanic control, and the global coverage offered by the motion of satellites in orbit, the motivation for an orbital ADS-B surveillance system may arise in the context of international co-operation. Already, the International Civil Aviation Organization (ICAO) co-ordinates standards and procedures for provision of Air Traffic Services, and has a Technical Co-operation Bureau dedicated to assisting states in implementing co-ordinated technical projects (ICAO, 2003a). It also co-ordinates the shared control of oceanic airspace and the establishment of procedures used therein (FAA, 1999). Development of a new surveillance system for oceanic control, or for surveillance over large areas of the Earth's surface covering several countries, may naturally include the involvement of ICAO. The actual development may occur at the national level, or through partnerships between national or transnational agencies. Canada and the United States, for example, share a continent and would in many cases both be in view of the same orbital sensor. Both countries share a common interest with European

authorities, due to the shared control of oceanic airspace and the large amount of intercontinental traffic across the Atlantic. Operators of that traffic would benefit from common standards on both sides of the ocean, and co-ordinated surveillance from takeoff on one continent to landing on the other.

In addition to co-ordination for the sake of transoceanic surveillance and standardization, national airspace management in third-party countries might benefit from such a system. Countries with limited budgets to establish a surveillance system, or to replace aging infrastructure, might use data from the orbital system to meet their needs. The example case of a satellite in GEO at 100° provides coverage over Canada, the United States, and Brazil, all countries with established space industries and a history of collaboration on space projects. But it also provides coverage of Suriname, Uruguay, Argentina, and many other parts of South America. These countries may not have the ability to launch an orbital surveillance system, and may have a wide range of budgets available for domestic air traffic surveillance. In all cases, the provision of data from an orbital surveillance system would be of benefit to aviation safety and efficiency, and is thus in the general interest. The involvement of multiple countries may also help to increase the demand for such a system, and reduce the cost borne by individual states. Should the development of an orbital ADS-B surveillance system occur in an international context, states and agencies leading the project may well decide to involve a broad range of interested parties, or to include in the planning a mechanism for providing data to third parties after the system is operational.

Such international co-ordination of technical projects may seem daunting, but precedent exists for collaboration in similar fields. ICAO has co-ordinated the technical, legal, and operational aspects of civil aviation the world over since its founding in 1947 (ICAO, 2005). On space matters, the European Space Agency, now with 18 member states, has undertaken complex space projects for over forty years (ESA, 2009b). Many other specific models exist of internationally-coordinated space-based services. The Galileo navigation system, now in its experimental stages, has been developed jointly by the member states of ESA and the European Union, and will provide global navigation services both inside and outside the contributing countries, on both a free and a commercial service (ESA, 2007). A long co-ordination has existed between Europe and the United States on provision of weather data from satellites, with the European Organisation for the Exploitation of Meteorological Satellites (EUMETSAT) and the National Oceanic and Atmospheric Administration (NOAA) collaborating on data sharing, system planning, and instrument standardization since 1991 (NOAA, 2003). The Cospas-Sarsat program was developed as joint undertaking

by four countries in 1979 (COSPAS-SARSAT, 2009b); it now provides search-and-rescue service through the deployment of standardized payloads on several satellites contributed by various states. All of these programs provide services which the participating states have deemed to be of enduring value and whose provision is in the public interest, often with important implications for the safety of life. A model of international co-operation, similar to these but adapted to the specific case of ADS-B surveillance and civil aviation, may be the context of development should an operational orbital ADS-B surveillance system be developed.

6.4 Stakeholders

Any development of an operational system would likely take into account the needs of the various stakeholders in the implementing states. Airlines and air operators would likely be consulted, particularly where the development of the system requirements relates to the operational needs of airspace users. Should new procedures be developed, new equipment be required, or new costs be passed on to system users, both commercial and governmental agencies will need to be involved. The consultation and co-operation of ATS authorities will be essential, to develop the requirements of the system and to ensure the functional utility of the data, and its integration into the airspace system. Depending on the program structure chosen, industrial interests may be involved to a greater or lesser degree in the system definition, design, or provision.

Within Canada, agencies which may take an interest in such a development program include, but are not limited to, Transport Canada (TC), Nav Canada, the Canadian Space Agency (CSA), the Department of National Defence (DND), and the Department of Foreign Affairs and International Trade (DFAIT). Numerous air operators, as well as commercial interests both inside and outside the space industry, may also take interest in such a program.

6.5 System characteristics

While many options exist for the mix of platforms to be used in establishing ADS-B surveillance – ground stations, satellites in various orbits, and supporting elements such as data relay systems – key aspects of its architecture will be driven by the needs of the air traffic management system. Such will by necessity be determined in consultation with ATS authorities and other stakeholders, but a central requirement will certainly be reliability. Any system on which the safety of aviation depends must

by design be continuously available, and interoperable with other airspace resources. The system must therefore be designed to interface with existing infrastructure and procedures, and must be highly reliable.

Other space-based systems have been deployed which have similar strict reliability requirements, such as GNSS services, which are expected to provide continuous service at all times. Long-term planning ensures periodic upgrade and replacement of GPS satellites, for example. Weather information provided by satellites is also of great importance, and so each operational Meteosat spacecraft is accompanied by an on-orbit spare (EUMETSAT, 2007) and replacement satellites are provided early and kept in storage as ground spares (EUMETSAT, 2005). Such program planning ensures the continuous provision of data whose availability has been deemed essential, and similar planning may be appropriate for an ADS-B surveillance system, to ensure the level of operational reliability needed by the air traffic system. This may also have implications for constellation design, for example in deploying a standby satellite for a GEO system, or providing spare satellites in each orbital plane of a LEO or medium Earth orbit (MEO) system. Alternately, a constellation might be designed to provide sufficient coverage overlap between adjacent satellites to minimize the impact of malfunction by one spacecraft.

6.6 Implementation

Numerous avenues exist for the implementation of a system for orbital ADS-B surveillance. It is likely that such a capability would be deployed in stages, with the technology, platforms, and organizational aspects evolving as the system grows. Initially, an experimental mission may be undertaken by a single agency, perhaps even a university space program, to demonstrate signal reception from orbit and verify the theoretical results presented in the preceding chapters. Such a program might employ a small-scale, simplified platform with limited capabilities as compared to an eventual operational mission.

The system need not be stand-alone. ADS-B receiver payloads might be integrated as passengers on other satellites, in the same way that search and rescue payloads are accommodated to support Cospas-Sarsat (COSPAS-SARSAT, 2009a). Satellite operators often offer positions for secondary payloads on large spacecraft; Canada's Telesat, for example, offers opportunities for hosted payloads on its geostationary communications satellites. Users of this service include the FAA, for which transponders aboard Telesat's Anik F1R satellite provide the navigation signals of

the Wide Area Augmentation System (WAAS) service (Rigley, 2009). WAAS is an overlay service for GPS, which provides an improvement to the navigational accuracy essential to the safe use of the system for civil aviation. Such an application may provide an implementation model for an ADS-B surveillance system, which has similar requirements and end users.

6.7 Further evolution

Should a space-based ADS-B surveillance system be deployed, its presence may influence the evolution of the standards applicable to ADS-B, the technology used, and the extent of its adoption as a surveillance mode. The availability of the system may, for example, drive an adjustment to the antenna pattern requirement for aircraft, to reduce the effect of the reception null at satellite nadir. It might also promote adoption of ADS-B surveillance in countries or regions where this was not previously planned. The system might come to be co-ordinated with other orbital services, such as navigation systems or maritime traffic monitoring programs. A possible future utility is the tracking of re-entering or even orbiting spacecraft. The message definitions for ADS-B over 1090 MHz ES are written to include identification of vehicle types, with a provision for “Space / Trans-atmospheric vehicle” as an option (DO-260B, 2009). An orbital ADS-B monitoring system would likely be capable of monitoring such traffic both in the atmosphere and outside it, depending on the vehicle’s orbit.

Chapter 7

Summary, Conclusion, and Future work

7.1 Summary

Air traffic management has historically relied on a combination of ground-based radar and radio voice messages to provide ATS agents with knowledge of the position, identity, and intentions of aircraft in flight. As traffic levels in both national and oceanic airspace increase, and as radar systems age, ATS authorities have begun the transition to a system using Automatic Dependent Surveillance – Broadcast (ADS-B) as a means of providing surveillance information. While ADS-B-based surveillance systems offer cost and accuracy advantages over radar, they still require deployment of arrays of ground stations, which can be difficult or impossible in remote land areas or the open ocean.

While ADS-B transmitters are designed primarily to be detected by neighboring aircraft and broadcast their signals primarily in the horizontal, the FLOAT experiment demonstrated that it is possible to detect these signals from altitudes well above the aircraft. The FLOAT-2 payload tracked 41 aircraft in all modes of flight – taxi, takeoff, climb, cruise, descent, and landing – receiving across all altitudes from the surface of the Earth to 92,950 feet (28.3 km) ASL, with aircraft reliably detected at ranges on the order of 200 km, and some aircraft detected at larger distances up to 528 km from the receiver. The experiment also demonstrated the effects of key parameters affecting the detection of ADS-B signals from high altitude, including the variation in transmitted power, the transmitter antenna pattern, and the effects on the signal of propagation through the Earth’s atmosphere.

The concept demonstrated in the FLOAT experiment has been extended to con-

sider detection of ADS-B signals using Earth-orbiting satellites. A model of the propagation of ADS-B messages from the transmitting aircraft to satellites at a range of relevant altitudes has been developed, considering the case of the widely-adopted 1090 MHz ES datalink system. The model accounts for the varying distances and geometries involved, the established standards for the transmissions, and the effects of propagation through the atmosphere. The atmospheric studies included absorption and refraction in the neutral atmosphere, attenuation due to atmospheric moisture, and limitations imposed by the ionosphere.

The result of the analysis is the value for the net gain needed at the receiver to reliably detect ADS-B signals from any chosen orbit, with results presented for commonly-used orbits including LEO, SSO, MEO, GEO, and molniya orbits, as well as for the case of stratospheric balloons. This gain requirement can be used to drive antenna, receiver, and constellation design for any future system to monitor ADS-B signals from orbit, whether experimentally or operationally. The basic design parameters for such a system using LEO orbits are given, and a preliminary antenna and constellation design is developed for the GEO case. The use of aerostats is presented as a possible future option.

Additional effects on the signal, apart from power-level detectability, are further considered. The importance of the Doppler effect is investigated, and concluded to be minor. The phenomenon of signal collisions – overlapping signals from multiple simultaneously transmitting aircraft – is also addressed, due to its importance for satellites having large fields of view. A statistical model of the rate of collisions is developed, which allows the identification of the driving parameters for system design. These parameters are the allowable length of time an aircraft may go undetected by the sensor, and the probability of successful detection over that time. Results are presented for a variety of values, referenced to the mandated system performance of conventional air-to-ground ADS-B surveillance.

Finally, in light of the scientific and technical results obtained, the utility of the findings has been explored in the context of development of an operational mission, and the likely benefits and co-operations that would stem from such a project.

7.2 Key findings

A summary of the key results is given below.

- ADS-B signals sent over the 1090 MHz ES can be detected from the stratosphere, even using simple, low-cost, low-power equipment.

- Due to the frequency of operation, atmospheric effects on the signal are minor except near the limits of the field of view, where elevation angles are very shallow.
- The Doppler effect is of limited importance, because the frequency shifts are small compared to the working frequency.
- At any altitude, atmospheric or orbital, a detection null exists at the sensor's nadir due to the antenna pattern of the aircraft transmitter. The strongest reception is therefore obtained for signals which are not directly below the sensor, but at a certain distance laterally from the nadir point. This distance is a function of the sensor altitude.
- From low Earth orbits (LEO), the signal is strong enough to be detected with a net receiver gain of 0 dB. The signal power available is 22-88% of that for the AIS system used for maritime traffic, which is already being monitored from LEO.
- The surface footprint of a satellite in LEO is very dependent on satellite altitude and, for higher altitudes, on antenna gain and pattern, meaning the design of a constellation will require co-ordination of these parameters. It can extend to radii of approximately 2100 km for an altitude of 400 km, and to approximately 3000 km at altitudes of 800 to 1200 km, if an antenna gain of 3-5 dB is applied.
- At LEO, the detection null at nadir is sufficiently narrow that, due to the orbital motion of the spacecraft, aircraft will be undetectable within it for no more than several tens of seconds.
- At GEO, net receiver gains of at least 25 dB are needed to detect ADS-B signals on the 1090 MHz ES transmitted at the maximum power of 500 W. A gain of at least 31 dB is needed for the minimum power of 125 W. As always, the needed gain varies with distance from the nadir point. A parabolic antenna with a 2-metre diameter gives a peak gain of 30 dB, and is sufficient to detect 500 W ADS-B transmitters with a gain margin of 10-11 dB over a broad area of the visible hemisphere.
- A single sensor with a 2-m parabolic antenna, in geostationary orbit at 100°W, would provide virtually complete ADS-B coverage of Canada, in addition to its oceanic approaches and the oceanic airspace for which Canada has responsibility. With a gain margin of 10 dB, virtually the entire United States is covered by

this same sensor, as well as most of South America and broad portions of the Atlantic and Pacific oceans.

- Due to the large fields of view available, signal collisions will be significant. The number of aircraft which a single sensor can handle is driven by two operational criteria: the length of time desired between aircraft position updates, and the probability of failing to detect an aircraft in that time. For a failure probability of 10^{-6} and a position update cycle of 5 minutes, it is possible to record signals from over 4000 aircraft simultaneously. Increasing the allowable aircraft population requires adjusting the update time or failure probability, or developing signal processing algorithms for deconflicting overlapping signals.

7.3 Future work

Significant opportunity exists to extend the present work, and much more work needs to be done before the monitoring of ADS-B signals from orbit can be achieved. Among the future work which could extend and refine the concept are the following tasks:

- **Adaptation to real equipment.** The present analysis makes use of the operational standards governing the ADS-B over 1090 MHz ES. A review should be made of the real-world performance of the transmitter technology used aboard aircraft, to determine in what manner and to what extent it may deviate from the standard, or be more specific than the standard requirements. The results may have implications for the assumed frequency stability, antenna pattern, transmission rate, power level, and other characteristics of the signal, which may drive receiver design.
- **Effect of aircraft orientation.** The present analysis has assumed that the transmitting aircraft is in level flight. This assumption is true over most of the duration of a long cruising flight, but manoeuvring and the resultant change in the orientation of the transmitter antenna may be significant for certain flight operations.
- **Bit error rate.** The calculation of link margins presented here does not consider limitations which may be posed by bit error rate behaviour of the pulse-position modulation scheme. While these errors may be minimized by match filtering or other receiver techniques, a bit error rate calculation should

be carried out, and, if it implies additional gain margin requirements, this effect should be applied to the link budget.

- **Survey of interference sources.** Other radio frequency systems may transmit signals which can interfere with the ADS-B signals. A survey of possible sources of interference would allow an estimation of the adverse effect that may be imparted on the reception of the signals. Such reduced reception may have implications for the system performance as determined by the analysis of signal collision probability.
- **Other datalink systems.** Besides the 1090 MHz ES, there exist other datalink technologies used for relaying ADS-B information. Their adoption is less extensive, and often serves different segments of the aviation community. A review should be made of the importance of these datalink technologies to the provision of air traffic surveillance, and whether it is necessary to include them in any orbital ADS-B surveillance system. If so, the present analysis can be adapted to the case of these datalink systems.
- **Traffic level analysis.** A key limitation imposed by the architecture of the 1090 MHz ES is the number of aircraft which can be simultaneously monitored, as a result of signal collisions. For various regions of interest for space-based air traffic surveillance, a survey should be made of present and projected levels of ADS-B-equipped air traffic, to determine the importance of this limitation. A count of the number of aircraft in view of a particular sensor will vary in time and space, as well as with the satellite altitude, requiring these aspects to be considered in the analysis. This survey could include an estimate of the power levels of the ADS-B transmitter equipment aboard the expected aircraft, to drive decisions about the antenna gain needed on-orbit. Knowledge of the numbers of aircraft in view will allow estimation of the fraction of time the receiver is active, which will in turn allow estimation of the importance of fading due to atmospheric scintillation, and statistical estimation of the rate of message loss due to this phenomenon.
- **Decollision algorithms.** In response to the traffic level survey, a need to address the aircraft population limit may become apparent. A technique to do so is the development of signal processing algorithms to disentangle overlapping signals after they are received. Such algorithms exist for AIS sensors, and might be adaptable to the ADS-B case.

- **Receiver design.** While ADS-B receivers are commercially available, no such device has yet been deployed in orbit. A program to define the requirements for such a payload, adapted to the conditions and needs of an orbital platform, could be begun as follow-on work to that described above.
- **Antenna design.** The present work has given examples of antennas which might be used on orbit. Many other possibilities exist, and may offer advantages for signal reception and overall system design, depending on the specifics of the mission and orbit chosen.
- **Experimental verification.** The theoretical results described in the present work could be verified and extended by the development of a space mission having as its goal the detection of ADS-B signals from orbit. Numerous options for such an experimental program exist, from microsatellite missions to hosted payloads on other spacecraft and orbital facilities. In addition to the scientific and engineering work described above, the program required to achieve such a mission would need to be developed, and the work carried out in consultation with relevant partners, including for example ATS authorities.

Bibliography

- AIC 21/09 (2009). *Aeronautical Information Circular 21/09*. Nav Canada.
- Air Canada (2009). Our Fleet: Boeing 777-300ER (77W). Online at <http://www.aircanada.com/en/about/fleet/77W.html>.
- Arianespace (2008). *Ariane 5 User's Manual*. Issue 5, Revision 0. Available online at http://www.arianespace.com/launch-services-ariane5/Ariane5_users_manual_Issue5.pdf.
- Bédard, D. & Spaans, A. (2007). Responsive space for the Canadian Forces. In *5th Responsive Space Conference*. Defence Research & Development Canada, AIAA: RS5-2007-3004. Los Angeles, California, 2326 April.
- Boeing (2007). Technical Characteristics – Boeing 777-300. Online at http://www.boeing.com/commercial/777family/pf/pf_300product.html.
- Bonin, G. (2008). Low-cost space qualification testing of potential microsatellite technologies - 2007. DRDC Contract Report CR 2008-337, Carleton University on behalf of DRDC – Ottawa. Available online at <http://pubs.drdc.gc.ca/PDFS/unc83/p531340.pdf>.
- Bonin, G., Sinclair, D., & Zee, R. E. (2009). Peak power tracking on a nanosatellite scale: The design and implementation of digital power electronics on the SFL Generic Nanosatellite Bus. In *23rd Annual AIAA/USU Conference on Small Satellites*. University of Toronto Institute of Aerospace Studies Space Flight Laboratory, and Sinclair Interplanetary.
- CAR (2009). *Canadian Aviation Regulations*. Transport Canada, 2009-2 edition.
- Cochrane, J. (2007). Update on Canadian implementation of ADS-B in Hudson Bay. In *EUROCONTROL ADS-B Certification Workshop*. Palma Mallorca 21-22 November.
- Cochrane, J. (2008). Canadian implementation of ADS-B Out. In *Airborne Separation Assistance Systems Thematic Network 2*. Nav Canada. 14 April 2008, Paris, France. Available online at: <http://www.asas-tn.org/workshops/final-seminar-paris-14-15-april-2008>.

- COSPAS-SARSAT (2009a). Cospas-Sarsat System Overview. Online at: http://www.cospas-sarsat.org/index.php?option=com_content&view=article&id=168&Itemid=56&lang=en.
- COSPAS-SARSAT (2009b). History of Cospas-Sarsat. Online at: http://www.cospas-sarsat.org/index.php?option=com_content&view=article&id=178&Itemid=143&lang=en.
- DAH (2010). *Designated Airspace Handbook*. Nav Canada. Issue No. 215, Effective 0901Z 11 February 2010. TP 1820E.
- DO-181D (2008). *Minimum Operational Performance Standards for Air Traffic Control Radar Beacon System / Mode Select (ATCRBS/Mode S) Airborne Equipment*. RTCA, Inc. October 2, 2008.
- DO-260B (2009). *Minimum Operational Performance Standards for 1090 MHz Extended Squitter Automatic Dependent Surveillance - Broadcast (ADS-B) and Traffic Information Services - Broadcast (TIS-B)*. RTCA, Inc. December 2, 2009.
- DRDC (2008). *CIMON Mission Concept & Enabling Technologies Development Study Statement of Work*. DRDC – Ottawa. Release 3.0, 5 September 2008. DRDC file: 15EA/08-SOW-0002.
- Dunstone, G. (2005). ADS-B performance. In *Report of the Automatic Dependent Surveillance - Broadcast (ADS-B) seminar and the Fourth meeting of the ADS-B Study and Implementation Task Force (ADS-B SITF/4)*. Airservices Australia. Nadi, Fiji, 26-28 October, 2005. Online at: http://www.icao.int/icao/en/ro/apac/2005/ADSB_SITF4/sp04.pdf, full report at http://www.icao.int/icao/en/ro/apac/2005/ADSB_SITF4/.
- Erçetin, O., Ball, M. O., & Tassiulas, L. (2000). Next generation satellite systems for aeronautical communications. Technical report, National Center of Excellence in Aviation Operations Research. Available online: http://www.lib.umd.edu/drum/bitstream/1903/6184/1/TR_2000-20.pdf.
- ESA (2007). Galileo services. Online at: http://www.esa.int/esaNA/SEMTHVXEM4E_galileo_0.html.
- ESA (2009a). Atlantis leaves Columbus with a radio eye on Earth's sea traffic. Online at: http://asimov.esrin.esa.it/SPECIALS/Space_Engineering/SEMIHX49J2G_2.html.
- ESA (2009b). History of Europe in space. Online at: http://www.esa.int/SPECIALS/About_ESA/SEM7VFEVL2F_0.html.
- EUMETSAT (2005). MSG-2 successfully launched. Available online at: http://www.eumetsat.int/Home/Main/News/Press_Releases/005023?l=en.

- EUMETSAT (2007). *Meteosat Second Generation: Space segment*. Online at: http://www.eumetsat.int/Home/Main/What_We_Do/Satellites/Meteosat_Second_Generation/Space_Segment/index.htm?l=en.
- EUROCONTROL (2007). *ADS-B for Dummies: 1090 MHz Extended Squitter*. European Organisation for the Safety of Air Navigation. Version 4. Available online at: <http://www.ans.dhmi.gov.tr/TR/Sistem/Dok/ADS-B%20for%20Dummies-1090ES%20v04.pdf>.
- FAA (1999). *North Atlantic International General Aviation Operations Manual*. Available online at: http://www.faa.gov/air_traffic/publications/atpubs/NAO/NAOTOC.htm.
- FAA (2002). *Small aircraft-to-satellite data link successfully tested*. Press release. Online at: http://www.faa.gov/news/press_releases/news_story.cfm?newsId=6367.
- FAA (2003). *Implementing the FAA ADS-B link decision: A near term strategic plan*. Technical report, Federal Aviation Administration (USA). Report of the FAA Strategic Plan workgroup, January 28 2008. Online at: http://www.faa.gov/about/office_org/headquarters_offices/ato/service_units/enroute/surveillance_broadcast/wsa/media/Implementing%20the%20Link%20Decision.pdf.
- FAA (2007). *ADS-B: Frequently asked questions*. FAQ attachment to press release of 30 August 2007. Online: http://www.faa.gov/about/office_org/headquarters_offices/ato/service_units/enroute/surveillance_broadcast/program_office_news/media/Follow%20Up%20Contract%20Award-ADS-B%20Q&As_8-30-07_Final.pdf Press release available online: http://www.faa.gov/about/office_org/headquarters_offices/ato/service_units/enroute/surveillance_broadcast/program_office_news/.
- FLOAT-RP-RMC-0001 (2009). *FLOAT – Flying Laboratory for Observation of ADS-B Transmissions – Space Mission Design Report*. Technical report, RMC.
- GTAA (2008). *GTAA 2007 Noise Management Report*. Greater Toronto Airports Authority. Available online at http://www.gtaa.com/local/files/en/Annual_Report_Noise_2007.pdf.
- IATA (2007). *Automatic Dependent Surveillance Broadcast (ADS-B) OUT*. IATA document reference TOPM-INS-001-00, Edition 2, 9 October 2007, online at http://www.eurocontrol.int/cascade/gallery/content/public/documents/cascade%20palma/ADS-B_OUT_Edition_02.pdf.
- ICAO (2003a). *ICAO's Technical Co-operation Bureau: Mission Statement*. Available online at <http://www.icao.int/icao/en/tcb/mission.htm>.

- ICAO (2003b). Operational use of ADS-B in Non Radar Airspace: Generic design safety case. Technical report, International Civil Aviation Organization (ICAO). Draft version from FAA <http://adsb.tc.faa.gov/RFG.htm>.
- ICAO (2005). Foundation of the International Civil Aviation Organization (ICAO). Available online at http://www.icao.int/cgi/goto_m.pl?icao/en/hist/history02.htm.
- ICAO ADS-B (2003). Report of the ADS-B Study and Implementation Task Force Meeting. Technical report, International Civil Aviation Organization. Brisbane, Australia, 24-26 March. Available online at: http://www.icao.int/icao/en/ro/apac/adsb_2003/ADSB-Report.pdf.
- Lydolph, P. E. (1985). *The Climate of the Earth*. Rowman & Littlefield Publishers, Inc.
- Maddalena, R. J. (2002). Refraction, Weather Station Components, and Other Details for Pointing the Green Bank Telescope (GBT). GBT Memo 112, National Radio Astronomy Observatory (United States). August 7, 2002. Available online at <http://www.gb.nrao.edu/~rmaddale/GBT/GBTMemos/GBTMemo112.pdf>.
- Martis, G. (2007). IATA policy on ADS-B OUT - IN. In *EUROCONTROL ADS-B Certification Workshop*. Palma Mallorca 21-22 November.
- MSC.140(76) (2002). *Resolution MSC.140(76)*. Maritime Safety Committee of the International Maritime Organization. Adopted 5 December 2002, available online: [http://www.imo.org/includes/blastDataOnly.asp/data_id%3D15510/140\(76\).pdf](http://www.imo.org/includes/blastDataOnly.asp/data_id%3D15510/140(76).pdf).
- NAT ASM (2009). *Application of Separation Minima - North Atlantic Region (NAT ASM) - Version 3.0 (2009)*. International Civil Aviation Organization. NAT ASM V-3.0(2009), Effective 26 June.
- NAT SPG (1999). *North Atlantic Region Air Traffic Management Concept of Operations*. ICAO North Atlantic Systems Planning Group. Version 0.34, available online at <http://www.nat-pco.org/nat/NC00-34.doc>.
- Nav Canada (2007). *Canadian NOTAM Procedures Manual*. Available online at <http://www.navcanada.ca/NavCanada.asp?Language=en&Content=ContentDefinitionFiles\Publications\AeronauticalInfoProducts\NOTAMProcedure\default.xml>.
- Nav Canada (2008). Hudson Bay ADS-B Implementation. Online at http://www.navcanada.ca/ContentDefinitionFiles/Services/ANSPrograms/ADS-B/ADS_B_Brochure_EN.pdf.
- NOAA (2003). U.S., European satellite agencies sign co-operation, data-sharing accord. Available online at: <http://www.publicaffairs.noaa.gov/releases2003/jun03/noaa03079.html>.

- Orfanidis, S. J. (2008). *Electromagnetic Waves and Antennas*. Rutgers University. www.ece.rutgers.edu/~orfanidi/ewa.
- Orlando, V. (2001). Automatic Dependent Surveillance Broadcast (ADS-B) Mode S Extended Squitter. In *Meeting No.8 of the RTCA SC-186 Working Group No.3 for the 1090 MHz Extended Squitter MOPS*. MIT Lincoln Laboratory. Online here: http://adsb.tc.faa.gov/WG3_Meetings/Meeting8.htm.
- Pascale, E., Ade, P. A. R., Bock, J. J., Chapin, E. L., Chung, J., Devlin, M. J., Dicker, S., Griffin, M., Gundersen, J. O., Halpern, M., Hargrave, P. C., Hughes, D. H., Klein, J., MacTavish, C. J., Marsden, G., Martin, P. G., Martin, T. G., Mauskopf, P., Netterfield, C. B., Olmi, L., Patanchon, G., Rex, M., Scott, D., Semisch, C., Thomas, N., Truch, M. D. P., Tucker, C., Tucker, G. S., Viero, M. P., & Wiebe, D. V. (2008). Balloon-borne Large Aperture Submillimeter Telescope: BLAST. *The Astrophysical Journal*, **681**, 400 – 414.
- Pranajaya, F., Zee, R., Cain, J., & Kolacz, R. (2009). Nanosatellite tracking ships: From concept to launch in 7 months. In *23rd Annual AIAA/USU Conference on Small Satellites*, number IV-11. University of Toronto Institute of Aerospace Studies Space Flight Laboratory and COM DEV Limited.
- PSC ADS-B-NRA (2008). Preliminary Safety Case for enhanced Air Traffic Services in Non-Radar Areas using ADS-B surveillance. Technical report, European Organisation for the Safety of Air Navigation (EUROCONTROL). Edition 1.1, 12 December.
- Quine, B. M., Strong, K., Wacek, A., Wunch, D., Anstey, J. A., & Drummond, J. R. (2002). Scanning the Earth's limb from a high-altitude balloon: The development and flight of a new balloon-based pointing system. *Journal of Atmospheric and Oceanic Technology*, **19**, 618–632.
- Rao, S. K. (2003). Parametric design and analysis of multiple-beam reflector antennas for satellite communications. *IEEE Antennas and Propagation Magazine*, **45**(4). Available online at <http://ieeexplore.ieee.org/stamp/stamp.jsp?arnumber=01241308>.
- Rigley, J. (2009). Opportunities to cost-effectively fly space payloads. In *Canadian Space Summit 2009*. Telesat.
- Rohan, P. (1991). *Introduction to Electromagnetic Wave Propagation*. Artech House, Inc., 685 Canton Street, Norwood MA 02062 USA.
- SOLAS (2002). *International Convention for the Safety of Life at Sea (SOLAS)*. International Maritime Organization. Adopted 1974; amendment of 2002.
- TC AIM (2009). *Aeronautical Information Manual*. Transport Canada, 2009-2 edition. Version 2009-2, effective 0901Z, 22 October 2009. TP 14371E.

- Tipler, P. A. (1999a). *Physics for Scientists and Engineers*, volume 2. W. H. Freeman and Company, 41 Madison Avenue, New York, NY 10010 USA, fourth edition.
- Tipler, P. A. (1999b). *Physics for Scientists and Engineers*, volume 1. W. H. Freeman and Company, 41 Madison Avenue, New York, NY 10010 USA, fourth edition.
- TIS (2010). Climate/humidity table. Published by TIS-GDV (Transportation Information Service of the German Insurance Association), available online at http://www.tis-gdv.de/tis_e/misc/klima.htm.
- Transport Canada (2003). *Canadian Procedures for Large Unmanned Balloon Operations*. Appendix A to the ANS&A Policies and Procedures Manual, TP 13391E, Rev 2.0.
- Wertz, J. R. & Larson, W. J., editors (1999). *Space Mission Analysis and Design*. Jointly published by Microcosm Press and Springer, 4940 W. 147th Street, Hawthorne, CA 90250 USA and 233 Spring Street, New York, NY 10013 USA, third edition.
- Wright, G. (2009). Nav Canada Implements ADS-B. In *9th Integrated Communications, Navigation, and Surveillance Conference*. Arlington, Virginia, USA, 13-15 May.
- Yamagami, T. (2003). Research on balloons to float over 50 km altitude. Available online: <http://www.isas.jaxa.jp/e/special/2003/yamagami/03.shtml>.

CURRICULUM VITAE

CURRICULUM VITAE

Name: Raymond Francis

Place of birth: Sudbury, Ontario, Canada

Date of birth: 5 April 1982

Raymond Francis enrolled in the Canadian Forces in 2003 as an officer in the Cadet Instructor Cadre. Currently holding the rank of Second Lieutenant, he is a member of the staff of the Northern Ontario Gliding Centre (NOGC) at Canadian Forces Base (CFB) North Bay, Ontario. His previous service includes a dual posting with NOGC and 200 Wolf Squadron Royal Canadian Air Cadets in Sudbury, Ontario, as well as three assignments as a flight instructor at the Central Region Gliding School (CRGS) at CFB Trenton, Ontario.

From July 2007 to August 2008, he held a Young Graduate Trainee (YGT) post at the European Space Agency (ESA) in Noordwijk, the Netherlands, working in the Payloads and Platform Division of the Directorate of Human Spaceflight. During this time he worked in the development of fluid science experiments for the International Space Station. His previous civilian work includes several posts in manufacturing, software, and space systems engineering in Canada and Belgium.

Post-secondary education: University of Ottawa
B.A.Sc. Mechanical Engineering (CO-OP)
2001-2006

Honours and Awards: Sponsored graduate studies post
Defence Research and Development Canada &
Royal Military College of Canada
2008 – 2010

University of Ottawa Entrance Scholarship
2001

University of Ottawa Faculty of Engineering Scholarship
2001

Sandvik Canada Scholarship
2001

St. Benedict Catholic Secondary School
RJ McCarthy Scholarship
2001

Publications:

Vincent-Bonnieu, S; Minster, O; Dewandre, T; Francis, R; Liggieri, L; Loglio, G; Miller, R; Steinchen, A; Antoni, M, Clause, D; Del Gaudio, L; Dalmazzone, C; Karapantsios, T; Dutschk, V; Rubio, R; Picker, G: FASES: An instrument for Fundamental and Applied Studies of Emulsion Stability, in *Third International Symposium on Physical Sciences in Space*, Nara, Japan, 22-26 October 2007

Vincent-Bonnieu, S; Minster, O; Dewandre, T; Francis, R; Langevin, D; Adler, M; Cohen-Addad, S; Hohler, R; Vandewalle, N; Saint-Jalmes, A; Weaire, D; Hutzler, S; Durian, D; Bellossi, F; Picker, G: FOAM: An instrument for coarsening of aqueous foam, in *Third International Symposium on Physical Sciences in Space*, Nara, Japan, 22-26 October 2007

Francis, R; Tremblay, P; Noël J: CIMON: The Canadian Magnetometric Observation Nanosatellites, *Second European Cubesat Workshop*, Noordwijk, the Netherlands, 20-22 January 2009

Francis, R: FLOAT: A stratospheric research balloon for education and payload development, in *Canadian Space Summit 2009*, Kingston, Ontario, 20-22 November, 2009